DEVELOPMENT OF A METHOD TO STUDY RETENTION OF HYDROPHOBIC ACTIVES FROM COSMETIC EMULSIONS ON OPTIMIZED SKIN BIOMIMICS

by

GEORGIOS GKOTSIS

A thesis submitted to

The University of Birmingham

for the degree of

DOCTOR OF PHILOSOPHY

School of Engineering

Department of Chemical Engineering

The University of Birmingham

January 2019

Acknowledgements

I would like to thank my supervisor Pola Goldberg Oppenheimer for her continuous support, guidance and motivation during these years. Thank you for all the help, inspiration and understanding.

Also thank Liam Grover, Serafim Bakalis, Anju Brooker and Mauro Vacaro for their support, feedback and scientific insight.

Many thanks to my colleagues JJ and Chiara for helping me and supporting me throughout these years

Many thanks to all ANMSA group members.

ABSTRACT

All-in-one products are a popular trend in cosmetics, personal and home care. In particularly, personal care products that serve multiple purposes are especially popular due to their multifunctional action which simultaneously provides cleaning, conditioning and protection of the treated area such as, skin or hair, in a fraction of the time in comparison to when using traditional products.

In this research programme, a dedicated method was developed towards the evaluation of the conditioning performance of 'all-in-one' cleansing products. Hence, all steps of product usage were replicated in a controlled environment and suitable characterization methods were employed.

Optimized skin mimics were fabricated to be used as test substrates and model systems of cosmetic formulations were produced, which demonstrated both cleaning and moisturizing capabilities as well as a repetitive and highly-controlled deposition set-up and a cleaning set-up.

The conditioning performance of the emulsions was studied and post-wash retention levels of the hydrophobic active on skin bio-mimics were systematically characterised. Techniques including fluorescent microscopy, gravimetric analysis and tribometry were employed to provide further, into-depth quantitative data of the retention.

Properties of the formulation including oil droplet-size, viscosity and volume-fraction and cleaning parameters including rinsing-duration and flow-angle were tested for their impact on retention.

TABLE OF CONTENTS

LIST OF FIGURES

LIST OF TABLES

LIST OF ABBREVATIONS

AFM	Atomic Force Microscopy
APG	Alky PolyGlucoside
BTAC	Behetrimonium Chloride
CAHS	CocoAmidopropyl HydroxySultaine
CMC	Critical Micelle Concentration
COST	Changing One Separate Factor
CTAC	Cetrimonium Chloride
DoE	Design of Experiment
JMP	Statistical Analysis Software
LSD	Large Size Droplet
MSD	Medium Size Droplet
MSS	Model Skin Surface
PVA	Poly Vinyl Acetate
RPM	Rounds Per Minute
RSM	Response Surface Methodology
RTV	Room Temperature Vulcanizing
SDBS	Sodium Dodecyl Benzen Sulphonate
SEM	Scanning Electron Microscope
SLES	Sodium Laureth Sulphate
SLS	Sodium Lauryl Sulphate
SSD	Small Size Droplet
TEWL	Transepidermal Water Loss

USA	United States of America
UV	Ultra Violet

LIST OF PUBLICATIONS AND CONFERENCE PROCEEDINGS

Papers:

Georgios Gkotsis, Jonathan James Stanley Rickard, Anju Brooker, Serafim Bakalis, Liam M. Grover, and Pola Goldberg Oppenheimer Fabrication of optimized skin biomimics for improved interfacial retention of cosmetic emulsions, *Journal of The Royal Society Interface*, Volume 15 Issue 143, 1 June **2018**

http://doi.org/10.1098/rsif.2018.0332

Conferences:

Oral Presentation at the *2nd International Conference on Advances in Chemical Engineering & Technology*, November 16-17, **2017**, Paris, France

Poster Presentation at the *RSC Biomaterials Chemistry Meeting*, 7-8th Jan **2016**, at the University of Birmingham

CHAPTER 1. INTRODUCTION AND THEORETICAL BACKGROUND

1.1 Introduction

Today's fast pace of life has created the paramount need to reduce time spent on skin and personal care in general by consumers, hence the development of products that serve multiple purposes is crucial [1-5]. All in one products, have been popular for a few years now, not only in skin care but in all personal care areas including dental, hair, cosmetics and fabric care. Similar pattern is followed in home hygiene as well as in the food industry. In the case of skin care, all in one products are designed in a way that enables consumers to treat their skin in various aspects but in a one-step process [2]. With conventional products, the consumer needs to clean their skin first with a cleaning product during the shower process, then in a second step use a revitalizing product that contains natural oils, vitamins, nutrients, etc. that nourishes the skin and enables maintaining a healthy appearance. In a third step the consumer can use a moisturizing product to ensure long-lasting hydration of the treated area and protection from atmospheric pollution. These many steps require a significant amount of time and the purchase of multiple products, resulting in consumers skipping the last two steps, not providing the important care required by their skin, hence neglecting one of the most important barriers of the human organism. All in one products can provide cleaning, moisturizing and treatment of the skin in a one step process without the need

for buying multiple products and in a fraction of the time needed compared to the use of conventional products [1-3].

It is crucial to evaluate the effectiveness of these products and evaluate the level at which the materials that have been engineered to deposit and be retained or absorbed by the skin structure after the use of the product actual perform. Here we introduce the term ‘retention’ which is defined as the phenomenon where an amount of a substance remains deposited on the applied surface after a specific process. Most skin care formulations contain some sort of surfactant, either for its cleaning properties or to emulsify the ingredients towards a homogeneous product and to produce and maintain specific structures within the emulsion. However, a problem arises here, and we refer to it as the counter effect of surfactants. In a product whose purpose is to clean but also deliver specific materials onto the skin surface like hydrophobic actives, natural ingredients, moisturizing agents, film forming polymers, cationic ingredients, etc., the desired materials are emulsified within the formulation using surfactants, giving them a dual, competitive function which includes both targeting soil, dirt and unwanted matter from the skin but also delivering the ingredients that we purposely included in the formulation to remain on the skin and as a result of the surfactants a significant portion of those ingredients are washed away during the rinsing of the skin.

Although a considerable research has been published on deposition of materials on human skin, the subject of retention is an understudied one. Consequently, a theoretical and experimental approach needed to be developed and understand retention, define the parameters that drive it and further develop a protocol that allows quantitative data generation that can be used to evaluate product effectiveness and formulation evaluation.

Our approach in this research included 5 steps in developing a retention focused system that should enable understanding of retention and generate quantitative data. These steps include the fabrication of an optimized human skin mimic, the development of adjustable model system emulsions similar to skin care products, the fabrication of a deposition set-up that is highly controlled and repetitive for all the control parameters that are encountered during deposition of a product, the development of a cleaning set-up that adequately represents the shower conditions and the variables that are involved in the shower process and lastly the evaluation of active retention on the tested samples. Additionally, the experimental approach was followed towards the generation of a model that allowed the study of the impact of all the independent factors such as oil viscosity, volume fraction, droplet size, rinsing time, rinsing angle to the response parameter, which in this study is retention, by using statistical analysis software and employing the least squared method.

1.2 Human Skin and Skin Mimicking Techniques

1.2.1 Human Skin

Being one of the most significant parts of the human organism, human skin is responsible for numerous functions of vital importance with most crucial being the physical protection of inner tissues from external molecules and threats like micro-organisms and bacteria [6-13]. Furthermore, human skin is responsible for the temperature regulation of the human body and enables the sensing of external alterations and/or stimulations. Additionally, skin protects the organism from UV radiation by altering its pigmentation through the function of melanocytes. Also, skin regulates the production of vitamin D, which is essential for the normal function of the organism [6-16].

As far as its structure is concerned, the human skin consists of three main layers, the Epidermis, the Dermis and the Hypodermis.

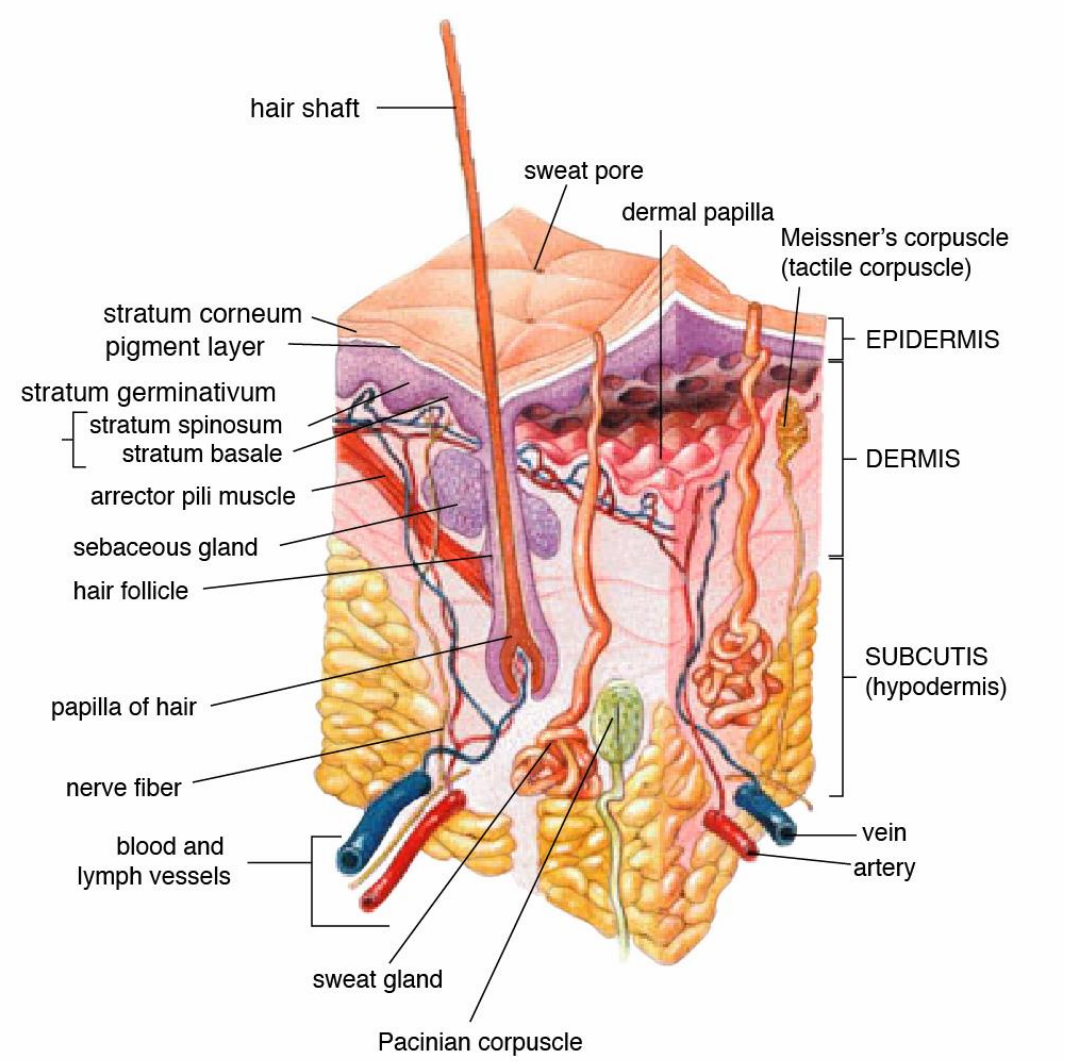

Figure 1.1: Structure of human skin [17]

By examining the epidermis in depth, distinguishable layers of cells can be observed and categorized depending on the cell characteristics and vitality. In detail, the inner layer of the epidermis is called stratum basale and it is where the keratin cells generate and the home of the melanocytes, which produce melanin and control the pigmentation of human skin. Furthermore, the next layer up is the stratum spinosum where the cells start to deform and assume a flat shape while moving to the external layers and

apoptose. The following layer is the stratum granulosum where lipid extrusion takes place and lastly the final layer is the stratum corneum where all the dead skin cells, mostly keratin, are stacked and assume a flat wide shape. The thickness of the stratum corneum is approximately 25 to 30 layers of dead, deformed cells and it is this part of the epidermis that gives skin its characteristic topography, surface energy and porosity. The living cells move gradually from the inner to the outer layers, where they will adopt a wider shape in a thicker structure and finally desquamate. Figure 1.2 is a graphic representation of the epidermis structure and its sublayers. [6,14,15]

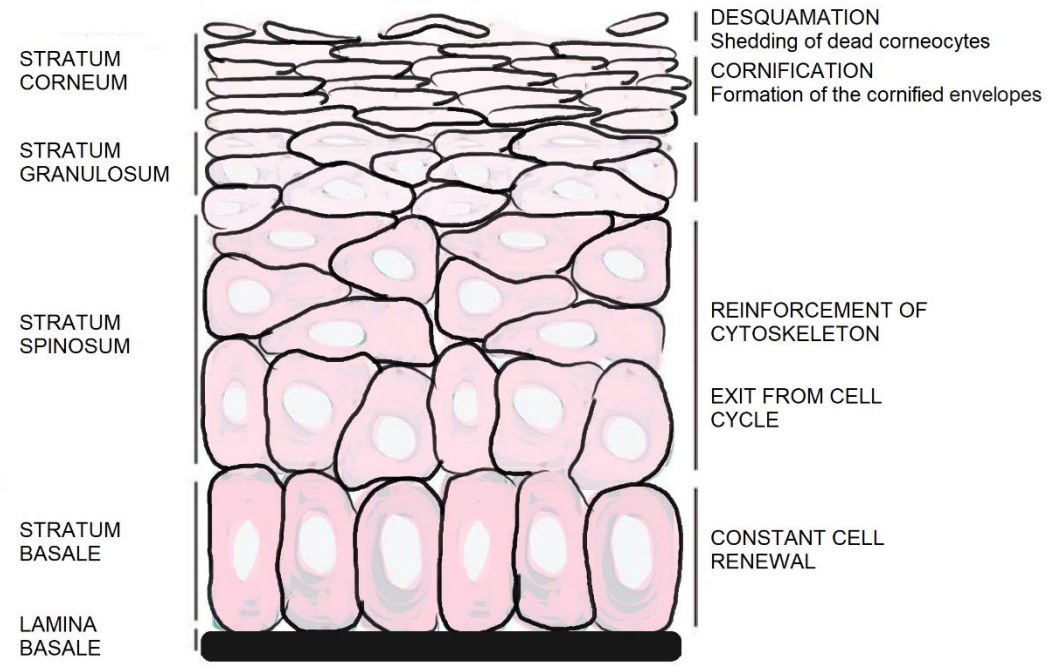

Figure 1.2: Structure of the epidermis

The inner part of the skin, the dermis, is a thicker layer that consists of all the crucial components that determine the proper function of the skin, including the blood vessels, the nerves and nerve endings, hair follicles, sweat glands, sebaceous glands and oil

glands. The nerves and nerve endings are those that enable the skin to perform as a large sensing organ, allowing the human body to detect external stimuli. Hair mostly contributes to the temperature regulation of the body and functions as stimuli receptors as well. Sweat glands have the function of temperature regulation by emitting sweat when the body is overheating in order to decrease its temperature via water evaporation. Oil glands provide the essential natural oils that protect hair and skin from dryness. Three types of cells can be found in the dermis which are the fibroblasts, the macrophages, and the adipocytes as well as matrix components such as collagen, elastin, and extrafibrillar matrix. Moreover, dermis consists of only two layers, the stratum papillae and the reticular layer. [6]

The final bottom layer of skin is the hypodermis, it is described as the inner layer after dermis and consists mostly of loose connective tissue, fats, large blood vessels and nerves.

1.2.2 Skin Mimicking

1.2.2.1 Replication Techniques and Materials

Mimicking skin properties and fabricating skin model substrates is a well-established subject in literature. The need for these substrates came from various concerns and disadvantages of using skin in vivo and animal skin for research, like sample reproducibility, cost, ease of use, tunability, storage requirements, supply availability, high variance of properties between samples and significant ethical issues. Therefore, multiple skin-oriented projects have presented solutions to these problems by developing skin mimics/replicas/model substrates, that replicate properties of interest

and demonstrate ease of use, high reproducibility, enhanced control of their characteristics, low cost, manageable shelf-life, stability and storage ease. Several crucial parameters that define skin are paramount and need to be considered when developing an efficient skin mimic and these include topographic characteristics, surface energy and mechanical properties [18]. The fabrication process and material choice are dependent on the end-product properties that are required by the mimic for the specific study that is tailored for.

A fundamental replication protocol is that of the resin replication technique, introduced by Facq [19]. It is one of the most widely used techniques due to its simplicity, accuracy and applicability with a variety of materials to a wide range of surfaces. The replication process starts by fabricating a negative mimic of the skin via pouring a skin safe material on the treated area of skin, allowing the material to cure, when applicable, and finally remove the mimic from the skin. The produced mimic demonstrates a negative image of human skin topography. However, it can be used to fabricate a positive mimic by employing the first as a mold where a choice of materials depending on the desired properties can be poured towards the production of a 1:1 positive skin replica that replicates accurately the topographic features of the area of interest. In Figure 1.3, a diagrammatic representation of the replication process described is illustrated where A is depicted as the surface to be replicated, in our case human skin, B illustrates the fabricated negative skin mimic, B is then inverted to be used as a mold to fabricate the positive mimic C which shows identical surface features with the initially replicated surface.

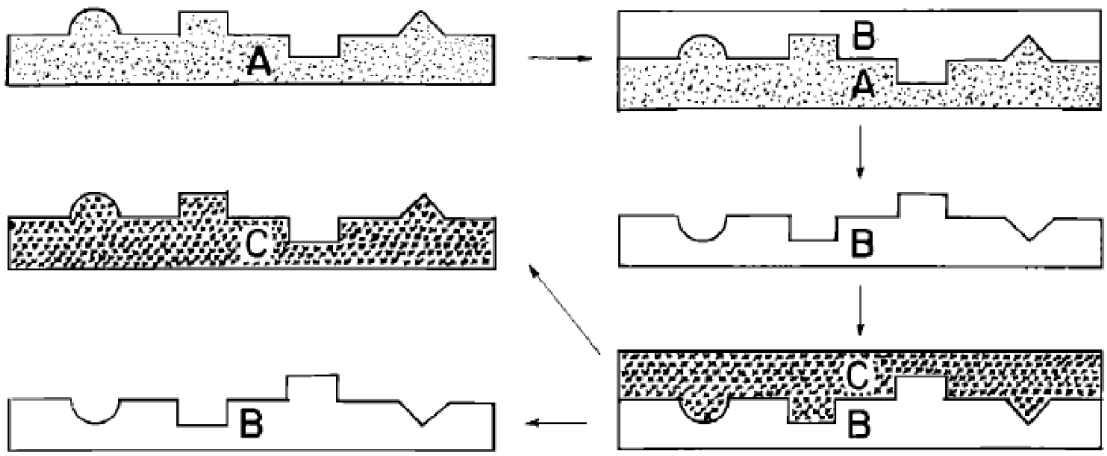

Figure 1.3: Diagrammatic representation of the replication process (Facq et. al 1962) [18].

Skin mimics can be divided in terms of fabrication materials into two major categories [18], biologically active and biologically inactive mimics or physical skin models. The first involve skin chemical composition reproduction by cell cultures in vitro, which generates close similarity of the test substrate to skin in terms of biology, chemical interactions and consistency. However, repetition between samples is difficult to achieve, there is high variance amongst fabricated biological mimics, the physical properties of the substrates are not within an acceptable range and the process cost is very high. Moreover, biologically active mimics demonstrate difficulty of use and complexity in storage [20-21]. On the other hand, physical skin models, which are replicas prepared using non-biologically active materials, exhibit high accuracy in topographic feature replication, they are usually cost effective and robust, reproducible and tunable substrates that show long term stability, high control, reliability and no ethical concerns. However, they cannot replicate the impact of substances on living cells and the absorption of materials within skin's biology, therefore, these substrates

are preferably used in studies that focus on the impact of superficial properties and not cell interactions.

Biologically inactive materials that are established in skin mimic model development, include gelatinous materials, liquid formulations, polymers, resins, metallic surfaces and textiles [18]. In the literature [22-24], gelatinous materials are used towards skin replicating samples due to their high modification abilities and significant control of the chemical and mechanical properties of the developed substrate. Further tuning of their pH, pressure and temperature enables adjustment of their capabilities towards the required specification leading to purpose made samples. Consequently, skin properties including elastic Youngs modulus, hardness and optical properties can be simulated to an advanced level. Popular materials for this approach include gelatins, agars, collagen and PVA gels.

Regarding liquid suspensions used towards skin model development, the benefits are mostly optical [25-27]. Systems incorporating lipids, polymer particles, inorganic compounds suspended to either aqueous or organic phases leading to suspension formations demonstrate light scattering properties that simulate those of skin in vivo. These systems are highly tunable and offer great manageability and reproducibility, however replication of the mechanical properties and topographical features of skin are not applicable.

One of the optimal material choices in skin mimicking are polymers, especially silicones and polyurethanes. These materials demonstrate a wide range of mechanical properties that are adjustable, allowing the production of samples of advanced mechanical precision. Also, access to a variety of polymers is easy, with global

suppliers providing great numbers of products depending the application, they are cost effective, easy to use, non-toxic and demonstrate astonishing shelf life. Silicones and more specifically polydimethylsiloxanes have been widely used in skin mimicking studies due to their affinity with human skin, low viscosity before curing that allows impregnation of the material even to the narrow furrows of skin topography, robustness and flexibility after curing. Silicone mimics demonstrate advanced morphological characteristics, accurate reproduction of the topographic features of the area and meticulous roughness simulation [28]. Amongst others, silicon mimics have been used in studies that focus on skin roughness [28-29], topography, absorption of substances [30-31], penetration [32], friction [33], etc.

Furthermore, Polyurethanes are widely employed in literature in skin mimicking projects, especially in those that focus on skin's superficial, outer properties like topography and surface energy, but also demonstrate skin-like mechanical properties, from elastic modulus to surface energy, and optical characteristics [34-39]. Their tunability, significant shelf life, ease of use and robustness, prove them an effective choice in a variety of skin research projects from friction focused studies to skin wound analysis [34-37]. An interesting use of polyurethanes in skin model development is in robotic skin tensile sensing, due to their potent simulation of human skin friction characteristics and to their wide range of mechanical properties [40-41].

Facq et. al. [19], suggested amongst others the use of replicating tapes to produce the negative replica, whereas for the positive they suggested aqueous solutions of polyvinyl alcohol, toluene softening of polystyrene films, heat casting of polystyrene and in situ polymerization of an epoxy resin.

Charkoudian et. al. [42], proposed a skin safe polydimethylsiloxane towards the fabrication of the negative mimic and introduced a biological system for the positive replica, known as model skin surface, MSS. This formulation was composed of a crosslinked protein (gelatin), a synthetic lipid-like substance (Ceraphyl GA) and adjustable amounts of water. This method allowed the production of replicas with advanced topographic features and tunable lipid to protein ratio which enabled the production of skin mimics with surface free energy and chemistry similar to actual human skin.

Goldman et. al. [43], fabricated positive replicas to study the impact of laser on the skin using SEM. They used silicon rubber for the negative mimics and several materials including silicone rubber, paraffin, wax, polyvinyl alcohol, latex rubber, alginates, plaster and acrylic resin, towards the production of the positive replica. Their goal was to achieve optimal topographic replication so that they could study skin topographic changes due to exposure of a high intensity light beam. They reported effective topographic replication with all materials tested.

Datta S. et. al. [44], fabricated mimics that demonstrate properties very similar to keratinous tissue and used them to study the effect of skin topography on the wettability of liquids. The use of alginates was proposed for the negative mimics and polyurethanes for the positive. Furthermore, they performed mechanical etching on a metal surface towards the fabrication of a substrate that exhibited human skin topographic features. The produced negative mimic demonstrated robustness, unlimited usability and shelf life due to the rigidity of the metal material. However, the low accuracy of the mechanical etching method could not achieve high levels of refinement on the micron scale topography, resulting in positive mimics that lacked

topographic accuracy. A polyurethane gloss paint, applied in layers, was the proposed material for the fabrication of the positive mimics.

Dabrowska et al. [18] presented an extensive review on materials used in the literature to replicate the physical properties of skin and the characteristics of interest that are used in skin focused studies when the use of human skin in vivo is not possible. Polymers due to their versatility and tunable properties are popular candidates in skin mimicking applications. Additionally, liquid suspensions, gelatinous materials, resins, metals and textiles are also mentioned as frequently involved in relevant projects.

Bhusan et al. [45] focused their studies on the friction forces of skin to hair or hair to hair interactions. To do so they fabricated skin mimic polyurethane films and mounted them to a flat surface on a tribometer and ran experiments against Caucasian, Asian and African hair of three levels of condition, undamaged, damaged and conditioned. They also evaluated the topography of the skin mimics and hair cuticles using AFM and stated that the produced mimics made by casting polyurethane materials on human skin polymer replicas achieved significantly relevant topography and similar surface energy compared to human skin, regarding them as an efficacious system to work with in such studies.

Fischer et al. [46] pointed out the importance of skin smoothness to the cosmetic industry and presented a study of methods towards that research on both human skin in vivo and a fabricated skin mimic, and evaluated these systems in terms of efficiency, ease of use, sensitivity and more. Their methods included SEM, surface evaluation of living cells, optical profilometry, mechanical profilometry, laser profilometry and skin visiometer. These methods are not compatible for use in vivo so the development of a

skin mimic was essential. They used a medical grade silicone with the trade name silasoft, due to its compatibility with skin and low viscosity before hardening, allowing the material to infuse within the furrows and wrinkles of the stratum corneum topography, developing enhanced topographic accuracy. The produced negative mimics where then used for smoothness evaluation.

Lagarde et al. [47] researched methods of quantitative evaluation of skin topography, to assess performance of anti-wrinkle and hydration products. They developed a negative replica to recreate a three-dimensional sample with the microstructure of human skin witch they characterized using dermatop, a system that employs interference fringe projection profilometry to generate 3-D information about the substrate including roughness, total height of surface irregularities and mean height of surface irregularities. The material chosen for the fabrication of the mimic was a skin safe silicone, used directly on human skin. The outcome was a transparent negative mimic with high topographic accuracy.

Another group of researchers, Grove et al., [48] used silicon skin replicas to study topographic characteristics of human skin and analyze the effect of tretinoin emollient cream on photodamaged skin. Mimics from the same skin area were fabricated in different time points to study the improvement of skin's topography by using a medicated cream. The replicas were fabricated using silflo silicone mixed with its curing agent and applied directly on the volunteers' cheek area. The properties evaluated were fine wrinkling, coarse wrinkling and roughness. They concluded that the emollient cream initiated and promoted skin recovery.

Yin et al., [49] performed an evaluation of skin's topography by developing volar forearm skin mimics and evaluating them with a computerized image process. The material used for the replicas was silflo silicone elastomer and the NIH image processing system was utilized for optical evaluation. Scanning of the mimics and image analysis took place using the software and the digitized images were evaluated for topographic characteristics, skin appearance, roughness and wrinkling. Their study showed that smoking greatly promoted wrinkling on skin with heavy smokers exhibiting deeper furrows and higher variance.

In conclusion, it is well established that polymers are highly popular in human skin replication studies due to the wide range of physical and mechanical properties that they demonstrate, ease of use, tunability and surface energy that can be controlled and produce mimics that highly resemble human skin in all parameters of interest [28-39].

1.2.2.2 Surface Properties

When studying human skin, or any solid surface, surface energy is a significant characterization property that needs to be evaluated. It is the surface energy that provides a great deal of information about the interaction of liquids and the surface of interest as well as its hydrophobicity/hydrophilicity. According to Fowkes [50-51], surface free energy of a solid surface is the sum of independent components which themselves are associated with specific interactions, as shown in equation 1.

$$\gamma_s = \gamma_s^d + \gamma_s^p + \gamma_s^h + \gamma_s^i + \gamma_s^{ab} + \gamma_s^o \quad (1)$$

where:

γ_s is the surface free energy

γ_s^d is the dispersive component

γ_s^p is the polar component

γ_s^h is the related to hydrogen bonds components

γ_s^i is the induction component

γ_s^{ab} is the acid-base component

γ_s^o represents all the remaining interactions

Owens and Wendt [51] later made the assumption that the sum of all interactions, except the dispersive component, could be associated with the polar component γ_s^p, and as a result the surface free energy of a solid could then be considered as a two-component number, the dispersive and the polar (or non-dispersive component).

Given the previous statements, the following equation 2, known as the Good's equation, describes the surface free energy of a solid surface in its interaction with a liquid:

$$\gamma_{sl} = \gamma_s + \gamma_l - 2\sqrt{(\gamma_s^d \gamma_l^d)} - 2\sqrt{(\gamma_s^p \gamma_l^p)} \quad (2)$$

where:

γ_{sl} is the solid surface to liquid interfacial free energy

γ_l is the surface tension of the liquid

γ_l^d is the dispersive component of the liquid's surface tension

γ_l^p is the polar component of the liquid's surface tension

and given the Young's equation 3 [52-56]:

$$\gamma_s = \gamma_{sl} + \gamma_l \cos \partial \tag{3}$$

where:

$\cos \partial$ is the contact angle between the solid surface and the liquid

the surface energy of a solid can be related with the contact angle of specific liquids using the equation 4, listed below:

$$\frac{\gamma_l (\cos \partial + 1)}{2} = \sqrt{\left(\gamma_s^d \gamma_l^d\right)} + \sqrt{\left(\gamma_s^p \gamma_l^p\right)} \tag{4}$$

Using this equation and the results from contact angle measurements of at least two liquids on a solid surface, the surface energy of a surface can be calculated. This method to calculate surface energy is popular in literature and usually referred to as the sessile drop technique. However, it is essential that one of the liquids used for the contact angle measurements must have only dispersive interactions with the surface such as diiodomethane which exhibits no polar component in its surface tension due to its molecular structure. Consequently, equation 4 is now expressed as follows:

$$\frac{\gamma_l (\cos \partial + 1)}{2} = \sqrt{\left(\gamma_s^d \gamma_l^d\right)} \tag{5}$$

and γ_s^d can now be calculated.

Using the calculated value of γ_s^d, and the contact angle measurements of the second liquid, the polar component of the solid surface can be calculated and by adding the two components the surface free energy of the solid surface since $\gamma_s = \gamma_s^d + \gamma_s^p$ [57-59].

Another well-known method to calculate surface free energy of a solid substrate is the van Oss theory, developed by Fowkes, van Oss, Good and Chaudhury [60-63], which describes the surface free energy of a solid substrate as the sum of the dispersive component or a Lifshitz van der Waals component and a polar component or Lewis acid base component that is divided in two, the acid and base components, making this method a three-component approach in calculating surface free energy. Theory states that the acid component demonstrates the dipole-dipole (or induced dipole) and/or hydrogen bond interactions of the surface and a liquid that tends to donate electrons hence exhibits base characteristics. On the other hand, the base component of the surface describes the interaction of the solid with liquids that have the potency to accept electron density hence act acidly. The following equation 6 illustrates the previous statements and the correlation of contact angle values and the three surface energy components of a solid:

$$\sigma_L(cos\theta + 1) = 2(\sigma_S^D \sigma_L^D)^{1/2} + 2(\sigma_S^+ \sigma_L^-)^{1/2} + 2(\sigma_S^- \sigma_L^+)^{1/2} \quad (6)$$

Where σ_L is the surface tension of the liquid, σ_S^D and σ_L^D the solid dispersive and liquid dispersive components respectively, θ the contact angle between the solid substrate and the applied liquid, σ_S^+, σ_S^- the acid and base components of the solid substrate and σ_L^+, σ_L^- the acid and base components of the applied liquid.

Using this equation and contact angle measurement values of three different liquids exhibiting different characteristics can be achieved. It is paramount that one of those liquids needs to exhibit no polar component, like diiodomethane so that the dispersive component can be calculated using equation 7:

$$\sigma_L(cos\theta + 1) = 2(\sigma_S^D \sigma_L^D)^{1/2} \quad (7)$$

With the substrate dispersive component calculated two further contact angle measurements need to take place to define the surface energy characteristics of the sample. One of them needs to exhibit no acid component and the other no base component so that the individual polar components can be calculated. For a liquid that demonstrates no acid component, the equation is reduced to the following equation 8:

$$\sigma_L(cos\theta + 1) = 2(\sigma_S^D \sigma_L^D)^{1/2} + 2(\sigma_S^+ \sigma_L^-)^{1/2} \quad (8)$$

Whereas the interaction of the solid substrate and a liquid that expresses no base component is described by equation 9:

$$\sigma_L(cos\theta + 1) = 2(\sigma_S^D \sigma_L^D)^{1/2} + 2(\sigma_S^- \sigma_L^+)^{1/2} \quad (9)$$

However, if no two liquids can be found that exhibit these characteristics, total surface free energy can be calculated with contact angle measurements of a liquid that has no polar component, a liquid that demonstrates either base or acid characteristics and a third liquid of no particular specifications. The initial equation and the information of the first two can lead to the calculation of the total surface free energy. This method provides surface free energy evaluation and feedback on the chemistry of the sample by generating data on the acid base components of the material, that are significant information especially in chemically heterogeneous substrates. However, due to the

three-component nature of this method, test liquids need to be chosen carefully and often compatibility issues arise between applied liquids and test surfaces making this method rather time consuming [61].

Thomsen *et* al., [55] have subsequently applied Fowkes theory while performing sessile drop experiments using a KRUSS drop shape analysis system to measure the surface energy of human skin, calculating values of 43.7 mJ/m^2 and 32.9 mJ/m^2 for the non-degreased and degreased skin, respectively.

Krawczyk J. [56] performed contact angle measurements on human skin in vivo using liquids of known surface properties like water, diiodomethane and formamide, and employed the van Oss approach for interfacial tension, to calculate in vivo human skin surface free energy. They concluded that the surface energy of non-degreased human forearm skin has a value of 44.78 ± 0.66 mJ/m^2 with a dispersive component of 38.82±0.93 mJ/m^2 and that the surface free energy of degreased human forearm skin is 36.05 ± 1.18 mJ/m^2 with a dispersive component of 34.09 ± 1.47 mJ/m^2.

Ginn et. al. carried out in vivo human skin surface energy characterization by measuring contact angles of water droplets on human forearm skin using a goniometer and obtained a value of 26.8 mJ/m^2. The skin area was degreased before performing contact angle measurements on it.

Rosenberg A. et. al. [64], have studied the wetting characteristics of numerous liquids on human skin. They employed the Zisman approach according to which the surface energy of a solid substrate is equal to the surface tension of the liquid with the surface tension that is just capable of a complete wetting of the surface which translates in a contact angle of 0° [65]. They concluded that human skin exhibits a maximum surface free energy of 37 mJ/m^2 with low polar interactions and that the hydrophobic behavior

of the skin can be attributed to the alignment of the polar groups present in keratin-A structures that are positioned against the skin air interface.

Mavon A. et. al. [66], have studied the wetting properties of human skin and correlated it with its protective abilities against chemicals, bacteria and harmful substances. They focused on surface energy values of human skin of different sebum concentrations to evaluate its effect to wettability by employing the Van Oss theory and contact angle measurements. Results showed that forearm skin demonstrates a non-polar character whereas forehead a monopolar, electron donating characteristic due to their different sebum concentration. For human forearm they presented a surface energy of 38.7±6.4 mJ/m^2 before ether treatment and 32.4±4.8 mJ/m^2 after. For human forehead 43.5±3.9 mJ/m^2 before and 34.5±4.1 mJ/m^2 after treatment.

Charkudian J.C. et. al. [42], tested their fabricated skin mimic, MSS, as far as surface energy is concerned. This was achieved by calculating contact angles of a series of liquids with known surface tension properties and then performed a critical surface tension analysis, a method developed by Zisman. The protein to lipid ratio that they used in the MSS formulation that they used for the positive replica, exhibited a surface energy of 33.4 dynes/cm. The small deviation of the mimic's surface energy to that found on literature for human skin was attributed to the absence of endogenous substances like sweat and sebum on the mimic.

Datta S., et. al. [44] have studied skin mimicking and introduced the technique of plasma coating of their produced skin mimic substrates with a monomer, to tune the mimic's surface properties and make it replicate human skin properties more accurately. The suggested coating material was 1,1,1, trimethyl pentene, as well as a

number of other hydrocarbons. To ensure that only a thin layer would be deposited, plasma deposition was decided upon. The surface energy of the mimic was evaluated using the sessile drop technique and the Fowkes theory. The human tissue values ranged from 29.60 to 37.16 mJ/m^2, whereas their replicas from 32 ± 1.0 to 45 ± 1.0 mJ/m^2, depending on the coating material.

1.2.2.3 Mechanical Properties

Human skin is a very complex organ with a lot of different variables that affect its properties including body part, sex, age, ethnicity, etc. Mechanical properties also vary significantly from skin type to skin type and hence it is challenging to attribute a single value of mechanical properties on skin. For comparison purposes though, a number of mechanical testing results on human skin will be presented in order to compare the effectiveness of the fabricated skin mimics. In this study, properties of interest, were the hardness and the Young's modulus.

In an effort to study mechanical properties of human skin in vivo, Manschot et. al. performed uniaxial tensile tests on human calf, across and along the tibial axis and found that across the axis, the maximum strain observed was 0.32, and the maximum Young's modulus was 4 MPa, whereas along the axis the maximum strain was 0.30 and the Young's modulus, 20 Mpa [67].

Agache et. al. investigated, amongst other properties, the stiffness of skin. To perform this measurement, a standard torque was applied to the dorsal forearm skin, that resulted in a rotation of 2-6◦. Following that, the Young's moduli E was evaluated for the linear part of the stress-strain curve using equation 10:

$$E=M/((2\pi \cdot 0.4 \cdot e \cdot r1 \cdot r2 \cdot \theta)) \quad (10)$$

It was concluded that the Young's modulus of human skin for the age group below 30 years old was E = 0.42 MPa and for the age group 30 and over was E = 0.85 MPa [68].

Romanelli et. al focused their research on human skin hardness evaluation using a durometer as a prognostic measure of skin disorders like lipodermatosclerosis, that has a direct impact on skin hardness. They carried out measurements using an O type durometer and concluded that normal skin exhibits a hardness of 25±5 shore O (approximately 20 Shore A) [69].

The use of polymers for the production of skin mimics covers effectively the mechanical specifications required since polymers exhibit a highly tunable character as far as their mechanical properties and they can be adjusted to match the value ranges of various human skin types.

1.3 Cosmetic Formulations

1.3.1. General About Emulsions

The term 'colloid' describes the mixture of two or more immiscible substances, and when all components of the 2-phase system are liquids, we refer to it as an emulsion. One of the liquids, the dispersed phase, is dispersed in the other, which we refer to as the continuous phase [158].

Depending on the role of the main components within an emulsion, different types can be identified. If the immiscible liquids are oil and water, a number of emulsion types can be produced given which of the two liquids will be the dispersed phase and which

the continuous. If oil assumes the role of then dispersed phase, an oil-in-water emulsion will form, whereas if the water phase becomes the dispersant, a water-in-oil emulsion will form. Apart from those types, there are more complex systems like water-in-oil-in-water emulsions, where the encapsulated in water oil droplets, also include water within them. The boundaries between the two phases are called interfaces, and in highly mixed systems, the increased interfacial area between the phases, scatters the light as it passes through the system giving to emulsions a cloudy/white appearance, however in cases of droplet sizes less than 100nm the emulsion appears translucent, because light waves can be scattered only by droplets with dimensions that are larger than a quarter of their wavelength. Given the dimensions of the droplets of the dispersed phase, the emulsions can be categorized in different groups like microemulsions and nanoemulsions. To produce a microemulsion, oil molecules are mixed with an aqueous phase together with a mixture of surfactants, co-surfactants, and co-solvents [5]. The amphiphilic surfactants are attracted by the interphases of the 2-phase system and promote stability. A microemulsion, generally requires higher surfactant concentration in comparison to a translucent nanoemulsion, however, significantly more energy and specific equipment is required for the second in order to generate droplets, in nano dimensions [158-159].

One of the most common weak points of an emulsion is its stability that is susceptible to thermal stress, pH changes and dilution. Hence, correct choice of surfactants, co-surfactants and structuring components is key to generate homogenous emulsion with long-lasting stability.

The parameters that define whether an emulsion consisting of an oil and an aqueous phase will form a water-in-oil or an oil-in-water emulsion depends on the concentrations of the two phases as well as the type of surfactant incorporated in the system. In general, according to the Bancroft rule, emulsifiers and surfactants tend to generate emulsions, with continuous phases, the ones that they dissolve easier to. For example, if a surfactant dilutes easier to water than in oil, hence has a stronger hydrophilic component, it tends to generate emulsions where the continuous phase is the aqueous [158-160].

1.3.1 General about Cosmetic Formulations

Cosmetic product formulations have been concurrently a topic of extensive research and applications [1-3, 70-76]. However, none of these studies have focused on the characterization and understanding of retention of selective actives from cosmetic emulsions on human skin, as well as an optimization of skin bio mimics for such purposes and generation of a method that studies this subject. For the scope of this project, a representative cosmetic emulsion has been fabricated as a model system to study the retention processes on the optimized skin mimics, consisting of water, anionic surfactants, stabilizing fatty acids and an oil phase as a moisturizing active. Three oil phases were tested with a range of viscosities, mineral oil, sunflower oil and petrolatum. Table 1.1 demonstrates a detailed example of the model system emulsions fabricated

Table 1.1: Model system formulations example. three different oils were used, mineral oil, sunflower oil and petrolatum, to study the impact of oil viscosity in retention. Moreover, formulations of three levels of oil phase concentration were produced.

	Low Oil Content	Medium Oil Content	High Oil Content
Water	60%	40%	20%
Anionic (Surfactant SDBS)	10%	10%	10%
Fatty acids (Lauric Acid)	10%	10%	10%
Oil Phase	20%	40%	60%

Petrolatum is still considered one of the most effective moisturizing actives in the cosmetic industry, [71, 77-78] known for its occlusive, film making, capabilities upon application that seals the skin and prevents trans-epidermal water loss [71]. This is a typical example of a skin cleaning formulation that also exhibits mild conditioning properties.

Skin care products can be divided into numerous categories depending on their purpose and method of use. Common products include cleansers, moisturizers, powders, sprays, creams and lotions. In the first category we can find most body wash products that are mainly used for their cleaning abilities. These products target soil and dirt as well as sweat and lipids from the skin, encapsulate them within their structure, and later remove them from skin during rinsing with water. Therefore, they incorporate strong anionic surfactants that demonstrate high foaming and cleaning efficiency. There are other types of cleansers in the form of lotions that can be applied using a cotton pad and mechanical shear, that operate with the same principles as body wash formulations, however they do not generate foam or require rinsing off after use. These products usually incorporate nonionic surfactants that are mild on the skin, and do not

require rinsing. Moisturizers are products that incorporate a moisturizing agent within their formulation. Depending on the type of the active the moisturization of skin can take place following different mechanisms, as we will demonstrate in the following chapters. There are two main types of actives, those that carry water to the skin enabling hydration, e.g. glycerin, hydrated humectants, etc., and those that create an occlusive layer on the skin, blocking trans-epidermal water loss and hydrate the external layers, e.g. petrolatum, oils, film forming polymers, cationic surfactants, etc [79-81].

1.3.3 Surfactants

The word surfactant comes from the term surface active agent and is defined as a material that can reduce the surface tension between a liquid-liquid, a gas-liquid or a solid-liquid interface, and hence enable mixing of otherwise immiscible substances [1, 152-153]. Their remarkable abilities derive from the nature of their chemical structure which involves a hydrophobic long chain group, the tail, and a hydrophilic component, the head, enabling the molecule to exhibit both hydrophilic and hydrophobic characteristics, an ability described as amphiphilic [82-83]. It is well known in literature [84-86] that surfactants can be used to alter the microstructure of the bulk they are incorporated into by interacting with each other or with other ingredients within the system, like fatty acids/ alcohols, co-polymers, etc. Depending on the concentration of surfactant, different structures/phases can be formed. In low concentrations surfactants remain in their monomer form and tend to bind to the interfaces of the bulk with air or the container surface. By increasing the concentration of the surfactant after

a characteristic for each surfactant value, the first micelle will form. A micelle is the simplest form of aggregation, usually spherical, and its size depends on the molecular structure of the surfactant. Micelle formation is driven by the urge of hydrophobic tails to avoid interaction with water, hence forming a spherical structure with hydrophilic heads in contact with water in the outer surface of the micelle and the hydrophobic tails within the aggregate, leading to a lower energetic level of the system. Every surfactant is characterized by a Critical Micelle Concentration, CMC, which describes the minimum concentration of surfactant required for the first micelle to be formed. CMC is usually used as an indication of the effectiveness of a surfactant for its cleaning abilities, given that higher CMCs enable higher concentrations of free monomers within the bulk before aggregating into micelles and those active monomers are those that target foreign matter and remove them from where they are deposited. Usually anionic surfactants exhibit higher values of CMC and hence exhibit enhanced cleaning abilities but also higher levels of skin irritation [82-83]. In Figure 1.4, the stages of surfactant dilution within a bulk and the formation of the first micelle at critical micelle concentration are illustrated.

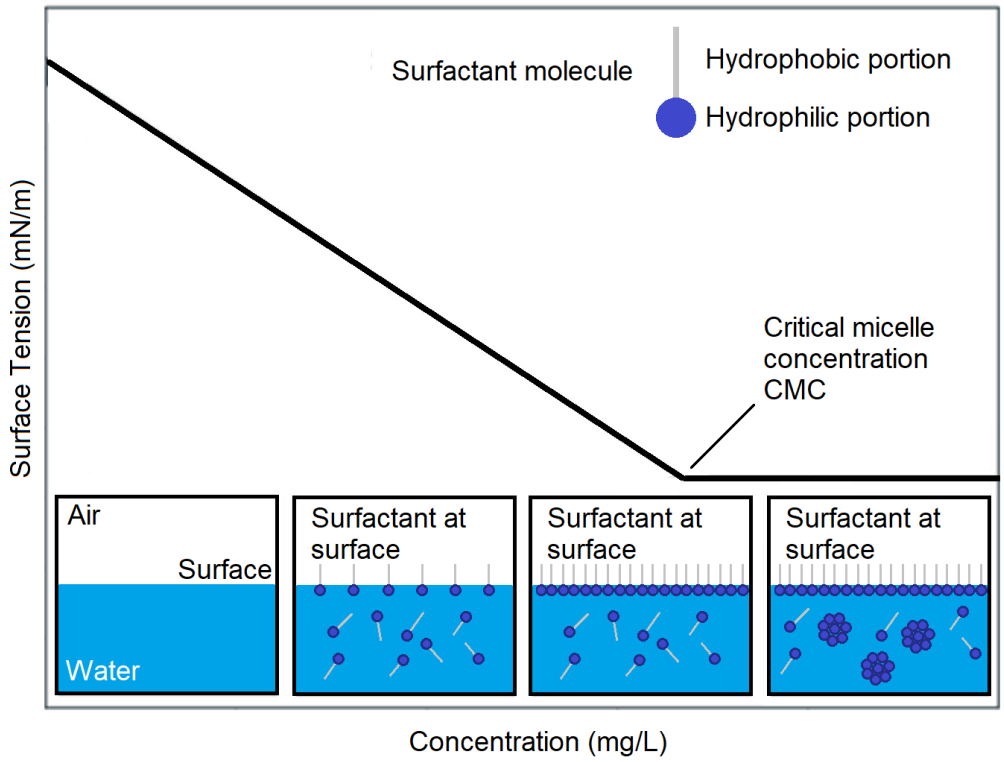

Figure 1.4: The different structures that surfactants assume depending on the concentration levels within a bulk, including micelle formation at concentrations higher than the CMC.

Due to the nature of their chemical structure, surfactants tend to occupy surfaces or interfaces of the system that they are incorporated in. When surfactants reach those boarders, of the otherwise immiscible materials, their structure is aligned so that the hydrophilic end is facing the aqueous phase and the hydrophobic part attaches to the non-water material. This way the interfacial surface free energy of the system is reduced. Surface free energy, in these systems, expresses the work required to create or expand the surface of a material against another phase. This term is mostly used in the case of solid surfaces against air whereas in the case of the adjacent phase being another, non-air material we use the term interfacial energy of the two phases. It is well known that molecules on the interfacial areas of a phase demonstrate higher energy

levels in comparison to molecules within the bulk, otherwise the material would tend to create surfaces to reach a lower energetic state. Hence the energy required to transfer molecules from the bulk of a phase to the interfacial areas is the work required to form this interface. That energy per unit of area is the measurable property known as interfacial tension between the two phases. Every liquid material exhibits a value of surface tension which describes the interfacial tension of that liquid against air and gives us information about its nature. The greater the dissimilarity in surface tension between two materials the larger their interfacial tension will be which translates in larger amounts of work required to create an interface between the two [82-84].

Now that the terms surface free energy, surface tension and interfacial tension are explained it is straightforward to comprehend the impact of surfactant molecules in lowering the interfacial tension between phases. Here we present the example of a vegetable oil, like castor oil, in water mixture, two renowned immiscible liquids. Castor oil demonstrates a surface tension of 39.00 mN/m at 20°C [87-90], whereas water demonstrates 72.75 at 20°C [91]. The difference in these values predicts the energy required to mix these two phases and create a higher interfacial area between the two. However, due to the difference in nature of those liquids and their high interfacial tension, in time after mixing, they will separate again creating two distinct phases. If a surfactant is then added to the system, its molecules will proceed to those interfaces and align their structure so that the hydrophobic part binds to the oily phase and the hydrophilic part to the aqueous phase and hence the interfacial tension is significantly reduced due to the chemical structure of the surfactant. Mixing the system increases the oil-water interfacial area with less energy required and stability through time due to the presence of surfactant. In the case of a single phase system of a beaker filled with

water, the addition of a surfactant would cause a reaction of the hydrophobic part of the surfactant molecules with water and the first would be expelled to the interfaces of the system either with air or the beaker walls facing away from the water. This amphipathic nature of the surfactant is what drives their molecules to attach to interfaces and prove useful materials in the cleaning industry [82-84].

Surfactants can be classified depending on the nature of the hydrophilic group. Anionic surfactants exhibit negative charge of the hydrophilic head and are well known for their cleaning and foaming abilities as well as harshness on skin and hair that can lead to irritation. Well known examples of these are sulphates, sulfonates, phosphates, carboxylates, etc. Common anionic surfactants include sodium lauryl sulphate, sodium laureth sulphate, and sodium dodecylbenzensulphonate, frequently used in cleansers for their foaming and cleaning capabilities. In surfaces that exhibit positive charge, the negatively charged head group of the surfactant is attracted by the charge of the surface and binds to it, driven by electrostatic forces, leaving the hydrophobic tail facing away from it hence promoting the hydrophobic nature of the system [84, 86, 92]. In Figure 1.5, the molecular structure of common anionic surfactants is illustrated.

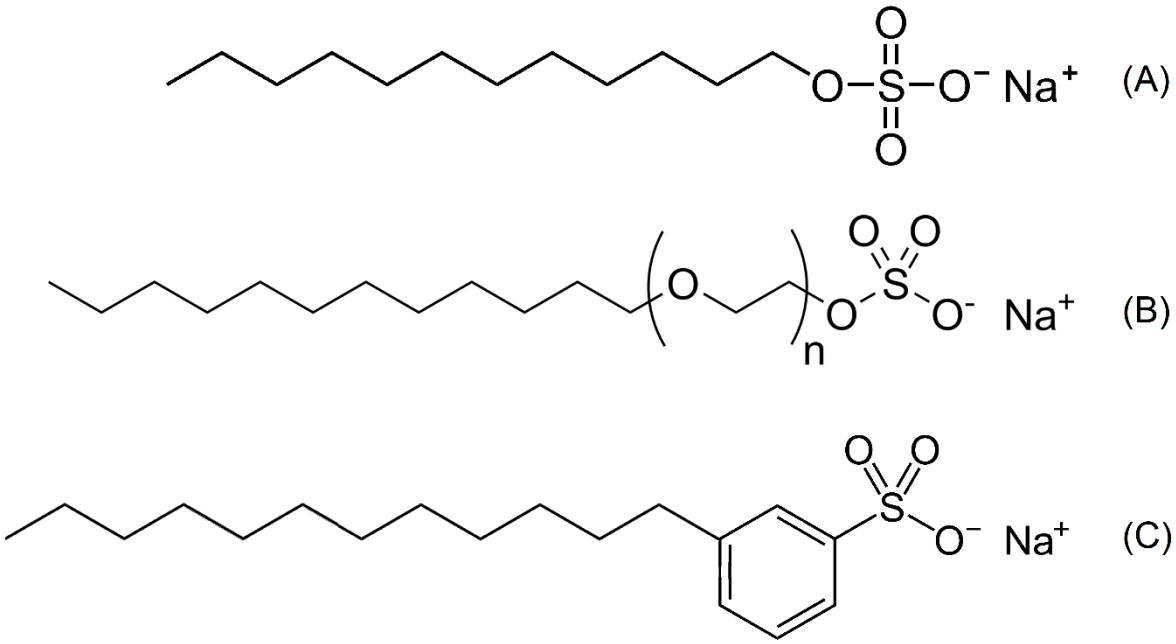

Figure 1.5: (A) SLS, (B) SLES and (C) SDBS chemical structure. In the SLES molecule, the ethoxylation group that makes it significantly less irritant against skin than SLS is illustrated. SDBS has an aromatic Benzene component in its molecule, also making it less irritant and milder on skin in comparison to SLS.

Cationic surfactant molecules demonstrate positively charged hydrophilic groups which are significantly milder and provide outstanding deposition properties on skin and hair, given that they are negatively charged resulting in electrostatic attraction between them and the cationic surfactants. Common examples are quaternary ammonium compounds like Behentrimonium chloride and Cetrimonium chloride. Interaction of a cationic surfactant with negatively charged surfaces induces hydrophobicity of the system. Interaction of cationic materials, with human skin and hair, is commonly used in cosmetic technology to promote deposition and/or coating by products [84-86]. The following Figure is an illustration of two common cationic surfactants, Behentrimonium chloride and cetrimonium chloride.

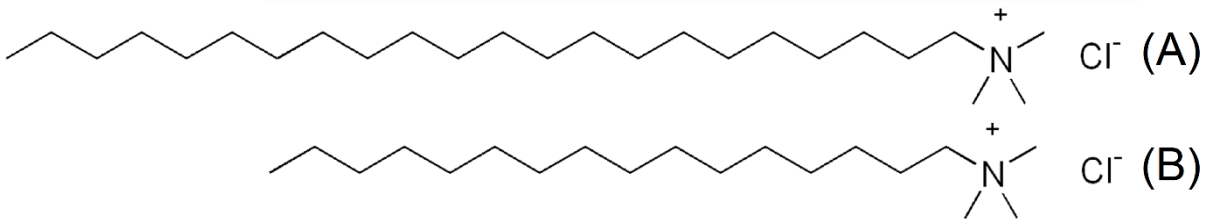

Figure 1.6: (A) Behentrimonium chloride chemical structure and (B) cetrimonium Chloride structure, a C25 and a C19 analogue structure cationic surfactants commonly used for their conditioning properties in cosmetic formulations.

Amphoteric surfactants are materials that exhibit both anionic and cationic behavior depending on the system properties they are incorporated into, the pH, the presence of co-surfactants, etc. Anionic properties usually derive from incorporated sulfonates in their structure whereas the cationic properties from amines or quaternary ammonium components. Furthermore, Cocamidopropyl hydroxysultaine, CAHS is commonly used in cosmetology as an amphoteric surfactant, known for its foam boosting properties and conditioning effect. Figure 1.7 illustrates its chemical structure where both the anionic and cationic components can be seen.

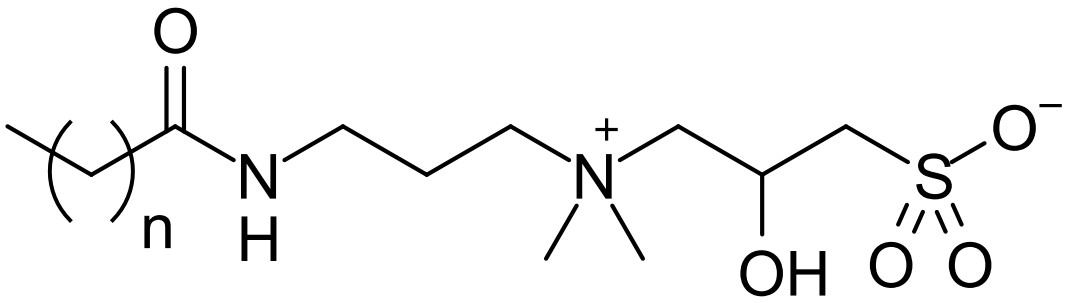

Figure 1.7: Chemical structure of Cocamidopropyl hydroxylamine (CAHS), a well-established amphoteric surfactant, known for its conditioning and foam boosting capabilities. The amine component is responsible for the cationic behavior of this substance whereas the sulphonate component for the anionic.

Lastly, the nonionic surfactants, that exhibit no charge in the hydrophilic part of their structure and are relatively non-toxic [154]. The lack of charge makes them mild surfactants, suitable for emulsification processes in lotions and in the food industry. However, due to their poor foaming capabilities they are not used as the main surfactant in cleansing products where foam generation is essential. Their hydrophilic properties are attributed to groups that contain oxygen which enable their molecule to perform hydrogen bonding and hence be water soluble. Nonionic surfactants are less affected by water hardness than anionic surfactants and keep performing even in higher $CaCO^3$ concentrations. Given that they show no charge, they bind to surfaces depending on the hydrophobic-hydrophilic nature of the surface. Common nonionic surfactant categories include ethoxylates, alkylphenol ethoxylates, fatty acid ethoxylates, ethoxylated esters, amines, fatty acid amides, fatty acid esters, glycerol, sorbitol, sucrose, amine oxides, sulfoxides and phosphine oxides, etc. Commonly used nonionic surfactants in the cosmetic industry include tween 20, 40, 60 and 80 that belong to the group of fatty acid esters and demonstrate great emulsification properties and mildness to skin and hair [85-86, 93]. Figure 1.8 shows the molecular structure of polysorbate 20.

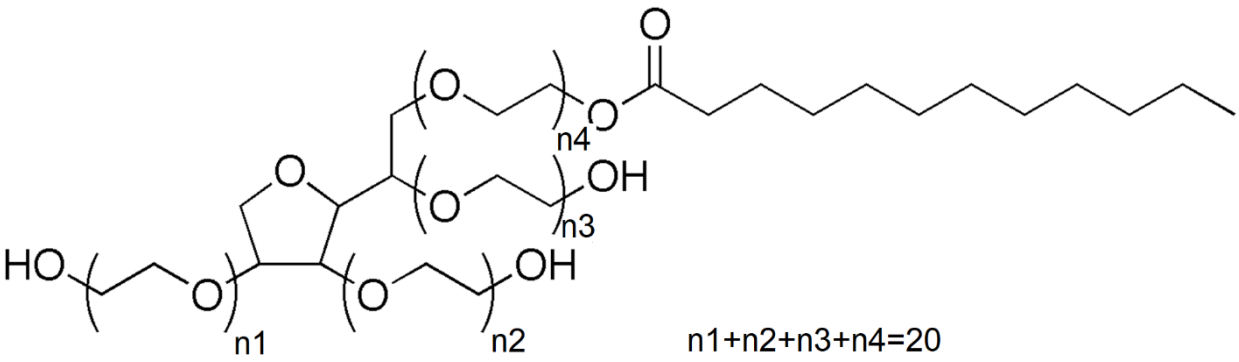

Figure 1.8: Chemical structure of the polysorbate 20 molecule, widely used in cosmetic formulations as the non-ionic surfactant.

The investigation of the self-assembly of surfactants within solutions is a widely studied subject in literature. The shape of the structures formed by surfactants, significantly influences the properties and behaviour of the surfactant within the solution and can affect properties including their solubilization capacity for hydrophobic materials, their viscosity and viscoelastic properties, their performance, foaming capabilities, interfacial properties, etc. The two approaches in studying the aggregations formed by surfactants, are the theoretical and the experimental approach and each can be used depending on the complexity of the system and the information we have about the amphiphilic molecule and structure of the surfactant [154-155].

Depending on the application, a specific surfactant structure might be required, like spherical, globular, rod-like micelles, bilayer, vesicles, etc. To achieve the desired structure, it is essential to choose a surfactant with a molecular geometry that enables the assembly of such geometries. The type and shape of these three-dimensional structures is determined by shape of the surfactant molecule and the concentration of it. Israelachvili, Mitchel and Ninham were the first to introduce the notion of packing parameter. They demonstrated the methodology that enables the prediction of the size, shape and structure of surfactant aggregations, when the molecular packing parameter of the amphiphilic molecule of interest and general thermodynamic principles are known. The critical packing parameter (p) is calculated by the following equation:

$$p=va_0l \tag{11}$$

Where:

v represents the volume of the hydrophobic tail of the surfactant,

a_0 is the area assumed by the hydrophilic head,

l the length of the hydrophobic tail

The value of the critical packing parameter together with the surfactant concentration within the formulation can be used for the estimation of the shape/type of the self-assembled aggregations formed be the molecules of the surfactant. It is generally speculated that surfactants with packing parameters within the range of $0<p<1/3$ lead to the formation of spherical micelles within a solution. Furthermore, surfactants with packing parameters between $1/3<p<1/2$, lead to the formation of rod-like shape or hexagonal aggregations. Higher packing parameter values within the range $½<p<1$, indicate a balance between the hydrophilic head group area and the hydrophobic tail volume and as a result the surfactant molecules tend to assume a plane structure in the form of sheets, bi-layers or vesicles. For surfactants with critical packing parameters higher than 1, the assemble of inverted micelles is expected. The following image, demonstrates the correlation of the critical packing parameter value and the predicted structure of the formed surfactant aggregations [154-157].

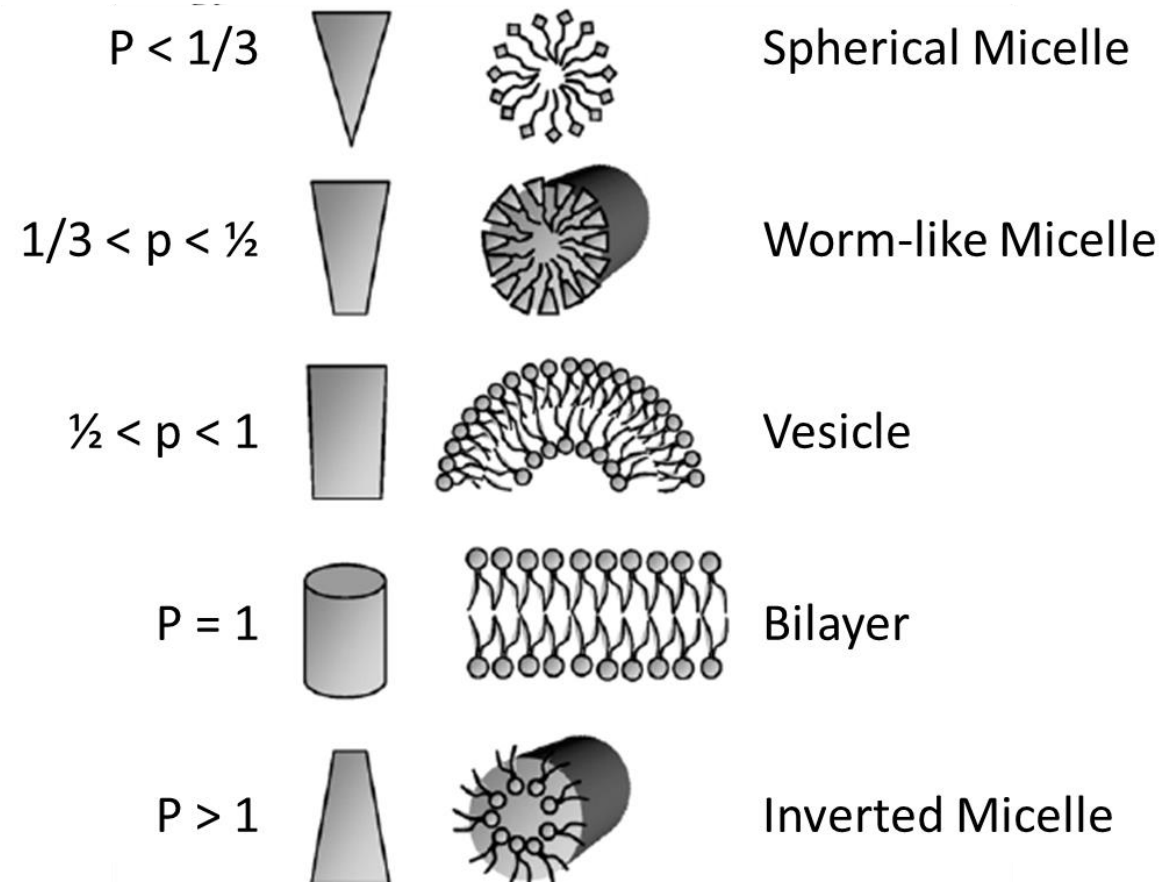

Figure 1.9: Packing parameter in correlation to the molecular structure of the surfactant and the aggregation type prediction.

The above speculations regarding the correlation of the critical packing parameter and the shape and type of aggregations as well as other features of them are based on the molecular characteristics of the amphiphilic component, like the area assumed by the hydrophilic head, a, the length of the hydrophobic tail, l, and the volume of the hydrophobic tail of the surfactant, v. These methodologies that define aggregation shape prediction by calculating the molecular packing parameter is a concept widely cited in literature in various disciplines including biology, chemistry and physics.

If we assume a spherical micelle that consists of g number of molecules and has a core diameter R, then the volume of then core V, can be calculated by the general geometrical relation

$$V=gv=4\pi R^3/3 \quad (12)$$

Where ‘V’ is the core volume of the aggregation, ‘g’ the number of molecules that the aggregate consists of, ‘R’ the radius of the aggregation and ‘v’ the volume of the hydrophobic tail of the surfactant. Also, the surface of the micelle ‘A’, can be calculated from the equation

$$A = ga= 4\ \pi R^2 \quad (13)$$

Where ‘a’ is the area assumed by the hydrophobic head

Combining these two equations the radius of the aggregation can be calculated by the following:

$$R = 3v_o/a \quad (14)$$

Assuming a spherical micelle where the molecules of the surfactant are packed with no empty space between them, the radius R cannot exceed the length of the hydrophobic tail lo. Hence for spherical micelles the value v_o/al_o needs to be within the range from 0 to 1/3. In a similar way, the radius of other types of aggregations can be expressed as a function of the surfactant molecule characteristic values, v,a and l. Table 1.2 demonstrates the equations that define the parameters of the aggregations. The only assumption here is that the radius cannot exceed the length of the hydrophobic tail lo. Using these equations, the defined ranges of packing parameter

that are used to predict the shape of the self-assembly surfactant structures are calculated.

Table 1.2: Geometrical Relations for Spherical, Cylindrical, and Bilayer Aggregates

variable	sphere	cylinder	bilayer
volume of core $V = gv_o$	$4\pi R^3/3$	πR^2	$2R$
surface area of core $A = ga$	$4\pi R^2$	$2\pi R$	2
area per molecule a	$3v_o/R$	$2v_o/R$	v_o/R
packing parameter v_o/al_o	$v_o/al_o \leq {}^1/_3$	$v_o/al_o \leq 1/2$	$v_o/al_o \leq 1$

The Critical packing parameter is considered a powerful tool in designing surfactants and in predicting the self-assembled aggregations of the amphiphilic molecules within a solution. However, these predictions are hypothetical and based on geometrical estimations of the molecular structure of the formed aggregations. in other words, complex systems, with components including co-surfactants, structuring components, particles, etc, might require an empirical approach for the more accurate estimation of the form and shape of the surfactant structures [157].

1.3.4 Effect of Surfactants on Skin

Cleansers in personal care are the products that aim dirt, sebum, oil and sweat removal from the skin or hair and as a result, anionic surfactants have been established as core ingredients in them due to their effective cleaning properties, foaming abilities and versatility. However, their outstanding performance may lead to complete removal of the natural oils of the skin and leave it unprotected against dryness, irritation and external pathogens. A widely used method to characterize surfactant harshness is the evaluation of trans epidermal water loss. This term describes the amount of hydration that passes from the dermis to the outer layer of epidermis and to the environment. This process is restricted by the natural lipids and sebum that human skin produces to control dehydration. By using a strong cleanser this natural barrier is interrupted, hence research has been carried out to lower the irritancy levels of these surfactants by tuning their chemistry, incorporating co-polymers, lipids to the formulation, etc. Furthermore, it is important to replace the disrupted lipid layer of the skin with conditioning actives to minimize irritation. There are numerous studies in literature that outline the need for conditioning components in cleansers due to the harshness of surfactants on skin and hair when used in their pure form [94-95].

Loffler et al. [96] tested the irritancy levels of sodium lauryl sulphate (SLS) and compared them with two popular surfactants, sodium laureth sulphate (SLES) and alkyl polyglucoside (APG). They applied surfactant patches of different concentrations for 6 to 24 hours on the back of volunteers and TEWL was monitored. The research concluded that SLS is significantly more irritant than the other two leading to increased water loss even at low times of exposure. According to literature [97], TEWL alterations is a viable indication of stratum corneum integrity and frequently used in surfactant

provoked irritation studies [97-101]. Furthermore, the regeneration time required from skin to assume normal TEWL values after treatment were higher in samples treated with SLS, not demonstrating adequate recovery even at 10 days, whereas the milder SLES and APG areas had recovered by day 7 and 3 respectively.

Agner et al. [98], studied the impact of SLS on skin, by using surfactant patches in a range of concentrations to evaluate the dose-reaction relation of SLS on normal skin. TEWL of skin treated with SLS patches was measured before and after application at 24h and 48h and was compared against that of normal skin. Skin color change was assessed using a colorimeter, blood flow was evaluated using a laser Doppler flowmeter and edema measurements using ultrasound A-scan. All applied techniques demonstrated the direct effect of SLS dose to skin irritation with higher concentrations leading to a higher irritation.

Wilhelm et al. [99], emphasized the correlation of surfactant exposure to several skin reactions. Treatment of skin with SLS containing patches took place, followed by evaluation of the area with an evaporimeter for TEWL, a Doppler flowmeter to measure blood flow increase and a tri-stimulus reflectance meter for optical evaluation of erythema. All methods provided data that prove the direct impact of SLS on human skin irritation, stratum corneum barrier deterioration and redness.

Van der Valk et al. [100], measured skin vapor loss using an evaporimeter, and then compared their findings with values of surfactant-treated skin. Surfactants used included SLS, SLES, polysorbate 60 and cocobetaine and they showed that skin treated with SLS exhibited the highest impact followed by cocobetaine, SLES and lastly polysorbate 60. The non-ionic surfactant samples demonstrated values similar to skin

treated with distilled water showing its astonishing levels of mildness in comparison to the harsh anionic surfactant SLS.

Furthermore, Charbonnier et. al. [101], studied the effect of SLS and SLES washing emulsions on dorsal skin and volar forearm in vivo. The washing emulsions used included 5% surfactant concentration and the protocol followed involved use of each model system formulation for 7 days prohibiting use of any other products. No noticeable difference was detected in the capacitance, TEWL and colour of the treated skin areas between the two surfactants. However, the squamometric analysis was sensitive enough to detect differences between the two surfactants and proved that SLS induced more damage on stratum corneum than SLES.

1.3.5 Moisturizing Agents

As mentioned before, trans epidermal water loss is a constant process of human skin, that the organism regulates by discharging natural lipids, oil and sebum, and physically restraining water loss by forming occlusive layers. Both the cosmetic and medical sector have carried out significant research on regimes to control excessive TEWL, which can result in dry skin, rigidity of the stratum corneum, psoriasis, xerosis, atopic dermatitis, rushes, ichthyosis, etc. due to defective epidermal barrier function. The use of moisturizing products that replenish the lipid concentration of the stratum corneum or attract hydration is a widely suggested proposition in literature to maintain TEWL levels. Moisturizers can be divided into four main groups, the film forming materials or occlusives, emollients, rejuvenators and humectants [102-103].

The first category, the occlusives, achieve skin conditioning by forming epicutaneous, occlusive films and blocking physically the corneocyte openings, maintaining high hydration levels to the outer layers of the skin. Their exogenous barrier mechanism, that restricts water evaporation from the cutaneous layers, makes them especially effective when the skin is already moistened [104]. The type and portion of the substance applied determines the effectiveness of film formation and the restriction of TEWL. Typically, a moderately thick layer of petrolatum of approximately 3mg/cm^2, reduces trans epidermal water loss by 50-75% whereas other moisturizers demonstrate lower performance [105-106]. Petrolatum is a well-established moisturizer due to its occlusive capabilities, affinity to the skin, ease of use, availability and low price making it the second most commonly used active agent in the industry of personal care products after water [104]. It is speculated that petrolatum has a positive impact on the epidermal barrier function of the skin by penetrating the stratum corneum and inducing intercellular lipid and fatty acid regeneration [107]. Furthermore, petrolatum is also classified as an emollient, meaning that it can occupy the gaps and fissures of stratum corneum, providing smoother texture and anti-wrinkle/fine line reduction. Dimethicone is another commonly used effective occlusive, from the family of silicones, which demonstrates prominent compatibility with skin, hypoallergic behavior, and enables skin hydration. Also, it allows improved skin oxygenation and a lighter feel by not plugging the pores. Use of occlusives has showed significant advantages in promoting the normal epidermal barrier function, however, use of these materials is usually accompanied with sensorial drawbacks like greasiness and feel of discomfort caused by skin pore blockage. Other well-known substances in this

category include mineral oil, cetyl alcohol, isopropyl palmitate, liquid paraffin, polyethylene glycols, silicones, stearyl alcohol, etc. [94-95, 102-103, 108].

Figure 1.10: Some of the first commercially available petrolatum products from the company that started it all ‘Vaseline’. The founder of Vaseline, Robert Augustus Chesebrough, was the one who discovered petroleum jelly, worked in depth on optimizing its refinement and purification process and studied its multiple benefits on skin that include wound and burn healing acceleration, medical benefits against skin conditions like eczema and dryness and lastly in cosmetics as an effective moisturizer [109].

The second group, the emollients, function very similarly to the occlusives and target texture improvement of skin by covering abnormalities, gaps, fine lines, wrinkles and roughness in the topography of the epidermis. Well established emollients include natural oils like castor oil, cocoa butter, olive oil, sunflower oil, shea butter, propylene glycol, silicones, petrolatum, etc. Natural oils are potent emollients due to their high concentration in fatty acids that are known to stabilize skin physiology and promote intracellular fatty acid regeneration.

The rejuvenators are generally a small category of materials that claim skin reconstruction and texture improvement by providing depleted proteins that are

essential for skin health. Rejuvenators are usually incorporated in anti-wrinkle and anti-age products. However, their effectiveness is questionable due to the significant dimensions of proteins making absorption and penetration of the stratum corneum challenging. Well established rejuvenators include collagen, keratin, elastin, etc. [110].

Humectants are substances usually exhibiting hygroscopic properties, meaning that they attract moisture from their environment. This is attributed to hydroxyl groups of hydrophilic character in their chemical structure, that bond with water molecules. Within a cosmetic emulsion, humectants hydrate and when applied onto the skin they maintain moisture in the stratum corneum, improving its properties and recovering its hydration levels. Furthermore, by occupying the external layer of the stratum corneum, these substances induce the transfer of water from the deeper layers of the skin to the epidermis, resulting in effective hydration. However, this effect might result in increased water loss through evaporation of the retrieved aqueous amounts, therefore it is generally suggested to accompany humectants with an occlusive ingredient [111]. Well established humectants include glycerin, aloe Vera, ammonium lactate, gelatin, hyaluronic acid, urea, etc.

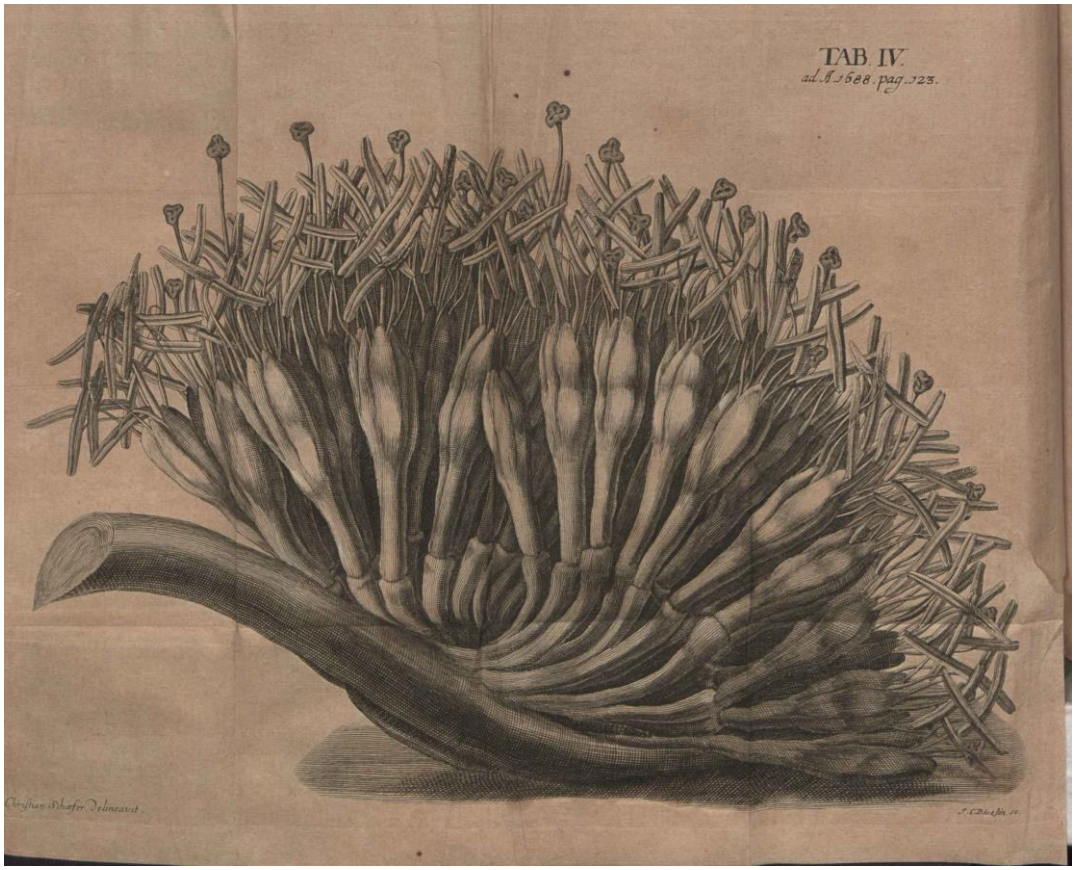

Figure 1.11: Illustration of Aloe Vera from 1688. Aloe Vera gel is a widely used natural humectant in multiple applications mostly cosmetic for its moisturizing capabilities [112].

When incorporating both a humectant and an occlusive in a moisturizing product, effective hydration is provided to the skin under a protective film that is covering texture imperfections and trapping moisture in the outer layer [102]. Humectants on the other hand, have been found to reduce the size of the superficial cells that occupy the interface between the epidermis and the product with the stratum corneum assuming a more compact texture with improved barrier function, which is attributed to osmosis forces driven by the hygroscopic character of humectants [77, 113].

Held E. et.al., have studied the impact of various moisturizers of different lipid content to the treatment of skin irritated by SLS. Therefore, forearm skin was treated with 0.5%

SLS infused patches followed by moisturizer applications 3 times a day for 5 days and then was evaluated for TEWL, electrical capacitance, laser Doppler flowmetry, Derma Spectrometry and clinical scoring. This project concluded that there is a direct relation between lipid concentration of moisturizers and skin barrier function recovery. High lipid content products demonstrated better regeneration of epidermal skin barrier function, even early in the treatment process. Petrolatum demonstrated outstanding skin conditioning capabilities and barrier function regeneration that outperformed even more sophisticated moisturizing systems [114].

Loden M. et.al., demonstrated the effects of urea-based moisturizers on barrier properties of normal skin, by treating forearm skin for 20 days, using two urea-based products, as well as other commercially available moisturizing products followed by treatment with SLS infused patches. Visual evaluation, evaporimeter and laser Doppler flowmeter measurements took place to estimate irritation levels and urea-based emulsions showed significant increase in skin electrical capacitance which translates to higher moisturization levels. All tested products exhibited reduction in TEWL, improved skin barrier capabilities and irritation inhibition even against the irritant SLS [115].

Buraczewska I. et.al. [116], focused their study on skin barrier function changes following long-term treatment with three moisturizing emulsions, a cream, a lipid free gel and a 5% urea cream. Methods of characterization included TEWL measurements, blood flow, skin capacitance evaluation, and visual assessment of the samples. Also, irritancy potential of SLS infused patches for 24h exposure was tested. They concluded that long term exposure of the cream and the lipid free gel resulted in an increase in TEWL meaning that the barrier function of the skin deteriorated accompanied by

increased SLS susceptibility. However, the urea-based cream demonstrated beneficial effects on skin, reducing TEWL and minimizing irritancy levels from SLS exposure.

Ghadially et. al. [77], studied the capabilities of petrolatum as an occlusive ointment related to stratum corneum barrier recovery following a controlled perturbation of it. Human forearm was artificially disrupted by treating the area with acetone solution and the samples were evaluated as for their TEWL using the evaporemeter and an electrolytic water analyzer. Results showed that Vaseline treatment accelerated skin barrier function recovery as soon as the first 3 hours after barrier disruption. After 72 hours from acetone treatment, no significant differences between Vaseline treated and untreated were observed.

1.4 Shower Habits and Conditions

Showering is a complex procedure with numerous parameters contributing to the process and affecting product performance. Water temperature, flow rate and mechanical shear are the profound variables that contribute to the process and overall experience. Consumer habits make these parameters vary significantly, however, there are regulations usually set by the government or a national health institution that provide guidelines for a safe shower experience and accident prevention. These guidelines are directed only to water temperature and flow rate. It is reasonable to speculate that higher values of shear and water flow rate inhibit active retention on human skin, and higher water temperature results in increased solubility of materials within rinsing water that could potentially result in reduced amounts of retained substances.

The UK Government Department for Environment, Food and Rural Affairs, has published standards for showers, taps, toilets and urinals where they state the mandatory levels of water usage should not exceed flowrates of 6 liters/min for showerheads [117].

In 2007, the UK government published a leaflet with information on shower flowrates and new showerhead technologies to minimize water use. They stated that 8-10 liters per minute, which is the UK mandatory limit, provides sufficient flow rate for consumer satisfaction. They also suggested new showerhead homologations like the aerating showerhead that mixes water with pressurized air before output to provide more efficient flow from flowrates as low as 6 l/min [118].

The energy saver department of the USA federal government published the mandatory changes on households towards reduction of hot water use for energy savings. They stated that all household shower heads should operate to a maximum flowrate of 9.5 liters per minute [119].

The New York City plumbing and administrative code published maximum flow rate limits for showers taps and urinals and suggested ways to reduce water usage to maintain water supplies and reduce the risk of droughts. According to them, modern showerheads should not operate at flowrates higher than 7.5 lpm at 80psi of pressure [120].

Governments have regulated safe temperatures for water in contact with skin during showering and have published health and safety guidelines and requirements to ensure safe conditions and avoid skin burns and accidents during showers. The UK government has published temperature regulations for water in showers stating that

no household should have showerheads operating at temperatures higher than 44°C [121-122]. US government regulations restrict water temperature for showers in most states to a maximum of 49°C. Canadian anti-scald codes and regulations suggest a maximum water temperature of 49°C for shower use. Whereas the French and Australian governments restrict water temperature to 50°C [123].

1.5 Design of Experiments and Modelling

Design of experiments, DoE, is a well-known approach to studies that involve a significant number of experimental components and levels, making a full factorial approach rather cost and time ineffective. It was initially introduced by Fischer in 1958 and used widely in agriculture and other sectors soon after [124-126]. Data generation is achieved by employing experimental design, performing limited experiments and using statistical tools to produce information as a full factorial approach would achieve. Full factorial approach is the plan of experiments that involves changing one separate factor at a time or as it is also known in literature with the term ‘COST’, and although it is a natural choice for most researchers, it is not as effective in terms of time and resources required. Furthermore, using the DoE approach the statistical analysis of the generated data allows the evaluation of the experimental factors chosen, by demonstrating their impact to the tested value. In time limited projects, statistical design of experiments allows the generation of valuable information on the system tested and enables crucial guidance to future researchers on the parameters of interest and focus.

The DoE approach in a study requires the employment of statistical tools. DoE packages that are available and usually tailored to specific applications with popular product names including Umetrics, JMP, gPROMS, statease, etc. For this project, JMP was used. To run a DoE approach necessary steps must be followed. Initially, it is crucial to identify the experimental factors of interest and their levels. It is important for the selected factors to have a great impact on the measurable outcome so that they benefit the created statistical model and promote the understanding of the study. The second step is to decide the experiment plan, combination of factors and levels and number of experiments that need to be carried out. This is usually generated by the statistical software that provides the design matrix/plan of experiments and the expected accuracy given the goal set by the researcher. The design choice is a compromise between the accuracy of the information required and the number of experiments that need to be performed. The experiments need to be performed following the order suggested by the matrix and ensuring repeatability throughout the process. Following, the results are used to generate a statistical model, using a statistical tool, generating plots that offer information including impact of factors, fitting of the model, accuracy, etc. Lastly, the significant step of investigating results, drawing conclusions, evaluating factor impact, level choice and redesigning the experiment if required [126]. The term ‘factor’, describes the control parameters of the experiment that exhibit either quantitative or qualitative values and that the researcher manipulates to evaluate their effect on the studied property. ‘Response’, describes the measurable property of the study, in other words the outcome of the process interaction, which describes the dependency of two or more factors with each other, something that usually needs to be kept at a minimum. ‘Confounding’, describes effects that derive

from factor interactions and cannot be evaluated by themselves. Finally, ‘resolution’, which describes the levels of confounding. Generally, minimum values of confounding enable high resolution.

Heather Tye et. al., [126] have used DoE to study drug discovery and focused on the benefits of designing the matrix of experiments from developing the chemical process to performing a fraction factorial design in discovering chemical, biological, analytical and purification applications. They concluded that the employment of statistical tools allowed an easier screening of the factors involved in the study and evaluation of their impact on the target response, hence allowing effective research that is target oriented and time efficient.

Brynn Hibbert et al., [127] pointed out the benefits of experimental design in chromatography, stating that it enables high effectiveness in data generation and information retrieved from time limited projects. Additionally, they displayed the benefits of a fraction factorial approach to a full factorial in chromatography, with the first allowing effective factor screening, model optimization and inclusion of a significantly greater number of factors and levels leading to optimal fit of the model generated. They also demonstrated the importance of randomization of the order of experiments to eliminate the effect of uncontrolled factors and ensure repeatability and minimum error.

Bieke Dejaegher et. al., [128] defined the experimental design as the simultaneous evaluation of several factors and their levels in the form of a predefined number and order of experiments. Furthermore, they focused on the process optimization part of this approach, explaining that optimization can be divided by screening of the factors

to evaluate the impact of each independent factor to the response, and then the optimization phase where the factors that show the highest influence in the target value are further exploited to enhance the response.

Luciana Vera Candioti et. al., [129] described the benefits of DoE in analytical processes, stating that a full factorial experimental plan can prove costly, time consuming and ineffective. Whereas the design of experiment approach can lead to optimization of analytical processes explaining that this term is referring to the improvement of the analytical process by evaluating the factors and levels at which the best response is acquired.

Riccardo Leardi, [130] carried out an extensive research on design of experiments and its benefits to chemical process optimization. They focused on all the components of DoE, and the different approaches that can be followed, pointing out the five essential steps to achieve optimization which are to define the aim of the experiments, to evaluate the factors as for their effect and their correlation, to design a plan of experiments, carry out the matrix of experiments and analyses of the data retrieved.

The goal in mechanistic understanding of a system following the DoE approach where a fraction factorial matrix of experiments has been developed, is optimization that can be achieved by applying certain statistical tools and methods to the generated data towards the production of a mathematical equation that describes the impact of experimental factors to the response and define the optimal result. One widely used method is the least squares approach which can be used to generate an equation that closely fits as accurately as possible to the experimental data and can be used later for response prediction, factor evaluation and response optimization. The least square

method belongs to statistical modelling methods, more specifically regression analysis which describes a process that estimates the impact of different variables/factors towards the generation of a model or mathematical equation that describes the relationship between the dependent variable (response) and one or more independent factors. The term residual describes the difference between the experimental value and the estimated one. The term least squares comes from the mechanism that the method employs which is to minimize the sum of squared residuals between the experimental points and the generated trendline for every mathematical equation. The least squares approach enables the production of a mathematical function that fits the experimental data as accurately as possible [131-132].

$$S = \sum_{i=1}^{n} r_i^2 \tag{15}$$

Equation 15 Describes the least square method for a model system that consist of n data pairs, where r_i is the residual of each data point to the fitted curve. To generate the model curve, polynomial regression is employed. There are many degrees of polynomial equations with the first degree being as simple as:

$$y = ax + b \tag{16}$$

and describes a linear curve that enables connection of two experimental points. The second degree is expressed in the following equation 17:

$$y = ax^2 + bx + c \tag{17}$$

and translates in an ellipsis that can correlate three experimental points. The third degree:

$$y = ax^3 + bx^2 + cx + d \tag{18}$$

That enables the accurate correlation of 4 points, etc.

Introduction of higher degree polynomial equations can lead to a better fit of the curve to the experimental data, however an excessive level of polynomials is not optimal due to the time and computational resources required to generate this function [133-134]. Additionally, data points that are questionable, or exhibit high error, might affect the curve in the case of a perfect fit approach, something that can be avoided by using simpler equations. Low order polynomials are usually smoother while providing the same level of information and understanding on the studied system. In literature, other types of approaches have been presented that use curves from trigonometric functions, Gaussian, Lorentzian, algebraic fit instead of geometric [133-135].

1.6 Thesis Outline

The aim of this research was to study and understand the drivers of retention of hydrophobic actives from cosmetic formulations on human skin during the use of an all in one cosmetic product that was designed to clean and moisturize human skin during the shower process. Our approach was to analyze this process, break it down to its fundamental components, study these separately and produce an innovative, robust and reproducible method of replicating the product use in a highly controlled way, while generating quantitative data of the retention levels of hydrophobic substances.

We assumed that the shower process and the use of a cleansing and hydrating formulation involves a skin area where the product is going to be applied, that has definite parameters of interest, including topographic features, roughness, surface energy, friction coefficient, hardness, etc. Human epidermis is a highly variable

substrate and its properties differ significantly depending on ethnicity, age, sex, environmental conditions, etc [136-140]. To achieve control of this aspect of the process we developed a skin replication technique that enabled the fabrication of optimized skin mimics, repetitively, at a low cost and with a relatively fast process that demonstrated high topographic replication accuracy, surface characteristics within a representative range to human stratum corneum, mechanical properties akin to human skin and a long shelf-life. Furthermore, we employed a significant number of characterization techniques that could accurately appraise retention.

The second element of this study was the cosmetic product or formulation and its characteristics. We targeted a cleaning formulation that provided an anionic surfactant system embodied with a hydrophobic component that served as a moisturizing agent. Complex cosmetic formulations usually incorporate a substantial number of ingredients that contribute to the stability, appearance, rheological properties, fragrance, texture and performance of the product. However, in this study, model system cosmetic emulsions were fabricated that incorporated only water, an anionic surfactant, a fatty alcohol and the oil phase to eliminate the impact of other components on the retention of the latter. In Table 1.1. the produced for this project model system formulations are demonstrated in detail. The anionic surfactant SDBS was used for its high foaming capabilities and cleaning strength while being mild to the skin [141-144]. A widely used moisturizing agent and one of the most potent and effective occlusives is petrolatum or Vaseline [145-148]. Its moisturizing capabilities are outstanding, and it is a very popular active ingredient in both cosmetology and pharmaceuticals. Consequently, it was selected as a highly viscous hydrophobic active to be incorporated in the model system formulations. Other hydrophobic actives that we tested were, the medium

viscosity sunflower oil and the low viscosity mineral oil to appreciate the impact of oil viscosity in retention. The fatty alcohol in this case serves as a co-emulsifier that interacts with the anionic surfactant towards the production of a lamellar structure, given the proper temperature and mixture energy to the formulation during production [149-151]. Additionally, the lamellar structure is known to deliver higher viscosity to the final product and shear thinning abilities that lead to improved sensorial benefits of the emulsion. For further evaluation of the retained hydrophobic active, a hydrophobic dye, pyrromethene, that is non-soluble to water and only dyed the oily phase was used, enabling the use of a fluorescent microscope and image analysis towards the evaluation of retention.

Another element is the product use during a shower, the application step, during which the cosmetic formulation is sheared against the human skin surface by applying a vertical force, to human epidermis. The conditions of this step are subjective and vary significantly amongst consumers. To maintain control and reduce the number of variables in this study, we assumed a standard force value, a standard number of cycles and speed during the application of the product while maintaining a skin on skin homologation. To control these parameters accurately a tribometer set up was modified and enabled precise, repetitive and automated application of the product to all skin mimic samples, reducing experimental error.

Lastly, the final element is the rinsing of the formulation with water to release debris, sweat, sebum, foam and formulation residues from human skin. Here, main parameters of focus are the water flow rate, the water temperature and the rinsing angle. To reduce the number of variables and simplify this process, we have assumed that the area of interest, is rinsed-off only through the showerhead and not by skin on

skin mechanical shear. We have selected the highest permitted water temperature according to government regulations and the highest possible water flow rates tested at three rinsing angles.

In conclusion, the four elements that affect retention of hydrophobic actives during product use, which are the skin mimic test substrate, the product formulation, the application method and the rinsing process, were identified, analyzed and reproduced in a controlled environment. Following, we will demonstrate the development of a method that efficiently accomplishes a series of characterization techniques and methods that enables product efficacy evaluation and retention quantitative data generation. Due to the high number of independent parameters and levels chosen, a full factorial approach took place only for the petrolatum-based emulsions. Whereas a design for experimental and a modelling approach was employed for the evaluation of the retention for all three oil model system emulsions.

1.7 References

1. Hohenstein, K. A. & Andrassy, G. Shampoo and body wash composition and method of use thereof. US6566313 B (2001).
2. Puchalski, E. & El-Menshawy, E.-S. Shampoo and bath and shower gel. US4690818 A (1986).
3. Wagner, J. & Smith, E. Mild body wash. US20050192188 A1 (2005).
4. Ertel, K., Bacon, K. R. Expanding the range of possible skin effects from moisturizing body washes. J. Am. Acad. Dermatol. 54, (2006).
5. Idson, B. Dry skin: moisturizing and emolliency. C&T 107, 69–78 (1992).
6. Marks, J. G., Miller, J. J. (Dermatologist), Lookingbill, D. P. & Lookingbill, D. P. Lookingbill and Marks' principles of dermatology. (Saunders Elsevier, 2006).
7. Proksch, E., Brandner, J. M. & Jensen, J.-M. The skin: an indispensable barrier. Exp. Dermatol. 17, 1063–1072 (2008).
8. Madison, K. C. Barrier Function of the Skin: "La Raison d'Être" of the Epidermis. J. Invest. Dermatol. 121, 231–241 (2003).
9. Grice, E. A. et al. Topographical and temporal diversity of the human skin microbiome. Science 324, 1190–2 (2009).
10. Pappas, S. Your Body Is a Wonderland ... of Bacteria. Sci. Dly. News (2009).
11. Maton, A. Human biology and health. (Prentice Hall, 1993).
12. Millington, P. F. & Wilkinson, R. Skin. (Cambridge University Press, 2009).
13. Kenneth Todar. Immune Defense against Bacterial Pathogens: Innate Immunity. (2017). Available at: http://textbookofbacteriology.net/innate_4.html. (Accessed: 26th September 2018)
14. Howard J. Bennett. Ever wondered about your skin? - The Washington Post. (2014). Available at: https://www.washingtonpost.com. (Accessed: 26th September 2018)
15. Stücker, M. et al. The cutaneous uptake of atmospheric oxygen contributes significantly to the oxygen supply of human dermis and epidermis. J. Physiol. 538, 985–994 (2002).
16. Uhlen, M. et al. Tissue-based map of the human proteome. Science 80. 347, 1260419–1260419 (2015).
17. Skin. Available at: https://web.archive.org/web/20090114060549/http://training.seer.cancer.gov/ss_module14_melanoma/images/illu_skin01.jpg. (Accessed: 26th September 2018)
18. Dąbrowska, A. K. et al. Materials used to simulate physical properties of human skin. Ski. Res. Technol. 22, 3–14 (2016).
19. Facq, J. L., Kirk, D. L., Rebell, G. A simple replica technique for the observation of human skin. Journal Soc. Cosmet. Chem. 15, 87–98 (1964).

20. Shevchenko, R. V., James, S. L. & James, S. E. A review of tissue-engineered skin bioconstructs available for skin reconstruction. J. R. Soc. Interface 7, 229–258 (2010).
21. Elliott, N. T. & Yuan, F. A Review of Three-Dimensional In Vitro Tissue Models for Drug Discovery and Transport Studies. J. Pharm. Sci. 100, 59–74 (2011).
22. Kozlov, P. V. & Burdygina, G. I. The structure and properties of solid gelatin and the principles of their modification. Polymer. 24: 651–666 (1983).
23. Glicksman, M. & Schierbaum, F. Gum Technology in the Food Industry. Starch - Stärke 23, 372–373 (1971).
24. Gómez-Guillén, M. C., Giménez, B., López-Caballero, M. E. & Montero, M. P. Functional and bioactive properties of collagen and gelatin from alternative sources: A review. Food Hydrocoll. 25, 1813–1827 (2011).
25. Hull, E. L., Nichols, M. G. & Foster, T. H. Quantitative broadband near-infrared spectroscopy of tissue-simulating phantoms containing erythrocytes. Phys. Med. Biol. 43, 3381–404 (1998).
26. Pravdin AB, Utz SR & Kochubey VI. Physical modeling of human skin optical properties using milk and erythrocytes mixtures. Proc SPIE 2627, 221–226 (1995).
27. Madsen, S. J., Patterson, M. S. & Wilson, B. C. The use of India ink as an optical absorber in tissue-simulating phantoms. Phys. Med. Biol. 37, 985–993 (1992).
28. Derler, S., Schrade, U. & Gerhardt, L.-C. Tribology of human skin and mechanical skin equivalents in contact with textiles. Wear 263, 1112–1116 (2007).
29. Gabriel, C. Tissue equivalent material for hand phantoms. Phys. Med. Biol. 52, 4205–4210 (2007).
30. Leveque, N., Raghavan, S. L., Lane, M. E. & Hadgraft, J. Use of a molecular form technique for the penetration of supersaturated solutions of salicylic acid across silicone membranes and human skin in vitro. Int. J. Pharm. 318, 49–54 (2006).
31. Khan, G. M., Frum, Y., Sarheed, O., Eccleston, G. M. & Meidan, V. M. Assessment of drug permeability distributions in two different model skins. Int. J. Pharm. 303, 81–87 (2005).
32. Shergold, O. A. & Fleck, N. A. Experimental investigation into the deep penetration of soft solids by sharp and blunt punches, with application to the piercing of skin. J. Biomech. Eng. 127, 838–48 (2005).
33. Guerra, C. & Schwartz, C. J. Development of a Synthetic Skin Simulant Platform for the Investigation of Dermal Blistering Mechanics. Tribol. Lett. 44, 223–228 (2011).
34. Bhushan, B., Wei, G. & Haddad, P. Friction and wear studies of human hair and skin. Wear 259, 1012–1021 (2005).
35. Cottenden, D. J. & Cottenden, A. M. A study of friction mechanisms between a surrogate skin (Lorica soft) and nonwoven fabrics. J. Mech. Behav. Biomed. Mater. 28, 410–426 (2013).

36. Gerhardt, L.-C., Schiller, A., Müller, B., Spencer, N. D. & Derler, S. Fabrication, Characterisation and Tribological Investigation of Artificial Skin Surface Lipid Films. Tribol. Lett. 34, 81–93 (2009).
37. Gerhardt, L.-C., Mattle, N., Schrade, G. U., Spencer, N. D. & Derler, S. Study of skin-fabric interactions of relevance to decubitus: friction and contact-pressure measurements. Ski. Res. Technol. 0, 070727080158004 (2007).
38. Bjellerup, M. Novel method for training skin flap surgery: polyurethane foam dressing used as a skin equivalent. Dermatol. Surg. 31, 1107–11 (2005).
39. Nakatani, M. et al. Relationship between perceived softness of bilayered skin models and their mechanical properties measured with a dual-sensor probe. Int. J. Cosmet. Sci. 35, 84–88 (2013).
40. Hwang, H. Y. Piezoelectric particle-reinforced polyurethane for tactile sensing robot skin. Mech. Compos. Mater. 47, 137–144 (2011).
41. KROL, P. Synthesis methods, chemical structures and phase structures of linear polyurethanes. Properties and applications of linear polyurethanes in polyurethane elastomers, copolymers and ionomers. Prog. Mater. Sci. 52, 915–1015 (2007).
42. Charkoudian John C. A model skin surface for testing adhesion to skin. J. Soc. Cosmet. Chem. 39, 225–234 (1988).
43. Goldman, L., Replica microscopy and scanning electron microscopy of laser impacts on the skin. J. Invest. Dermatol. 52, (2006).
44. Datta, S. et al. Methods of use of substrate having properties of keratinous tissue. US8417474 B2 (2007).
45. Bhushan, B., Wei, G. & Haddad, P. Friction and wear studies of human hair and skin. Wear 259, 1012–1021 (2005).
46. Fischer, T. W., Wigger-Alberti, W. & Elsner, P. Direct and Non-Direct Measurement Techniques for Analysis of Skin Surface Topography. Skin Pharmacol. Physiol. 12, 1–11 (1999).
47. Lagarde, J. M., Rouvrais, C., Black, D., Diridollou, S. & Gall, Y. Skin topography measurement by interference fringe projection: a technical validation. Ski. Res. Technol. 7, 112–121 (2001).
48. Grove, G. L. et al. Skin replica analysis of photodamaged skin after therapy with tretinoin emollient cream. J. Am. Acad. Dermatol. 25, 231–237 (1991).
49. Yin, L., Morita, A. & Tsuji, T. Skin premature aging induced by tobacco smoking: the objective evidence of skin replica analysis. J. Dermatol. Sci. 27, 26–31 (2001).
50. Fowkes, F. M. Attractive forces at interfaces. Ind. Eng. Chem. 56, 40–52 (1964).
51. Owens, D. K. & Wendt, R. C. Estimation of the surface free energy of polymers. J. Appl. Polym. Sci. 13, 1741–1747 (1969).
52. Żenkiewicz, M. Methods for the calculation of surface free energy of solids. Journal of Achievements in Materials and Manufacturing Engineering (2007).
53. Young, T. An Essay on the Cohesion of Fluids. Philos. Trans. R. Soc. London 95, 65–87 (1805).

54. Wu, S. Calculation of interfacial tension in polymer systems. J. Polym. Sci. Part C Polym. Symp. 34, 19–30 (2007).
55. Thomsen, F. Measuring the surface free energy of human skin. KRÜSS Appl. Note 1 (2006).
56. Krawczyk, J. Surface free energy of the human skin and its critical surface tension of wetting in the skin/surfactant aqueous solution/air system. Ski. Res. Technol. 21, 214–223 (2015).
57. Dann, J. . & R., J. Forces involved in the adhesive process. J. Colloid Interface Sci. 32, 302–320 (1970).
58. Gindl, M., Sinn, G., Gindl, W., Reiterer, A. & Tschegg, S. A comparison of different methods to calculate the surface free energy of wood using contact angle measurements. Colloids Surfaces A Physicochem. Eng. Asp. 181, 279–287 (2001).
59. Wu, S. Polar and Nonpolar Interactions in Adhesion. J. Adhes. 5, 39–55 (1973).
60. Fowkes, F. M. Role of acid-base interfacial bonding in adhesion. J. Adhes. Sci. Technol. 1, 7–27 (1987).
61. Van Oss, C. J., Good, R. J. & Chaudhury, M. K. Additive and nonadditive surface tension components and the interpretation of contact angles. Langmuir 4, 884–891 (1988).
62. Van Oss, C. J., Chaudhury, M. K. & Good, R. J. Monopolar surfaces. Adv. Colloid Interface Sci. 28, 35–64 (1987).
63. Good, R. J. & Van Oss, C. J. Modern approaches to wettability : theory and applications. (Plenum Press, 1992).
64. Rosenberg, A., Williams, R. & Cohen, G. Interaction Forces Involved in Wetting of Human Skin. J. Pharm. Sci. 62, 920–922 (1973).
65. Rulison, C. So You Want to Measure Surface Energy? KRÜSS GmbH (1999)
66. Mavon, A. et al. Sebum and stratum corneum lipids increase human skin surface free energy as determined from contact angle measurements: A study on two anatomical sites. Colloids Surfaces B Biointerfaces 8, 147–155 (1997).
67. Manschot J. F. M. & Brakkee, A. J. M. The measurement and modelling of the mechanical properties of human skin in vivo—II. The model. J. Biomech. 19, 517–521 (1986).
68. Agache, P. G., Monneur, C., Leveque, J. L. & De Rigal, J. Mechanical properties and Young's modulus of human skin in vivo. Arch. Dermatol. Res. 269, 221–32 (1980).
69. Romanelli, M. & Falanga, V. Use of a durometer to measure the degree of skin induration in lipodermatosclerosis. J. Am. Acad. Dermatol. 32, 188–91 (1995).
70. Flick, E. W. Cosmetic and Toiletry Formulations. Noyes Publications. Second edition, Vol 2 (Elsevier, 1992).
71. Morrison, D. Petrolatum A Useful Classic. Cosmet. Toilet. Mag. 111, (1996).
72. Brooker, A. D., Vaccaro, M., Robles, E. S. J., Somerville, R. N. P. & Cuthbertson, M. A process for making a consumer goods product comprising a benefit delivery composition. EP3031893 A1 (2015).

73. Calvo, L. C. Cosmetic emulsion compositions having skin moisturizing properties. US4216201 (1978).
74. Lodén, M. Effect of moisturizers on epidermal barrier function. Clin. Dermatol. 30, 286–296 (2012).
75. Nikitakis, J., Lange, B., E., et al. International Cosmetic Ingredient Dictionary and Handbook Volume 1. (1973).
76. Wehr, R. F. & Krochmal, L. Considerations in selecting a moisturizer. Cutis 39, 512–5 (1987).
77. Ghadially, R., Halkier-Sorensen, L. & Elias, P. M. Effects of petrolatum on stratum corneum structure and function. J. Am. Acad. Dermatol. 26, 387–96 (1992).
78. Rentsch, S. F. Non-greasy petrolatum emulsion. US 5387417 (1991).
79. Knowlton, J. & Pearce, S. Handbook of cosmetic science and technology. (Elsevier Advanced Technology, 1993).
80. Rosen, M. & Rosen, M. Delivery System Handbook for Personal Care and Cosmetic Products : Technology, Applications and Formulations. (Elsevier Science, 2005).
81. Barel, A. O., Paye, M. & Maibach, H. I. Handbook of cosmetic science and technology. (CRC Press).
82. Porter, M. R. Handbook of Surfactants. (Springer US, 1991).
83. Salager, J.-L. Surfactants Types and Uses. Univ. Los Andes Publ. (2002).
84. Rosen, M. J. & Kunjappu, J. T. Surfactants and interfacial phenomena. (Wiley, 2012).
85. Ogino, K., Abe, M. & Ogino, K. Mixed surfactant systems. (M. Dekker, 1993).
86. Kosswig, K. Surfactants. in Ullmann's Encyclopedia of Industrial Chemistry (Wiley-VCH Verlag GmbH & Co. KGaA, 2000).
87. National Institute of Industrial Research (India). Board of Consultants & Engineers. Modern technology of oils, fats & its derivatives. (Asia Pacific Business Press, 2007).
88. Florence, A. T. (Alexander T. & Attwood, D. Physicochemical principles of pharmacy : in manufacture, formulation, and clinical use. (Pharmaceutical Press, 2011).
89. Chakrabarty, M. M. Chemistry and technology of oils and fats. (Allied Publishers, 2003).
90. Flingoh, C. & Chiew, L. Surface tensions of palm oil, palm olein and palm stearin. Elaeis 4, 27–31 (1992).
91. Vazquez, G., Alvarez, E. & Navaza, J. M. Surface Tension of Alcohol Water + Water from 20 to 50 .degree.C. J. Chem. Eng. Data 40, 611–614 (1995).
92. Mannhardt, K., Schramm, L. L. & Novosad, J. J. Adsorption of anionic and amphoteric foam-forming surfactants on different rock types. Colloids and Surfaces 68, 37–53 (1992).
93. Schick, M. J., Dekker, M. & van Oss, C. J. Nonionic Surfactants: Physical Chemistry. J. Dispers. Sci. Technol. 11, 437–438 (1990).

94. Othmer, K. Kirk-Othmer Chemical Technology of Cosmetics. (Wiley, 2012).
95. Burns, T., Breathnach, S., Cox, N. & Griffiths, C. Rook's Textbook of Dermatology. (John Wiley & Sons, 2013).
96. Löffler, H. & Happle, R. Profile of irritant patch testing with detergents: sodium lauryl sulfate, sodium laureth sulfate and alkyl polyglucoside. Contact Dermatitis 48, 26–32 (2003).
97. Nilsson, G. E. Measurement of water exchange through skin. Med. Biol. Eng. Comput. 15, 209–218 (1977).
98. Agner, T. & Serup, J. Sodium lauryl sulphate for irritant patch testing--a dose-response study using bioengineering methods for determination of skin irritation. J. Invest. Dermatol. 95, 543–7 (1990).
99. Wilhelm, K.-P., Surber, C. & Maibach, H. I. Quantification of sodium lauryl sulfate irritant dermatitis in man: Comparison of four techniques: skin color reflectance, transepidermal water loss, laser Doppler flow measurement and visual scores. Arch. Dermatol. Res. 281, 293–295 (1989).
100. Van Der Valk, P. G. M., Nater, J. P. & Bleumink, E. Skin Irritancy of Surfactants As Assessed by Water Vapor Loss Measurements. J. Invest. Dermatol. 82, 291–293 (1984).
101. Charbonnier, V., Morrison, B. M., Paye, M. & Maibach, H. I. Subclinical, non-erythematous irritation with an open assay model (washing): sodium lauryl sulfate (SLS) versus sodium laureth sulfate (SLES). Food Chem. Toxicol. 39, 279–86 (2001).
102. Parker, J., Scharfbillig, R. & Jones, S. Moisturisers for the treatment of foot xerosis: a systematic review. J. Foot Ankle Res. 10, 9 (2017).
103. Nolan, K. & Marmur, E. Moisturizers: Reality and the skin benefits. Dermatol. Ther. 25, 229–233 (2012).
104. Draelos, Z. D. Active Agents in Common Skin Care Products. Plast. Reconstr. Surg. 125, 719–724 (2010).
105. Buraczewska, I., Broström, U. & Lodén, M. Artificial reduction in transepidermal water loss improves skin barrier function. Br. J. Dermatol. 157, 82–86 (2007).
106. Lodén, M. The increase in skin hydration after application of emollients with different amounts of lipids. Acta Derm. Venereol. 72, 327–30 (1992).
107. Grubauer, G., Feingold, K. R. & Elias, P. M. Relationship of epidermal lipogenesis to cutaneous barrier function. J. Lipid Res. 28, 746–52 (1987).
108. Hachem, J.-P. et al. The effect of two moisturisers on skin barrier damage in allergic contact dermatitis. Eur. J. Dermatol. 12, 136–8
109. The Vaseline Story | Vaseline. Available at: http://www.vaseline.co.uk/article/vaselinestory.html. (Accessed: 26th September 2018)
110. Kraft, J. N. & Lynde, C. W. Moisturizers: what they are and a practical approach to product selection. Skin Therapy Lett. 10, 1–8 (2005).

111. Anderson, P. C. & Dinulos, J. G. Are the new moisturizers more effective? Curr. Opin. Pediatr. 21, 486–490 (2009).
112. IV botanica. Acta Eruditorum (1688). Available at: https://commons.wikimedia.org/wiki/File:Acta_Eruditorum_-_IV_botanica,_1688_–_BEIC_13396043.jpg.
113. Fluhr, J. W., Bornkessel, A. & Berardesca, E. Glycerol - Just a Moisturizer ? (2016).
114. Held, E., Lund, H. & Agner, T. Effect of different moisturizers on SLS-irritated human skin. Contact Dermatitis 44, 229–234 (2001).
115. Lodén, M. Urea-containing moisturizers influence barrier properties of normal skin. Arch. Dermatol. Res. 288, 103–107 (1996).
116. Buraczewska, I., Berne, B., Lindberg, M., Törmä, H. & Lodén, M. Changes in skin barrier function following long-term treatment with moisturizers, a randomized controlled trial. Br. J. Dermatol. 156, 492–498 (2007).
117. Department for Environment, Food and Rural Affairs Government Buying Standards for showers, taps, toilets and urinals. (2014) Available at: https:// http://www.europeanwaterlabel.eu/ (Accessed: 26th September 2018).
118. Why think about showers? Available at: https:// www.opsi.gov.uk/si/si1999/19991148.htm. (Accessed: 26th September 2018)
119. Reduce Hot Water Use for Energy Savings | Department of Energy. Available at: https://www.energy.gov/energysaver/water-heating/reduce-hot-water-use-energy-savings. (Accessed: 26th September 2018)
120. ENHANCE WATER EFFICIENCY STANDARDS URBAN GREEN NYC GREEN CODES TASK FORCE: FULL PROPOSALS WE 1 1. Available at: https:// http://www.nyc.gov/html/gbee/downloads/pdf/water_efficiency.pdf (Accessed: 26th September 2018)
121. Health Services – Scalding and burning. Available at: http://www.hse.gov.uk/healthservices/scalding-burning.htm. (Accessed: 26th September 2018)
122. Angel, C. & Director, C. Controlling Scalding Risks from Bathing and Showering 2 of 12 Guidance on Bathing and Showering-Version 3. (2010).
123. Anti-Scald Hot Water Regulations & Temperatures - laws regulating safe hot water temperature to avoid scalding burns, summarized by country, state, province & authority. Available at: https://inspectapedia.com/plumbing/Hot_Water_Temperature_Laws.php#AU. (Accessed: 26th September 2018)
124. Rose, S. Statistical design and application to combinatorial chemistry. Drug Discov. Today 7, 133–8 (2002).
125. Montgomery, D. & Jones, R. Design and Analysis of Experiments. Qual. Reliab. Eng. Int. 18, 163–163 (2002).
126. Tye, H. Application of statistical ‘design of experiments’ methods in drug discovery. Drug Discov. Today 9, 485–491 (2004).

127. Hibbert, D. B. Experimental design in chromatography: a tutorial review. J. Chromatogr. B. Analyt. Technol. Biomed. Life Sci. 910, 2–13 (2012).
128. Dejaegher, B. & Vander Heyden, Y. Experimental designs and their recent advances in set-up, data interpretation, and analytical applications. J. Pharm. Biomed. Anal. 56, 141–158 (2011).
129. Vera Candioti, L., De Zan, M. M., Cámara, M. S. & Goicoechea, H. C. Experimental design and multiple response optimization. Using the desirability function in analytical methods development. Talanta 124, 123–138 (2014).
130. Leardi, R. Experimental design in chemistry: A tutorial. Anal. Chim. Acta 652, 161–172 (2009).
131. Charnes, A., Frome, E. L. & Yu, P. L. The Equivalence of Generalized Least Squares and Maximum Likelihood Estimates in the Exponential Family. J. Am. Stat. Assoc. 71, 169–171 (1976).
132. Stigler, S. M. Gauss and the Invention of Least Squares. Ann. Stat. 9, 465–474 (1981).
133. Arlinghaus, S. L. Practical handbook of curve fitting. (CRC Press, 1994).
134. Kolb, W. M. Curve fitting for programmable calculators. (Syntec, Inc, 1984).
135. Halli, S. S. & Rao, K. V. Advanced Techniques of Population Analysis. (Springer US, 1992).
136. Alaluf, S. Atkins D., Barrett K., Blount M., Carter N., Heath A., Ethnic Variation in Melanin Content and Composition in Photoexposed and Photoprotected Human Skin. Pigment CELL Res. 15, 112–118 (2002).
137. Chiller, K. G., Passaro, D. & Frieden, I. J. Hemangiomas of Infancy. Arch. Dermatol. 138, 1567–1576 (2002).
138. Lin, F. R. et al. Association of Skin Color, Race/Ethnicity, and Hearing Loss Among Adults in the USA. J. Assoc. Res. Otolaryngol. 13, 109–117 (2012).
139. Roberts, W. E. Skin type classification systems old and new. Dermatol. Clin. 27, 529–33, viii (2009).
140. Rawlings, A. V. Ethnic skin types: are there differences in skin structure and function?1. Int. J. Cosmet. Sci. 28, 79–93 (2006).
141. Bettley, F. R. The toxicity of soaps and detergents. Br. J. Dermatol. 80, 635–642 (1968).
142. Wood, D. C. F. & Bettley, F. R. The effect of various detergents on human epidermis. Br. J. Dermatol. 84, 320–325 (1971).
143. Ray Bettley, F., The influence of detergents and surfactants on epidermal permeability. Br. J. Dermatol. 77, 98–100 (1965).
144. Rieger, M., Foam Wet Processing in the textile industry. in Foams 339–380 (Taylor & Francis Group, 2017). doi:10.1201/9780203755709-10
145. Czarnowicki, T. et al. Petrolatum: Barrier repair and antimicrobial responses underlying this “inert” moisturizer. J. Allergy Clin. Immunol. 137, 1091–1102.e7 (2016).

146. Rawlings, A. V., Canestrari, D. A. & Dobkowski, B. Moisturizer technology versus clinical performance. Dermatol. Ther. 17, 49–56 (2004).
147. Mygind, K., Sell, L., Flyvholm, M.-A. & Jepsen, K. F. High-fat petrolatum-based moisturizers and prevention of work-related skin problems in wet-work occupations. Contact Dermatitis 54, 35–41 (2006).
148. Lodén, M. & Lindberg, M. The influence of a single application of different moisturizers on the skin capacitance. Acta Derm. Venereol. 71, 79–82 (1991).
149. Attwood, D. & Florence, A. T. Surfactant Systems: Their chemistry, pharmacy and biology. (Springer Netherlands, 1983).
150. Tadros, T. F. Applied surfactants: principles and applications. (2005).
151. Ribeiro, H. M., Morais, J. A. & Eccleston, G. M. Structure and rheology of semisolid o/w creams containing cetyl alcohol/non-ionic surfactant mixed emulsifier and different polymers. Int. J. Cosmet. Sci. 26, 47–59 (2004).
152. A. M. Schwartz, J. W. Perry, Surface Active Agents; their Chemists, Technology, R.E. Krieger, New York, (1978).
153. M. J. Rosen, Surfactants and Interfacial Phenomena, Wiley, New York (1978).
154. G.P. Kumar, P. RajeshwarraoNonionic surfactant vesicular systems for effective drug delivery – an overview (2000)
155. Rabah A. Khalil, Al-hakam A. Zarari, Applied Surface Science, Volume 318, (2014)
156. B. Lindman, K. Holmberg, D.O. Shah, M.O. Schwuger (Eds.), Handbook of Applied Surface and Colloid Chemistry, John Wiley & Sons, New York, NY (2002)
157. Stuart MC1, Boekema EJ, Two distinct mechanisms of vesicle-to-micelle and micelle-to-vesicle transition are mediated by the packing parameter of phospholipid–detergent systems, Biochimica et Biophysica (2007)
158. Khan, A. Y.; Talegaonkar, S; Iqbal, Z; Ahmed, F. J.; Khar, R. K. "Multiple emulsions: An overview". Current Drug Delivery. 3 (2006)
159. Loi, Chia Chun; Eyres, Graham T.; Birch, E. John, "Protein-Stabilised Emulsions", Reference Module in Food Science, Elsevier (2018)
160. Mason TG, Wilking JN, Meleson K, Chang CB, Graves SM. "Nanoemulsions: Formation, structure, and physical properties" (PDF). Journal of Physics: Condensed Matter (2006)

CHAPTER 2: EXPERIMENTAL TOOLS AND ANALYTICAL TECHNIQUES

2.1 Materials

During this project, a significant number of polymer materials were screened for their suitability for skin replication and the development of mimics that deliver properties like those of human skin. For the fabrication of negative skin mimics, the skin safe PDMS silicone Body-Double was used as well as alja-safe and alja-safe breeze liquid alginates supplied by Bentley Advanced Materials. For the development of positive skin mimics, the employed materials included, VytaFlex® 10 and VytaFlex® 20 polyurethanes supplied by Bentley Advanced Materials, Polytek Poly74–29 Flexible Polyurethane Rubber and Polytek Poly PT Flex 20 Liquid Casting Rubber that were supplied by MB Fibreglass.

Contact angle measurements on the produced surfaces involved water, HPLC grade, diiodomethane ReagentPlus® 99%, and ethylene glycol, anhydrous 99.8%, all supplied from Sigma Aldrich.

For the fabrication of the model system emulsions, the materials used included Sodium Dodecyl Sulphate, BioUltra ≥99.0%, sodium dodecylbenzenesulfonate, technical grade, cationic surfactants-WP, certified reference material, lauric acid, Vaseline®, Sunflower seed oil from Helianthus annuus, cetyl-alcohol and difluoro{2-xx1-(3,5-

dimethyl-2h-pyrrol-2H-pyrrol-2-ylidene-N)ethyl]-3,5-dimethyl-1H-pyrrolato-N}boron Pyrromethene546, all purchased from Sigma-Aldrich. Furthermore, mineral oil, baby oil® by Johnson and Johnson was purchased from the market.

2.2 Skin Replication Technique

The first step of the mimic replication was the marking and prepping of the skin area of interest. Various skin parts were replicated throughout the duration of this project, but all required the essential skin preparation steps that included marking a 5x5 cm^2 area, shaving the area with an unused razor, degreasing the area using mild soap and warm water, rinsing the skin with water until all residues are removed, towel drying and letting air dry for 10 minutes in ambient conditions. Following, the skin safe silicone used for the negative mimics was assembled (specific gravity: 1.17 g cm−3, viscosity: 5000 mPa·s), the two parts were mechanically mixed in a ratio of 1:1 by weight, for 1 minute. Using a spatula, the mixture was applied directly on the skin surface and let to cure for 20 min (according to manufacturer's directions). The cured negative imprint was then removed and cleaned with mild soap and water and left to dry in ambient conditions for at least 1 hour before use. Following, the polyurethane materials used for the fabrication of the positive mimics were prepared. All materials used consisted of two parts that were mixed accordingly in a 1:1 ratio and poured directly on the patterned side of the negative mimic. The system was moved to a vacuum chamber for 10 minutes to remove trapped air from the interface of the negative mimic and the polyurethane material. Following, the mimics were moved to an oven set at 70°C and

left overnight to cure (approx. 12 hours required). Following, the positive mimics were detached from the negative and stored until further use.

2.3 Model System Emulsion Fabrication

Initially, the anionic surfactant (Sodium dodecylbenzenesulfonate with the linear formula: CH3(CH2)11C6H4SO3Na and molecular weight of 348.48 g/mol), the fatty acid (lauric acid with the linear formula CH3(CH2)10COOH and molecular weight of 200.32) and the oily phase (petrolatum, sunflower oil, mineral oil), where weighed in separate beakers. A high accuracy, Ohaus, analytical balance was employed for the weight measurement requirements of this project.

Figure 2.1: Ohaus analytical balance that was used for gravimetric analysis of this project.

The anionic surfactant concentration was 10% (0.29 M) and the fatty acid was 10% (0.50 M) for all fabricated emulsions. As far as the oil phase is concerned, to study the effect of the hydrating active concentration on retention, model system emulsions of variable oil volume fractions were produced. The chosen levels were 20%, 40% and

60%. The higher oil fraction levels where chosen towards the formation of a highly concentrated in hydrating component gel. Moreover, three oil phases of a range of viscosities were selected, to study the effect of oil viscosity on retention. The selected low-viscosity oil was mineral oil, the medium-viscosity oil was sunflower oil and the high-viscosity oil was petrolatum.

A solution of 0.05% hydrophobic dye (Pyrromethene 546) to acetone was prepared and premixed with the oil phase. The solution portion added, equaled 0.5% of the weight of the oil phase used. The two were mixed and stirred mechanically until homogenous. Following, the container was completely covered with aluminum foil due to the photosensitivity of pyrromethene. The following protocol was followed for the fabrication of the model system emulsions.

The anionic surfactant, was initially mixed in a beaker with half of the water portion required and mechanically stirred, using an overhead stirrer at 500 RPM, until homogenous and then heated in an oven at 80°C.

Following, the fatty acids were measured in a beaker and put in the oven at 80°C until they assumed their liquid form. Then they were added to the mixture and stirred. The surfactant molecules react with the fatty acid to form a lamellar structure which is visible by the immediate thickening of the mixture and viscosity build-up due to the formation of those structures.

The oil phase was measured and placed in the oven at 80°C and blended with the hydrophobic fluorescent dye, pyrromethene. The addition of the dye enabled the optical evaluation of retention using a fluorescent microscope. When the oily phase

reached a thin fluid state it was incorporated in the gel chassis and stirred at 500 RPM for at least 10 min.

Balancing water was added to the beaker to reach 100% of the formulation recipe and then the blend was stirred at 500 RPM till homogenous. Due to the photosensitivity of the dye, the mixture container was covered with aluminum foil at all times.

The system was then moved to the high shear homogenizer (silverson), towards the application of various shear levels to produce emulsions of different droplet sizes. Screen, is the cylindrical component that attaches on the work head and controls the flow of the emulsion to the mixer through its holes/openings. Given the shape and size of its holes the screen serves on different purposes like high shear emulsification. The screen used in this project has the model name emulsor and was also supplied by silverson. The emulsor was equipped on the probe and the homogenizer was operated at various speeds depending on the desired droplet size of the formulation.

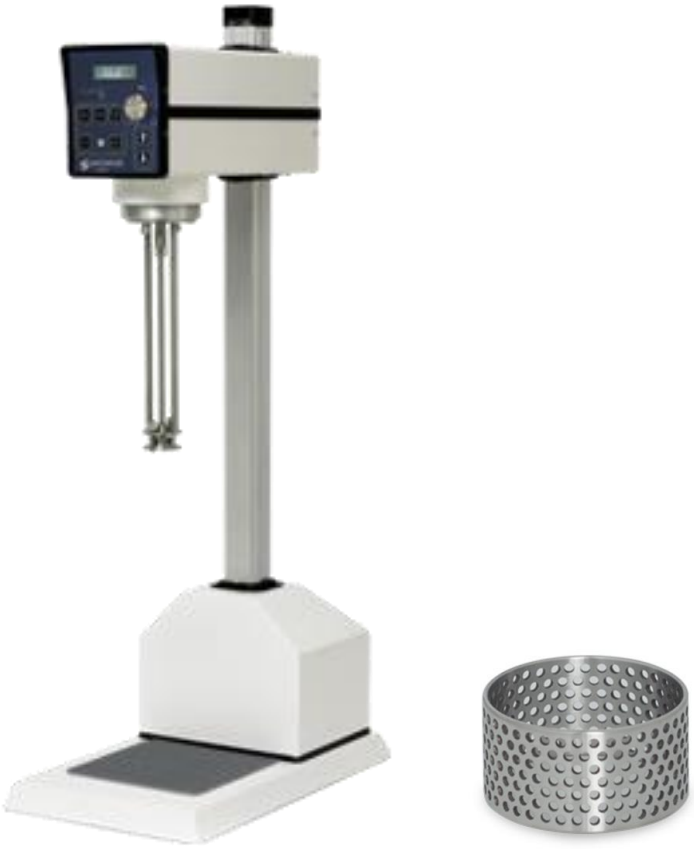

Figure 2.2: (Left) Silverson high shear lab homogenizer, (Right) emulsor screen that attaches to the homogenizer's probe.

The formulated emulsions were removed from the beaker and placed in sealed plastic containers, wrapped with aluminium foil for protection against light. The samples were stored in a lab cupboard until further use at ambient temperature.

2.4 Deposition Set-Up

To apply the fabricated model system emulsions on the skin mimics in a repetitive and highly controlled way, a deposition set up was developed by modifying a tribometer set up. The tribometer apparatus consists of a base and a sample holder, a highly

controlled upper moving arm with an incorporated balance, digital sensors for linear and lateral forces, a control screen and a computer. The modifications that took place included the replacement of the sample holder with a heating plate and a custom-made skin mimic sample holder placed on top of it. This enabled the inclusion of human skin temperature in the control parameters of the deposition process. The temperature was set at 35°C. Also, the upper moving part was replaced with a custom-made part where a skin mimic could be attached, to achieve a skin mimic on skin mimic interface. The deposition process started by placing the mimic samples on the sample base on the heating plate and leaving them for 5 minutes to reach the set temperature. Following, 2ml of emulsion was retrieved using a syringe and deposited on top of the mimic. The top moving part with mimic was then balanced and placed on top of the sample and deposited emulsion. A weight of 100g was placed on top of the moving part to set the lateral force. Using the control screen, the speed was set at 10mm per second and the number of cycles was set at 5. Following, the start button was selected, and the deposition process was initiated. At the end of the process the samples were dismounted, the sample holder and heating plate were cleaned of any excess emulsion and the top moving part mimic was replaced with a new one before the following experiment. Figure 2.3 shows images of the modified tribometry set-up.

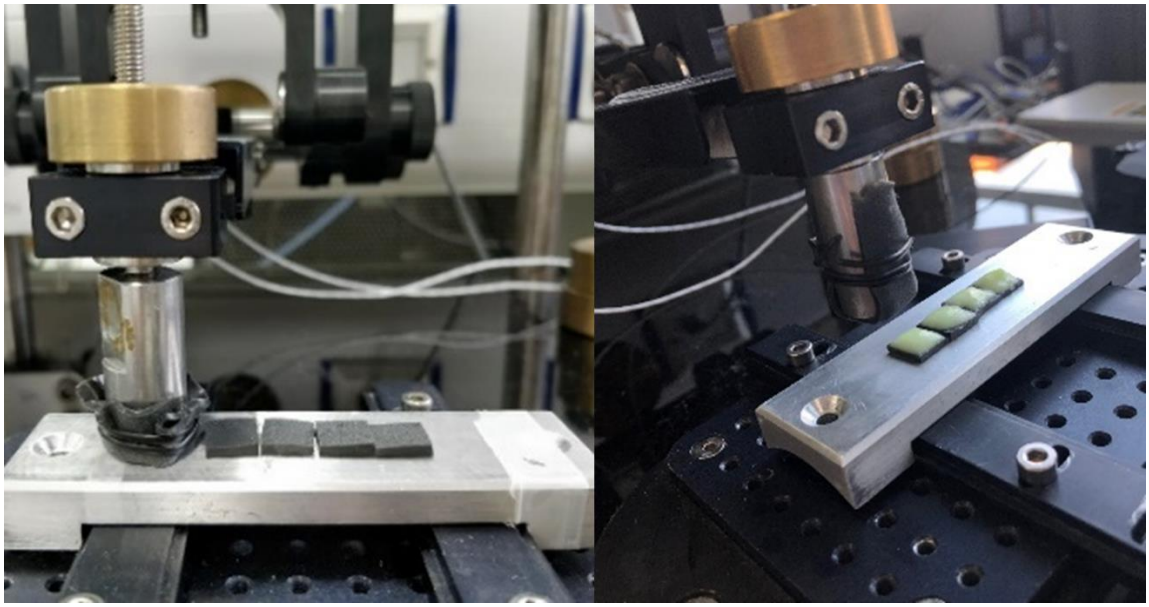

Figure 2.3: Initial deposition set-up design images, showing the modified tribometer set-up. (Left) Image showing the rod where the weights are added to control lateral force, and four 1x1 cm skin mimics double taped on the sample holder, (Right) image of the bottom skin mimics after a 2ml portion of emulsion has been deposited on them, but before the mechanical shear by the instrument. In later experiments the mimics were placed on a bespoke sample holder attached on a heating plate.

2.5 Cleaning Set-Up

The developed cleaning set-up needed to accurately re-produce the parameters of a shower that include water temperature, water flow rate, angle of flow and water jet diameter. The parts required to develop this set up included a high accuracy water pump (qdos03 supplied by Watson Marlow), a heating plate (provided by Corning Incorporated), a water collection box, a bespoke, angle adjustable sample base, water cables, beakers, a chronometer and a custom, 3D printed, 1mm nozzle.

Figure 2.4: High accuracy water pump, model qdos03 supplied by Watson Marlow, that was used to provide water in the shower spec cleaning apparatus. It is a versatile peristaltic chemical metering pump, which is able to provide a range of flowrates from 0.1 – 500ml/min at a steady pressure of 100psi.

The beaker served as a water container and was filled with tap water and place on top of the heating plate that was set at 40 degrees Celsius. The water temperature was measured using a thermometer to ensure that only 40°C water was used throughout the experiments. The input water pipe was placed and held in the water tank and fed the water pump with the warm water. The water pump was set at 100ml/min and the output pipe was positioned using a clamp over the sample holder. The temperature of the water was selected according to NHS regulations and suggestions for shower habits [1-2]. The water flow rate was selected from regulations as described by the UK government [3] and calculated for a single water jet making the assumptions that a typical showerhead is incorporated of approximately 90 waterjets of 1mm diameter each. Hence, a water jet nozzle of 1mm diameter was designed on Tinkercad, an online digital design CAD software, and 3D printed out of PLA using a 3D printer. The nozzle was attached on the tip of the output water pipe of the pump and sealed using

Teflon tape. The adjustable angle sample base was glued on the base of the water collection container. Figure 2.5 demonstrates the developed cleaning apparatus and its major components.

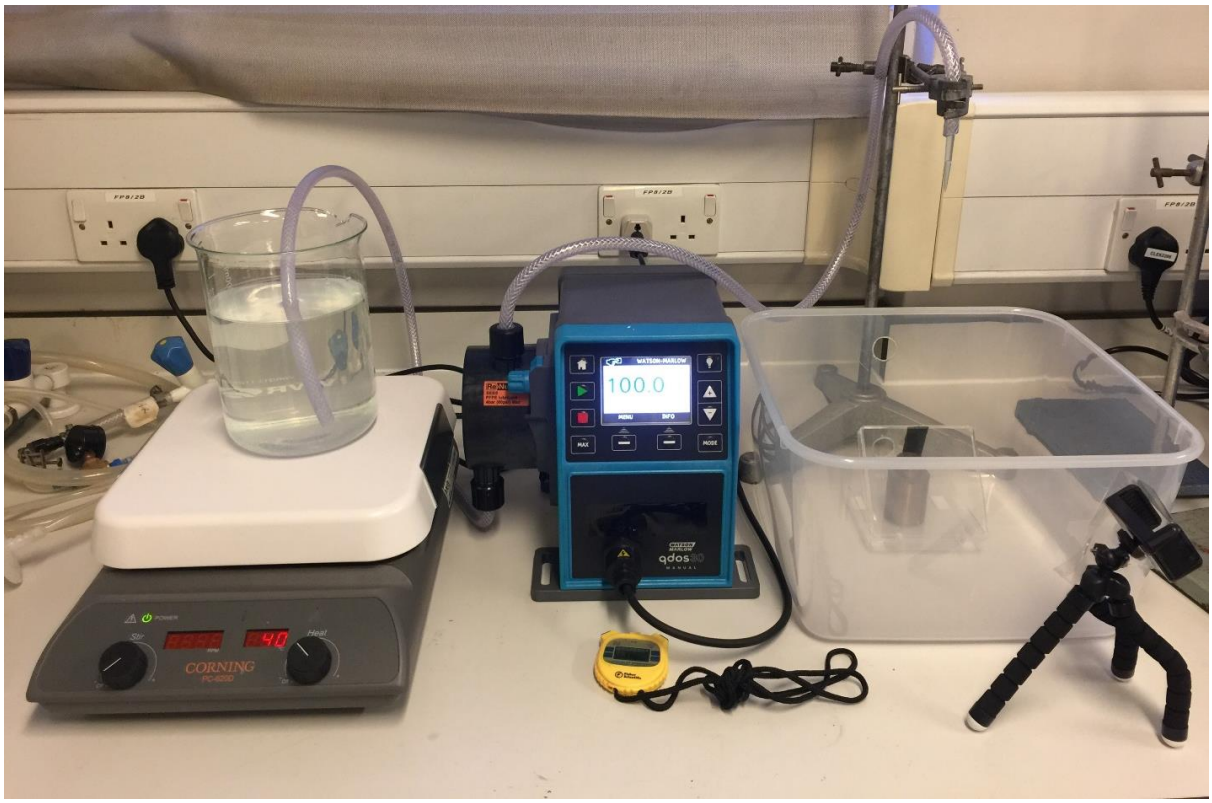

Figure 2.5: The cleaning apparatus and its major components that include from left to right, a heating plate, a filled beaker with deionized water serving as a water container, water input pipe, a high accuracy water pump, a chronometer, output water pipe with a fitted bespoke 1mm nozzle, a water collecting container and a variable angle sample base.

The cleaning process started by placing the samples with the deposited product on the sample holder. Following, the selected angle of flow was adjusted by changing the settings of the sample base. For the aims of this project, three options were tested, 90, 67.5 and 45 degrees of flow angle. Following, the water temperature was tested and when it reached 40°C, the pump was set at 100ml/min and the rinsing initiated

alongside the chronometer for time keeping. During this project, three levels of rinsing time were evaluated, 30, 60 and 90 seconds. When the selected amount of time had passed, the samples were removed and left to dry. The selected water was carefully disposed, and the water tank was refilled if required. The sample base was cleaned of any excess product deposits before installing the next samples.

2.6 Scanning Electron Microscopy

The scanning electron microscope, SEM, model name Hitachi S3400 SEM with a tungsten hairpin source with a lateral resolution of 5–10 nm, was used for the optical evaluation of the fabricated skin mimics. Initially, the samples were cut to the desired dimensions, 1x1 cm and 3x4 cm. The samples were positioned in the sample holder using a conductive double-sided tape. No gold or other metal sputtering was required prior to the mimic examination. The microscope was set at 10.0 kV in a variable pressure mode at 70 Pa. the captured pictures were used for optical evaluation of the achieved accuracy of the samples and defect investigation. Figure 2.6 is an example of a raw image with an incorporated scale bar from the SEM of a skin mimic showing the high accuracy of the instrument.

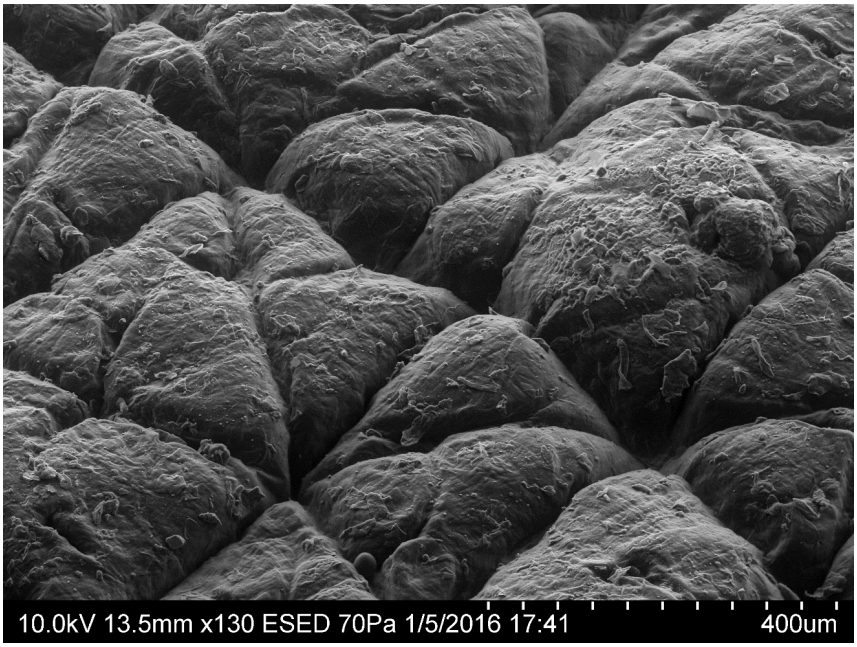

Figure 2.6: SEM raw image of a skin mimic sample. The images came with incorporated scale bars and the specifications used to capture it.

2.7 Optical Microscopy

Like SEM, white light optical microscopy was employed for the evaluation of the fabricated mimics and comparison with commercially available mimics provided by P&G. The microscope used was a Leica, model DM1750 M white light microscope and the images were captured using a DMC5400, 20 MP colour CMOS camera.

2.8 Interferometry

Further optical characterization of the mimics as well as roughness evaluation required the use of a MicroXAM-1200 3D non-contact interferometer. The skin mimic samples were required to be sputtered with a film of gold to enhance the accuracy of the measurements. An Agar Scientific sputter coating system was used to cover the

sample surface with gold. The layer achieved had a thickness of approximately 10nm according to manufacturer directions. The white light interferometry was used to generate high-resolution 3D images with a high vertical resolution and the MapVUE®AE analysis software package enabled the calculation of average surface roughness values of the tested samples. Figure 2.7 illustrates the interferometer set up used and Figure 2.8 demonstrates the prepped skin mimic samples coated with a layer of gold to enhance the instruments accuracy by increasing the reflectivity.

Figure 2.7: Interferometer set up, showing the main microscope, the light source controller and the intensity control.

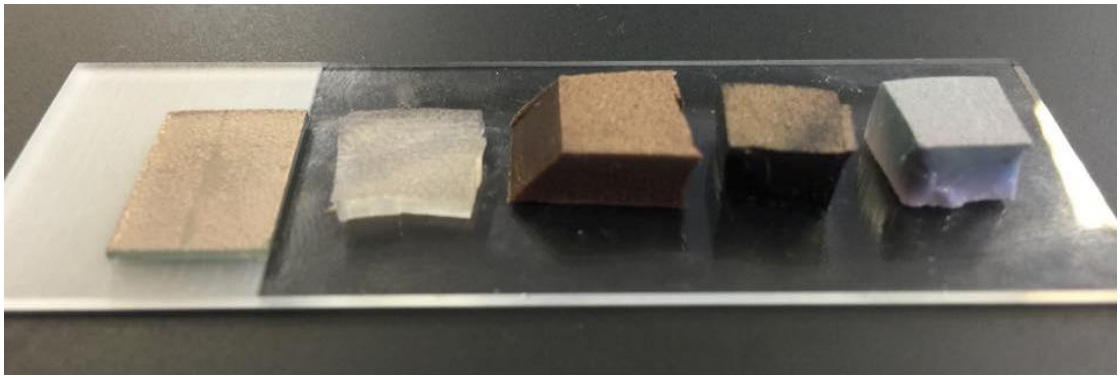

Figure 2.8: Image of skin mimic samples prepared for interferometer evaluation. The samples have been sputter coated with gold using an Agar sputter coating system to enhance the signal received by the interferometer and assume better quality images and higher accuracy results.

2.9 Contact Angle Measurements

The produced skin mimic samples were evaluated as for their surface free energy. The sessile drop technique was used for the purposes of this project according to which contact angle measurements, the Fowke's theory and surface energy principles enable the calculation of the surface free energy of solid surfaces, by employing the following equation whose synthesis and components are explained in detail in Chapter 1.2.2.2:

$$\frac{\gamma_l(\cos\partial+1)}{2} = \sqrt{\left(\gamma_s^d\gamma_l^d\right)} + \sqrt{\left(\gamma_s^p\gamma_l^p\right)} \quad (19)$$

Water and diiodomethane were used as reference liquids for the contact angle measurements. A microscopic camera, supplied from Andostar, was used to capture photos of the droplet/mimic interface. A 2-20 μl pipette from Eppendorf was used for the measurement and deposition of the liquid droplet. Initially, 20 μl of water was measured and deposited on the mimic using the pipette. The tip of the pipette needed to be as close to the surface of the sample as possible before releasing the liquid. The moment the droplet contacted the surface, a photo of the developed interface was

captured. The acquired image was uploaded on the ImageJ software for contact angle analysis using the angle measurement tool from the software toolbox. The same process was repeated for the evaluation of diiodomethane contact angles. Every liquid was tested at least 3 times for each skin mimic sample. The acquired contact angle values were then used for the calculation of surface free energy of the replicas by applying them on the Fowke's equations as described in literature. Figure 2.9 shows an example of a droplet to skin mimic image that was used to calculate contact angles.

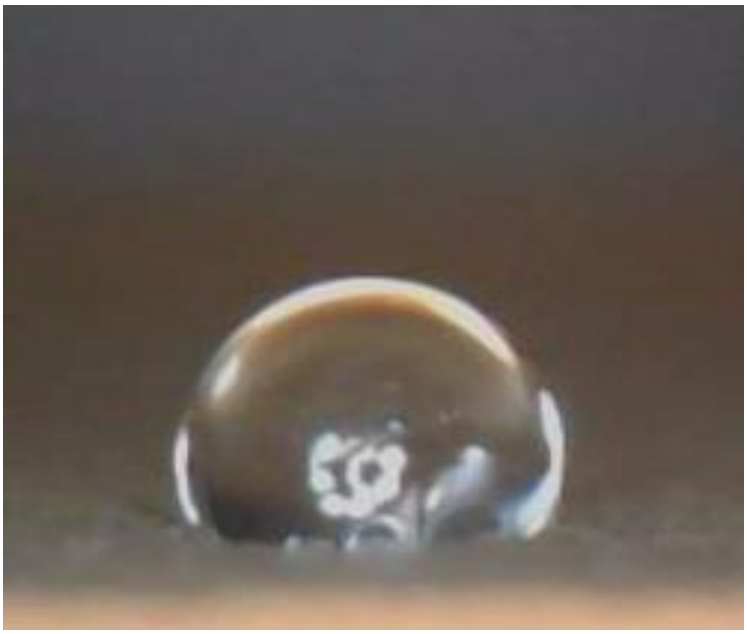

Figure 2.9: Example of a droplet/skin mimic image used to measure contact angles of specific liquids on the fabricated samples towards the calculation of surface free energy. The ImageJ software was used to evaluate the contact angle of the two using the angle measuring tool.

2.10 Mastersizer

For the evaluation of the achieved oil droplet size of the produced emulsions, a Mastersizer was used provided by Malvern, model Malvern-2000. This instrument uses

the principles of static light scattering and laser diffraction techniques and targets the sample with a light beam to acquire a scattering pattern from the field of droplets and uses it to produce droplet size distribution data of the tested sample [4]. For these calculations the instrument required the input of the refractive index and absorption values of the dispersive and continuous phase of the emulsion, which could be found in the literature. The dispersive phase was either petrolatum, mineral oil or sunflower oil, whereas the continuous phase was always water. The instrument comprised of a water tank with an incorporated stirrer and input/output pipes that provided the solution on a cell were the laser beam hit the sample. The process of using the Mastersizer started by flushing the water tank with a 5% DECON solution. Following, the tank needed to be rinsed with deionized water repeatedly to ensure that no residues of DECON were present. The software used, was then calibrated to reduce background noise of the measurement. Then the formulation was added gradually, ensuring that the stirrer mixed it in the water tank and created a homogenous solution. The software indicated when enough material had been added and after that the measurement could start. After the completion of the measurements the water tank was emptied and refilled with clean water and flashed with DECON and deionized water enough times to prepare for the following experiment. The following graph in Figure 2.10, illustrates a raw file as derived from the Malvern software showing the droplet size distribution of an emulsion in three repetitions.

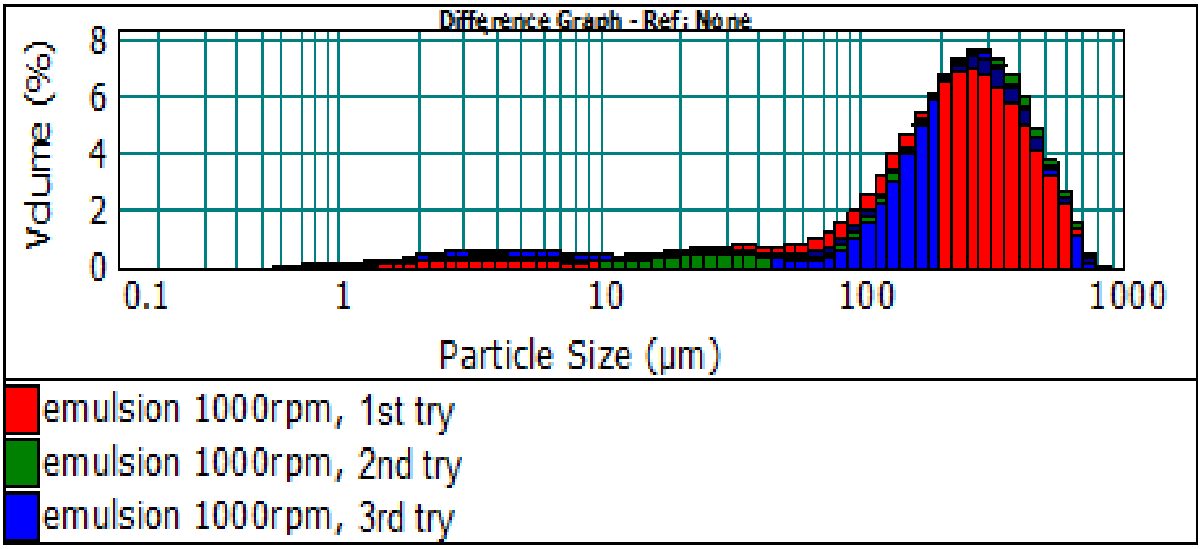

Figure 2.10: Typical example of the raw graph of droplet size distribution as derived from the instrument's software. The software plots the data of the three repetitions and presents them in a droplet size (µm) to volume (%) graph where the accuracy of the measurements can be evaluated by how close the three graphs fit. In this case the three-repetition data match closely so the measurement can be trusted.

2.11 Rheometer

For the rheological characterization of the produced formulation, the Kinexus pro+ rheometer by Malvern was used. The rheometer enabled the evaluation of the shear viscosity from flow tests as well as dynamic material properties like the viscoelastic modulus and phase angle from oscillation tests. In this project, the viscosity of the model system emulsions and the pure oils (petrolatum, sunflower oil, mineral oil) were measured. The geometry of a vane rotor rotating in a container cylinder was used, which was suggested by the manual for formulations of low to medium viscosities. The formulation was poured in the cylinder until it covered the top part of the rotor vane, then the temperature was set at 40°C, and then the experiment started. The derived data were plotted using Microsoft Excel.

2.12 Fluorescent Microscopy

The staining of the oil phase of the emulsions with the fluorescent dye, Pyrromethene-546 enabled the use of a fluorescent microscope to target the dye and hence the deposited oil phase on the skin mimic samples after rinsing of the product from their topography. Pyrromethene has an absorption peak at 495nm and an emission peak at 505nm. By adding these limits on the software of the fluorescent microscope, the single wavelength LED light source, purchased from CoolLED, enabled the emission of the correct wavelength to detect this specific dye. The microscope was supplied by Leica and the camera used to capture the images was supplied by Ximea and had the model code MR285MU_BH. The control software used for these measurements was the μManager. The captured, 8-bit images were uploaded to the imageJ software for the measurement of their fluorescent intensity signal by selecting the area of interest and selecting the measure intensity option in the software toolbox. This value represented the presence of the deposited oil phase given that it was the only phase of the product containing the hydrophobic dye, hence emitting fluorescent signal. This method was used for comparison purposes amongst the formulations and not for direct measurement of the deposited oil portion that was retained on the samples. This could be achieved by generating calibration curves and is suggested as further/future research of this project.

2.13 Tribometry

The tribometer, as mentioned before, was used for the controlled deposition of the formulated model system emulsions on the skin bio mimic's topography. However, due to the high accuracy of friction readings and the fact that deposited oil on skin functions as a lubricant, making the surface of the skin smoother and reducing its friction, this instrument was used as another method to target retention and cross-validate the fluorescent microscope and gravimetric analysis data.

The instrument used was a bespoke, custom-built tribometer, with most parts purchased from CSM Instruments. The instrument consisted of a base, a highly controlled upper moving part with height adjusters and a balance, x and z axis sensors that detected linear and normal load, a control tower with an incorporated touch control screen and a computer. The control parameters of this experiment included the travel distance of the top part, the speed of movement, the number of cycles performed, and the normal load applied on the sample. For the purposes of this project, a flat 1x1 cm mimic surface was equipped on the upper moving part so that it is sheared against the samples. The travel distance of the moving part was set at 1 cm, given that the samples were 1x1 cm^2 and as a result it covered all of its length. The speed of travel was set at 10mm per second and the number of cycles was set at 10. Using the balancing weights, the upper part was balanced so that no force was applied on the samples. Following that, accurate weights of 100g were placed directly over the edge were the skin mimic samples were making the normal load approximately 1N. When all parameters were in place the measurement started and the retrieved data were plotted, and the coefficient of friction was calculated using the following equation:

$$\mu = \frac{F}{N} \tag{20}$$

where μ is the coefficient of friction, F the linear or frictional force and N the lateral or normal load. Friction is a more tangible evidence of oil retention and this method is generally used in the industry for performance evaluation of lubricants and occlusive materials like petrolatum, mineral oil and sunflower oil.

2.14 References

1. Health Services – Scalding and burning. Available at: http://www.hse.gov.uk/healthservices/scalding-burning.htm. (Accessed: 26th September 2018)
2. Angel, C. & Director, C. Controlling Scalding Risks from Bathing and Showering 2 of 12 Guidance on Bathing and Showering-Version 3. (2010).
3. Why think about showers? Available at: https:// www.opsi.gov.uk/si/si1999/19991148.htm. (Accessed: 26th September 2018)
4. Laser Diffraction Particle Sizing (Malvern Mastersizer) Available at: https://www.crodalubricants.com/en-gb/discovery-zone/how-we-test-our-products/laser-diffraction-particle-sizing (Assessed: January, 2019)

CHAPTER 3: DEVELOPMENT AND FABRICATION OF THE OPTIMIZED SKIN MIMIC

3.1 Fabricating a Skin Mimic Substrate

Human skin *in-vivo* is a restrictive choice in skin focused studies due to the significant number of sample destructive methods that are subsequently excluded when choosing living skin as a substrate. Therefore, skin mimicking, bio-mimics and skin-like substrates have been developed and employed in skin focused researches from as early as 1964 [1-3]. Moreover, pork skin is a valid proposition in such researches as well, due to its affinity to human skin, analogous surface energy characteristics and similar chemistry. However limited shelf life, complex maintenance, high variability between samples and preservation requirements make pork skin an unsuitable option in studies in which chemistry and cell structures are not essential. Hence the development of robust test substrates that accurately replicate skin's topography, surface and mechanical properties and follow a production method that is easy, cost and time effective was crucial.

3.2 Current Skin Mimics

Universal personal care industries and R&D laboratories often acquire their skin mimics from third party artificial skin substrate manufacturers like Beaulax, IMS, Organogenesis, Skinethic Tissue Culture Laboratories, etc. Their products are robust, repetitive and provide a variety of characteristics depending on the application. However, they are expensive and often challenging to modify in order to match the criteria of a specific study. As a first step in our study we examined three different skin mimics with different topographic features provided by Beaulax, that can be found by the trade name BIOSKIN. These three mimics were used for wetting experiments of fragrances.

The distinction amongst them macroscopically was their colour, Brown, Black and White, and they all underwent optical analysis, surface energy estimation by contact angle measurements, roughness characterization and hardness measurements to use them as a benchmark against our own produced skin mimics. The Images in Figures 3.1, 3.2 and 3.3 show interferometer and optical microscopy images of the three BIOSKIN replicas to evaluate their topographic features.

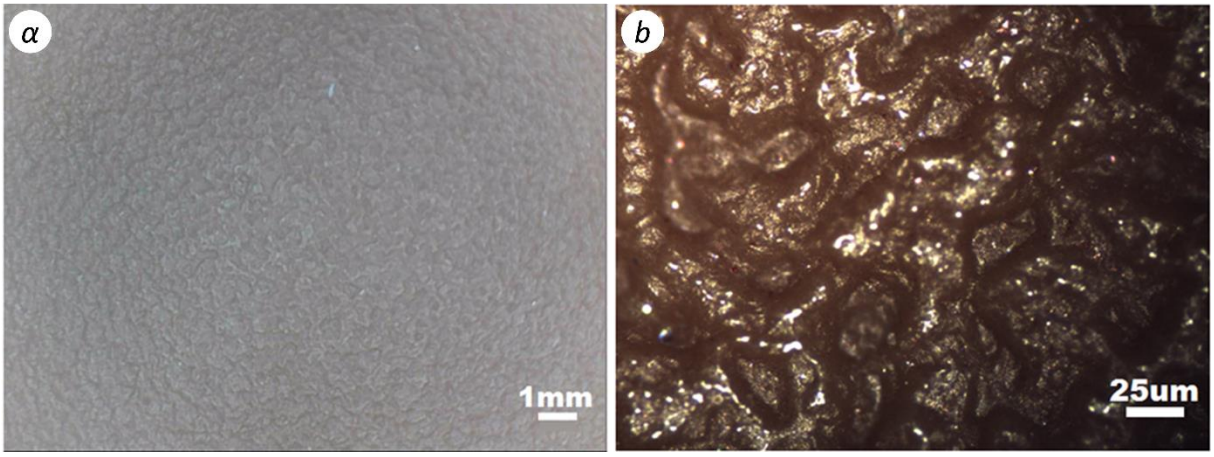

Figure 3.1: Optical interferometer image of Brown BIOSKIN skin mimic (α) and optical microscopy image (b), showing evenly distributed roughness but low resemblance to human skin topography.

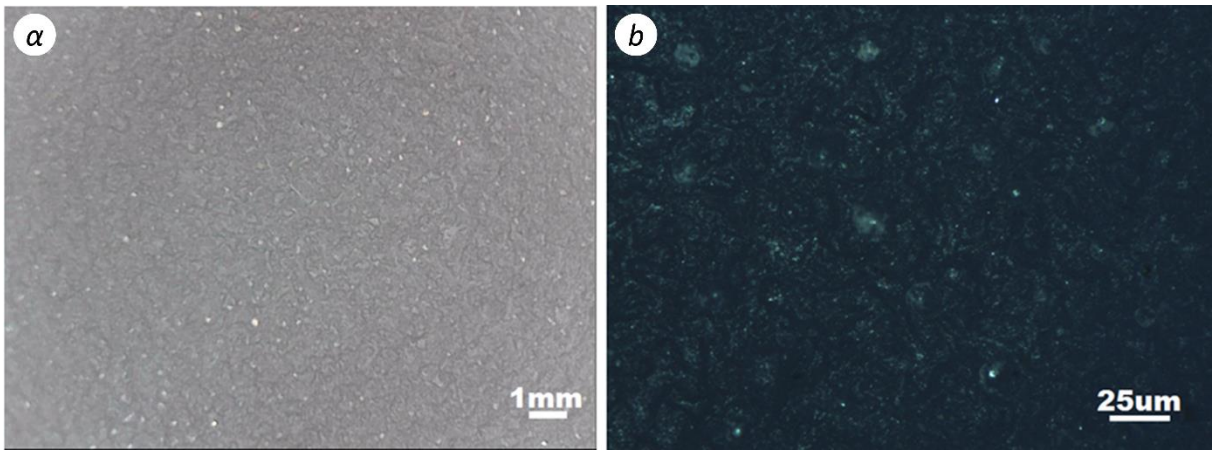

Figure 3.2: Black BIOSKIN skin mimic interferometer (α) and optical microscopy image (b) where an even but lower than the Brown BIOSKIN mimic roughness is shown.

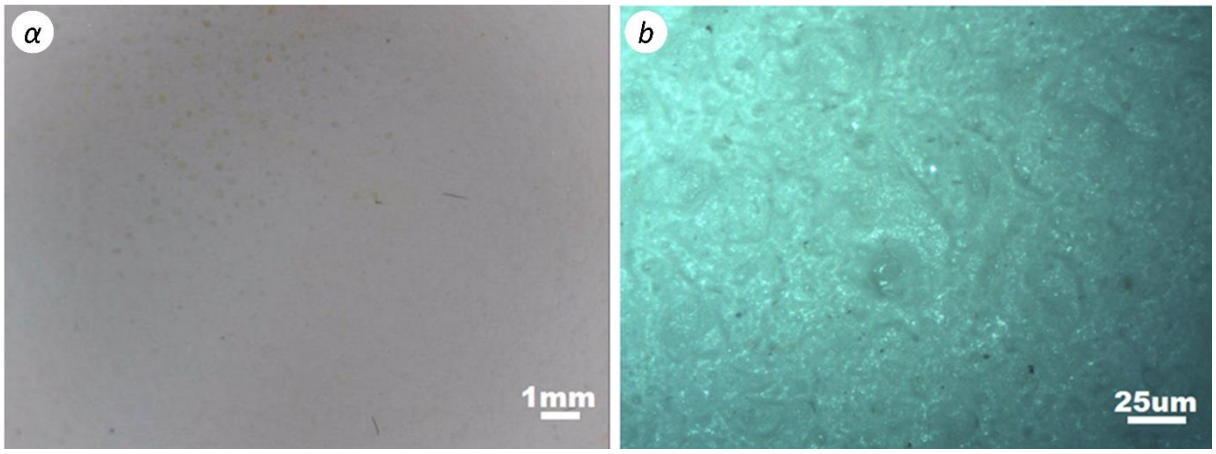

Figure 3.3: White BIOSKIN skin mimic interferometer (α) and optical microscopy image (b) of the topography. Very low, almost flat topographic features are observed.

Interferometry and optical microscopy images showed a very distinctive differentiation of topographic features amongst the different skin mimics, with Brown BIOSKIN exhibiting intense topographic features and high roughness whereas the White BIOSKIN demonstrated the mildest topographic characteristics. In all cases, the surface characteristics were even, throughout the skin mimic surface and didn't resemble human skin topographic features. The reason behind the large variation in roughness values is attributed to a potential effort to cover a larger range of human skin types and ethnic groups. In the following Table 3.1 the roughness values of the three mimics is presented to show the broad span of values that they covered and are compared to the roughness values of human skin from literature.

Table 3.1: Average roughness values Sa of the three different BIOSKIN mimics in comparison with human forehead and human forearm in vivo measurements from literature showing the wide range that the mimics cover.

	Brown BIOSKIN	**Black BIOSKIN**	**White BIOSKIN**	**Human Forehead[4]**	**Human Forearm[5]**
Average Roughness	19.3±3.0	14.7±3.6	9.8±2.1	18.8±4.3	18.2±2.8

In Table 3.1, the wide range of roughness that the BIOSKIN mimics cover is demonstrated, however only the Brown BIOSKIN replica shows roughness values similar to human skin, according to other studies, making it the most potent of the three for skin research projects.

Furthermore, contact angle measurements of deionized water and diiodomethane took place on all the skin mimics, allowing the calculation of the surface energy, using the Fowke's theory and the sessile drop technique, and comparison with that of human skin.

Table 3.2: Contact angle values of water and diiodomethane on BIOSKIN mimics and calculated surface energy.

	Brown BIOSKIN	**Black BIOSKIN**	**White BIOSKIN**	**Human Forearm**
Water contact angle	95.5 ± 2.4	85.8 ± 4.0	81.50 ± 1.3	N/A
Diiodomethane contact angle	34.2 ± 2.4	29.5 ± 3.5	31.22 ± 3.0	N/A
Surface energy	42.5 ± 1.2	45.7 ±1.5	46.04 ± 1.9	36.1±1.2 [5]

In Table 3.2, the contact angle measurements of water and diiodomethane for BIOSKIN skin mimics as well as the comparison of the calculated surface free energy of the mimics and human skin *in-vivo* from the literature are demonstrated. The Brown BIOSKIN skin mimic exhibited the closest surface energy values to that of human forearm. This is attributed not only to the affiliation of the construction polymer materials of the mimic to human skin in terms of chemistry but also to the similar roughness values between the two which is known to affect both contact angle measurements and surface energy of a solid surface.

Following the evaluation of the commercially available skin mimics the development of a skin replication technique based on a literature review and optimized to the requirements of this project took place. We fabricated robust and repetitive polymer skin substrates that demonstrated stability, long shelf life and were time and cost effective to produce.

3.3 Skin Replication Technique

3.3.1 Skin Preparation

Primarily, the skin mimics were derived from a Caucasian male volunteer in the age group of 25-30 years old. The skin area of interest was selected and marked. Areas that were chosen for replication in this project included, forearm, forehead, cheek, thigh, and chest. The selected areas, at least 5x5 cm^2, were initially shaven to remove any hairs and then washed with a mild shampoo. The washing consisted of 1-minute lathering with moderate shear, 1-minute rinsing off with warm water, towel drying the test area followed by air drying in ambient conditions for the next 10 minutes. The skin was then ready for replication.

3.3.2 Negative Mimic Fabrication

A skin safe silicone was chosen for the development of the negative mimics. The two parts of the polydimethylsiloxane were mechanically mixed for at least 1 minute using a spatula. The mixture was applied onto the prepped skin area forming a thin layer of approximately 1-2mm thickness. The material was allowed to cure and set for at least 20 minutes (manufacturer recommendations involved 5 minutes working time and 20 minutes demoulding time). The material was then carefully removed, and the fabricated negative imprints of human skin topography were used as a mould to fabricate the positive mimics.

3.3.3 Positive Mimic Fabrication

The negative mimics were washed with a mild soap, towel dried and air dried to ensure that no natural lipids from the skin were present. The mimics were then placed on a petri dish on a horizontal bench. The materials chosen for the fabrication of the positive mimics were a series of polyurethanes due to their outstanding mechanical properties, the large span of hardness that they provide, their affinity to human skin as far as surface energy and hydrophobicity is concerned and their low pre-cured viscosity that allowed them to flow within the microstructure of the negative mimic's topographic features, enabling the production of accurate mimics. The range of polyurethanes used included Vytaflex 10, Vytaflex 20, Poly74-29 and Polytec poly pt-flex due to the hardness characteristics they demonstrate, that range from 10 to 30 Shore A, with human skin hardness values in literature ranging from 10 to 40 Shore A [6,7], showing yet again the superiority of polyurethanes for skin replication projects. For simplicity, these polyurethanes were termed PU1, PU2, PU3 and PU4 respectively throughout this study. The prementioned materials, all incorporate two parts that need to be mixed in a 1:1 ratio to initiate polymerization. The two parts were mixed for at least 1 minute. The mixture was then poured on the topography of the negative mimic. The petri dish containing the negative mould and the polyurethane material were placed in a vacuum chamber to remove air bubbles within the polyurethane bulk that were trapped during mixing. Additionally, the vacuum enhanced the replication accuracy by removing air from the microtopography of the negative mimics which was trapped in the interface between the two materials. After approximately 10 minutes the mimics were removed from the chamber and placed either in an oven at 60°C where the curing time was 1-2 hours or left in ambient conditions in a fume cupboard where curing durations were

approximately 24 hours. Once the curing time was passed the positive mimics were then carefully demoulded and cut in 1x1 cm^2 squares.

3.3.4 Characterization of the Mimics

The fabricated mimics were characterized to evaluate their replication accuracy and similarity to human skin for the parameters of interest, which were topographic features, roughness, pore distribution and dimensions, surface energy and hardness.

An initial optical evaluation took place using Scanning Electron Microscopy to ensure that topographic accuracy had been achieved and to assess the surface characteristics of the positive mimics. The following images demonstrate the surface features of the poly pt flex polyurethane positive mimics, PU4.

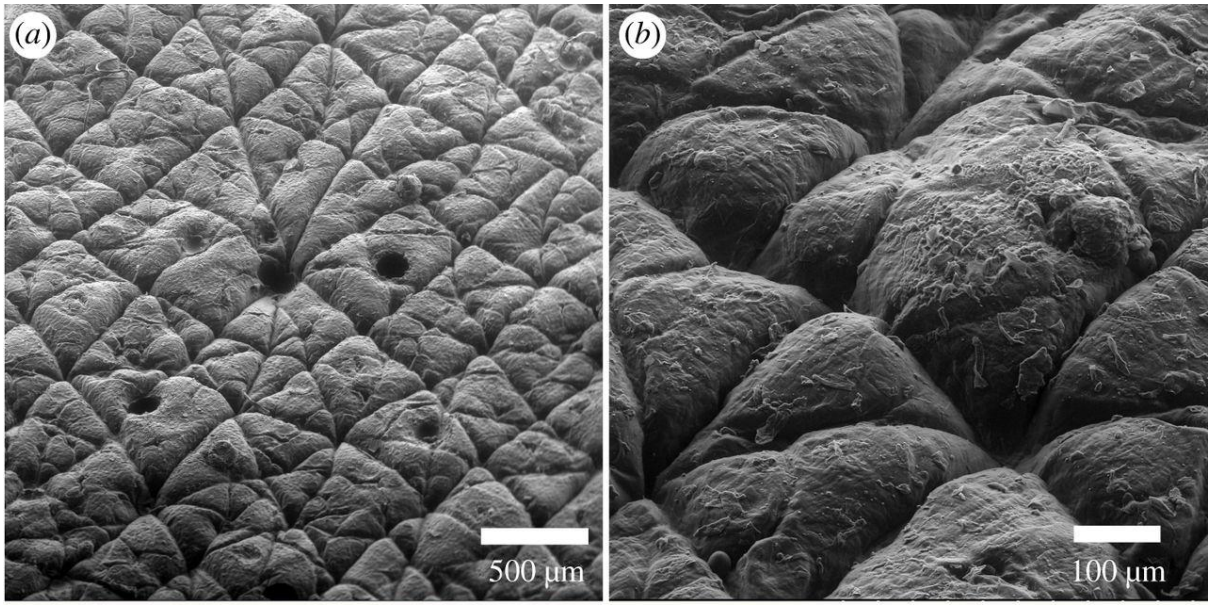

Figure 3.4: Poly pt Flex polyurethane positive mimic SEM images exhibiting the achieved topographic accuracy and the resemblance to human skin.

Figure 3.4 demonstrates the obvious resemblance of the fabricated mimics to human skin and the superiority of these mimics compared to the BIOSKIN as far as skin topography is concerned.

Furthermore, the mimics roughness was characterized by employing white light interferometry. This method was also used to generate 3 dimensional images of the mimic topographic structure, due to the multilayer scanning capabilities of this technique. Moreover, additional pore dimension and distribution measurements took place via image analysis of these images.

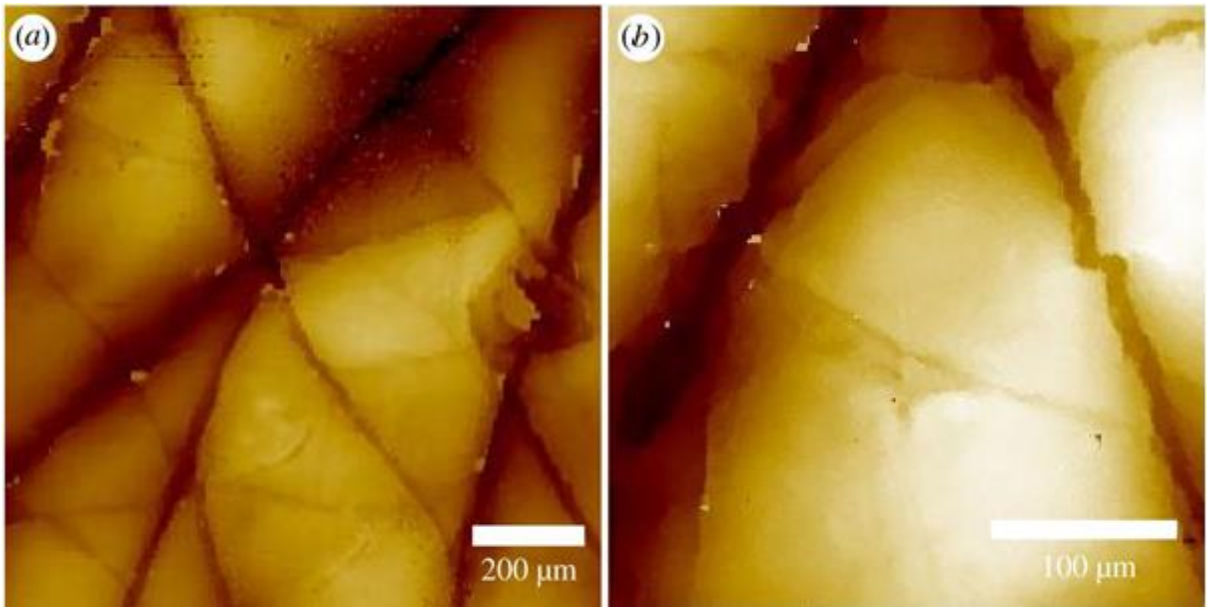

Figure 3.5: Poly pt Flex polyurethane positive mimic interferometry images showing (α) the achieved topographic features of the fabricated substrates and (b) a pore site, measuring 82μm in diameter.

The image analysis software ImageJ was employed towards the examination of interferometer Figures to calculate average pore dimensions and distribution. To carry out these measurements, ten 100x100 μm^2 images were randomly captured from a

skin mimic. The pore sites were identified and counted, and the pore diameters were measured using the scale bar embedded in the image, using the length calibration tool of ImageJ. Therefore, the average number of pores per cm^2 was calculated and found to be 188±17 pores/ cm^2 whereas the average pore diameter was calculated and showed a value of 84.7 ± 0.6 μm. Human skin in vivo measurements of these values in literature have shown pore distribution values of approximately 200 pores/ cm^2 and an average pore diameter of 60-80 μm [8,9,16], proving the significant topographic accuracy of the fabricated mimics and their strong similitude to human stratum corneum.

Table 3.3: Measured average surface roughness of skin mimic in comparison to human forearm roughness by in-vivo measurements in literature.

	PU4 skin mimic	**Human Forearm [5]**
Roughness (μm)	15.5 ± 0.3	18.2 ± 2.8

In Table 3.3, the roughness values of the positive mimics are presented showing a slight difference to human skin in vivo roughness measurement values from literature. However, skin roughness is a property that varies a lot depending on multiple components including sex, age, ethnicity, etc. According to literature, valid skin roughness values range from 10 to 30 μm [8,10-12], consequently the positive skin mimic accurately falls within this range, providing precise representation of human skin surface characteristics.

Furthermore, the fabricated skin mimics were evaluated for their surface energy by performing contact angle measurements and employing the Fowke's theory towards the calculation of their surface free energy. In Table 3.4, the calculated values for all polyurethane mimics are presented and compared to the surface energy value of

human skin as measured in-vivo in literature. However, by observing the dispersive and polar components of the mimics separately, the dominance of the dispersive component is obvious. Human skin also demonstrates a significantly lower polar component in comparison to its dispersive, although remarkably higher than that of the mimics. Literature has shown that degreasing human skin with ether or ethanol before surface energy calculations, lowers the polar component significantly, underlining the correlation of that component with the natural lipid concentration on the stratum corneum [13-15]. Hence it is only natural that the polyurethane mimics, due to complete lack of any lipids, cannot represent this aspect of human skin. Nevertheless, there are artificial lipids, sebum and sweat commercially available that could be deposited sparingly on the mimics to optimize them even further as far as their surface energy characteristics and lipid concentration are concerned. All replicas exhibit values closely to those of human skin and outperformed the commercially available mimics that were tested to provide a benchmark as seen in Table 3.2. However, due to the combination of efficient manual handling, pre-cure rheological characteristics, the achieved topographic accuracy and comparable surface energy, PU4 was selected as the main material for our skin replication process to provide positive mimic substrates.

Table 3.4: Surface energy characteristics, polar and dispersive components, of the fabricated skin mimics in comparison to human skin from in-vivo surface energy characterization in literature.

	PU1	**PU2**	**PU3**	**PU4**	**Human skin [16]**
Surface Energy (mJ cm^{-2})	40.7 ± 0.1	34.9 ± 0.1	41.5 ± 0.1	38.1 ± 0.5	36.1 ± 1.9
Dispersive Component	40.6 ± 0.1	34.6 ± 0.1	41.5 ± 0.0	37.7 ± 0.1	34.1 ± 1.5
Polar Component	0.4 ± 0.1	0.3 ± 0.1	0.1 ± 0.1	0.4 ± 0.5	2.0 ± 0.5

3.4 Conclusions

Skin mimicking is an essential and widely studied part of skin focused researches. There are commercially available mimics provided by numerous companies that provide relatively similar properties to human skin, depending on the application. For the purposes of this study, a skin replication technique was developed that enabled the production of robust, accurate, time and cost effective skin mimics, by following a well-established skin replication method and adding innovative steps towards the optimization of the specifications of the produced substrates. The developed mimics were characterized against human skin and a benchmark commercially available mimic to assess the achieved performance. The produced mimics demonstrated optimal performance in the parameters of interest which included topographic accuracy, surface free energy and mechanical properties. Their similarity to human skin was ideal, outperforming the tested skin mimics available in the market. The substrates also exhibited long shelf life, low maintenance requirements, high reproducibility and flexibility. The developed method could be used in various applications and could potentially be used in different projects where skin replication of other body parts is required.

3.5 References

1. Facq J. 1964 A simple replica technique for the observation of human skin. J. Soc. Cosmet. Chem. 15, 87–98.
2. J. Waters, L. Recent Developments in Skin Mimic Systems to Predict Transdermal Permeation.
3. Wang MBBS, X., Albahrani, Y., Pan, M., Levitt FAAD, J. & Levitt, J. Review Skin simulators for dermatological procedures. 21, (2015).
4. Korn, V., Imanidis, G., Skin Surface Topography and Texture Analysis of Sun-Exposed Body Sites in View of Sunscreen Application, Skin Pharmacol Physiol ;29:291–299 (2016)
5. Hof and hopperman Comparison of replica and in vivo measurement of the microtopography of human skin, SOFW Journal, Vol. 126, pp. 40-46 (2000)
6. Naser ST., Mechanical properties and the in-vivo response to porous polyurethane: an evaluation to provide an effective subdermal barrier against infection. In 56th Annual Meeting of the Orthopaedic Research Society, New Orleans, Louisiana, 6–9 March. Univ. PA Orthop J. 20, Poster no. 2169 2010
7. Kuwahara Y., Quantification of hardness, elasticity and viscosity of the skin of patients with systemic sclerosis using a novel sensing device (Vesmeter): a proposal for a new outcome measurement procedure. Rheumatology 47, 1018–1024. (2008)
8. Flament F, Bazin R. Facial skin pores: a multiethnic study. Clin. Cosmet. Investig. Dermatol. 8, 85–93. (2015)
9. Nigel AS, Christiano A. Regional variations in transepidermal water loss, eccrine sweat gland density, sweat secretion rates and electrolyte composition in resting and exercising humans. Extrem Physiol Med 2, 4. (2013)
10. Wilke K, Bie SS. A short history of sweat gland biology. Int J Cosmet Sci 29, 169–179. (2007)
11. Goldman L. Replica microscopy and scanning electron microscopy of laser impacts on the skin. J. Investig. Dermatol. 52, 18–24. (2006)
12. Datta S. Methods of use of substrate having properties of keratinous tissue. US 8,417,474 B2. (2013)
13. Mavon, A. et al. Sebum and stratum corneum lipids increase human skin surface free energy as determined from contact angle measurements: A study on two anatomical sites. Colloids Surfaces B Biointerfaces 8, 147–155 (1997).
14. Rosenberg, A., Williams, R. & Cohen, G. Interaction Forces Involved in Wetting of Human Skin. J. Pharm. Sci. 62, 920–922 (1973).
15. Mavon, A., Redoules, D., Humbert, P., Agache, P. & Gall, Y. Changes in sebum levels and skin surface free energy components following skin surface washing. Colloids Surfaces B Biointerfaces 10, 243–250 (1998).
16. Krawczyk J. Surface free energy of the human skin and its critical surface tension of wetting in the skin/surfactant aqueous solution/liquid system. Skin Res. Technol. 21, 214–223 (2015)

CHAPTER 4: FABRICATION AND CHARACTERIZATION OF CONTROLLABLE MODEL SYSTEM EMULSIONS

4.1 Introduction

Following the establishment of an efficient, robust and repetitive mimic that accurately replicated all aspects of interest of human skin, the fabrication of controllable model system emulsions that incorporated the basic structures and ingredients of current cosmetic products, yet are simple and tunable, was essential. Modern cosmetic products contain a significant number of ingredients serving multiple purposes including appearance, fragrance, rheological characteristics, preservation, claims, etc. However, in this study we focused on the impact of the chassis ingredients on retention of hydrophobic actives from the produced formulation on human skin, to exclude the impact of other ingredients, towards optimal understanding of the drivers of retention.

4.2 Fabricating Model System Emulsions

The purpose of this project was to study the retention of hydrophobic actives from a cosmetic cleansing and moisturizing product on human skin, hence the formulation required the incorporation of at least one anionic surfactant for its cleaning and foaming capabilities, in this case SDBS or sodium dodecyl benzensulphonate, a fatty acid for its structural capabilities when incorporated together with a surfactant and the

formation of lamellar colloid assembly, in this case lauric acid, a hydrophobic moisturizing agent for its hydrating capabilities, in this case petrolatum, sunflower oil and mineral oil, and finally water. The three different oil phases were chosen to evaluate the impact of oil viscosity in retention. The formulation process followed to fabricate the model system emulsions is described in detail in chapter 2.3. Table 4.1 demonstrates the Ingredient list and concentrations that were used to fabricate the model system emulsions. All three oil phases are products of the refining process of petrochemical or natural oils that consist of components of various molecular weights and as a result a representative molecular weight for each can-not be calculated. Hence the concentrations of the oils are expressed in w/w.

Table 4.1: Model system formulations. As oil phases, mineral oil, sunflower oil and petrolatum were used to study the impact of oil viscosity in retention.

	Low Oil Content	**Medium Oil Content**	**High Oil Content**
Anionic (Surfactant SDBS)	10% (0.29 M)	10% (0.29 M)	10% (0.29 M)
Fatty acids (Lauric Acid)	10% (0.50 M)	10% (0.50 M)	10% (0.50 M)
Oil Phase	20%	40%	60%
Water	Up to 100%	Up to 100%	Up to 100%

The following chart illustrates the number of model system emulsions produced, their characteristics and the focus points that each target. As demonstrated in the Figure 4.1, three parameters of interest were selected at three different levels each.

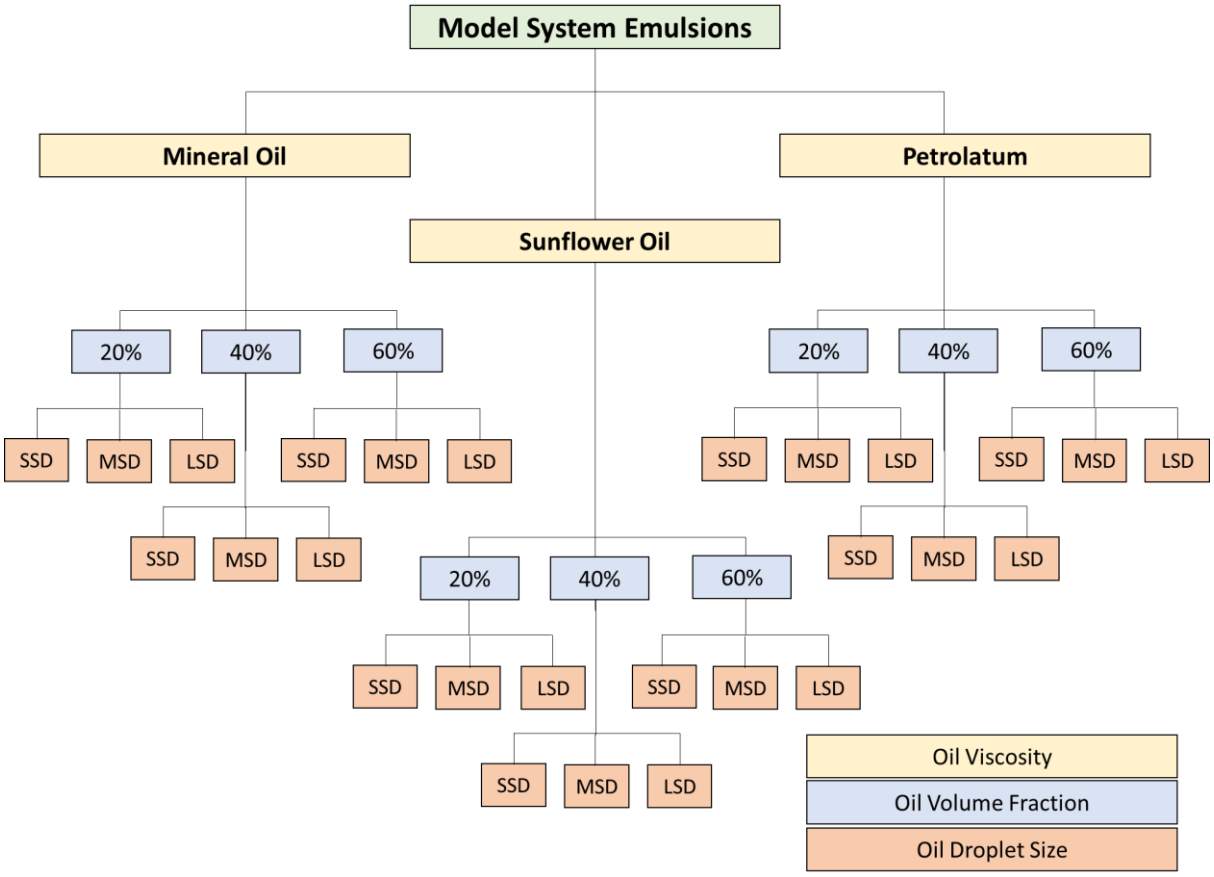

Figure 4.1: Illustration of the model system emulsions that were fabricated for the evaluation of hydrophobic active retention. Three independent parameters were selected, oil viscosity, oil volume fraction within the formulation and oil droplet size, and three levels for each of these parameters, leading in a total of 27 formulations required for this research. SSD represents the small size droplet emulsions, MSD the medium size droplet emulsions and LSD the large size droplet emulsions.

4.3 Oil Viscosity

The first independent parameter was oil viscosity and three levels were selected by choosing three different oils, mineral oil that shows a low viscosity at approximately 15cP at 25°C, sunflower oil that shows a medium viscosity of approximately 48cP at 25°C, and lastly petrolatum that represents an example of high viscosity being a semi solid, showing a value of 64000cP at 25°C [1,2]. Because of its semi solid nature, petrolatum demonstrates a significantly higher viscosity than the other oils used in

cosmetology at room temperature. Consequently, in order to present a more relevant comparison of the rheological profiles of the three oily phases, viscosity measurements of the selected oils took place at 40°C which is above petrolatum's melting point [3,4]. Furthermore, 40°C was the temperature of operation during the cleaning process in our experiments as well. Table 4.2 presents the results of the viscosity evaluation of the nominated oils and the differences amongst them.

Table 4.2: Viscosity values of mineral oil, sunflower oil and petrolatum at 40°C. A distinctive variance amongst the selected oils viscosity is observed.

	Mineral oil	**Sunflower oil**	**Petrolatum**
Viscosity (Pa.s) at 40°C	0.01±0.0	0.02±0.0	2.33±0.1

By choosing these three oils that exhibit a distinctive viscosity difference, the impact of oil phase viscosity will be studied as a driver of retention.

4.4. Volume Fraction of Oil

The second independent parameter was volume fraction of the oil phase in the cosmetic emulsion and three levels were selected, 20%, 40% and 60%. It is reasonable to expect that higher amounts of initial oil portion within the formulation would potentially lead to higher retention levels. However, the retained portion to initial portion fraction serves as a potent indication of effectiveness that supports the understanding of retention. Oily substances are expensive materials, hence the determination of an optimal oil phase concentration that would deliver sufficient retention on skin, yet avoid wasting material during rinsing, which could potentially provide significant cost savings during product development.

4.5. Oil Droplet Size

The third independent parameter that was accounted for during model system emulsion production was the droplet size of the oil phase. We have established that the synergy of anionic surfactants and fatty acids generated a lamellar structure within which the oil phase was dispersed. It is known that the mixing energy we apply to the system affects oil droplet size drastically, something that can be detected using a Mastersizer an instrument that measures droplet size distribution within emulsions given the refractive index and laser absorption values of the target material and the dispersant.

It is important to state here that to study the effect of oil droplet size in retention, given that we tested a significantly large number of emulsions that used three different oils at three different concentrations each, it was crucial that the three levels of droplet size targeted were the same for all the formulated model systems. The three levels chosen were small size droplet emulsions, SSD, that would exhibit average oil droplet dimensions below 5μm, medium size droplet emulsions, MSD, that demonstrate average oil droplet dimensions between 35-55 μm and lastly large droplet size emulsions, LSD, that demonstrate large oil droplets of at least 100μm. The droplet size range was selected after careful consideration of human skin topographic features, dimensions, roughness levels and our hypothesis of physical entrapment of the droplets within the patterned surface of the mimics that contain pores and patterns in the range from 40 to 80μm, just like human skin as presented in the literature [8,9]. The small size droplet emulsions were designed to have very small dimension oil

droplets that would slide within the pores, wrinkles and texture of the skin. The medium size droplet emulsions exhibited oil droplets of similar dimensions to human skin pores to evaluate the impact of physical entrapment within pores to retention. Lastly the large size droplet emulsions demonstrated significantly larger dimensions, way above stratum corneum topographic texture.

However in such complex systems, like the formulated model system emulsions, it was hard to correlate a specific shear value or RPM settings of the high shear homogenizer to a specific oil droplet size outcome, especially when different oil phases have been selected. Consequently, a significant amount of trial and error took place to identify the RPM settings of the high shear homogenizer that delivered a similar range of oil droplet size in all the formulated systems. It was found that higher shear was required to achieve the same levels of droplet dimensions for higher viscosity oil phases in comparison to thin, less viscous, oils. Petrolatum, that demonstrated the highest viscosity of all the tested oils, required 1000 RPM mixing for 10 min in the high shear homogenizer to produce formulations of LSD, as described above, 2500 RPM for 10 minutes to produce MSD emulsions and 4000 RPM for 10 min to produce SSD emulations. Sunflower oil emulsions required 500 RPM, 750 RPM and 1000 RPM for 10 min accordingly in order to produce LSD, MSD and SSD emulsions of equivalent droplet dimensions to the petrolatum formulations. The mineral oil emulsions required the least amount of shear with 400 RPM for 10 min towards the production of LSD emulsions, 600 RPM for the MSD emulsions and 800 RPM for the SSD emulsions. All the formulated systems were tested in the Mastersizer to evaluate the achieved droplet size distribution. Figure 4.2 presents the distribution results.

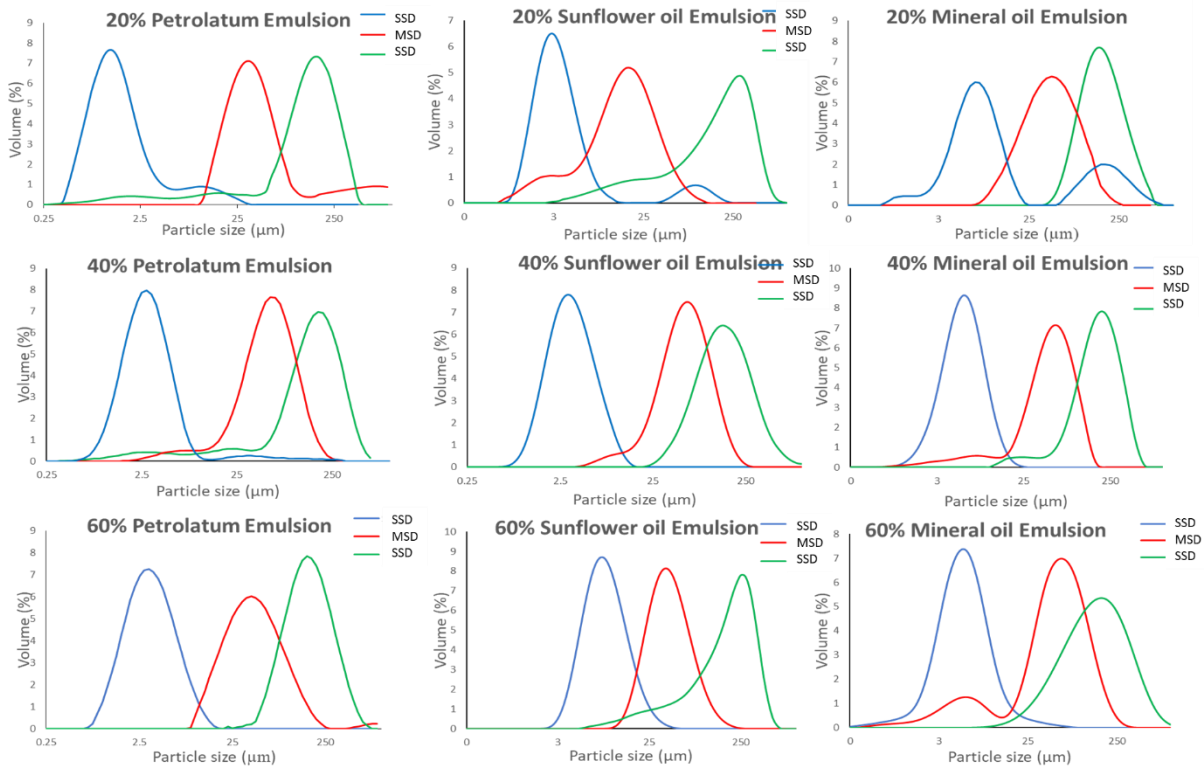

Figure 4.2: Mastersizer graphs exhibiting the achieved droplet size distribution in all 27 produced model system emulsions.

It is evident in Figure 4.2 that all the model system formulations demonstrated significant similarities across the levels of oil droplet size. This enabled us to trust the results and accurately study the impact of droplet size on retention. The difference in shear levels required amongst the three different oil phases to achieve similar levels of droplet size is remarkable with petrolatum emulsions undergoing the highest levels of shear and mineral oil the lowest.

In the Gaussian distributions, illustrated in Figure 4.2, the median value is often used as the representative droplet size distribution of the tested emulsions. This value, D50, expresses the droplet dimension that separates the distribution of droplets in half. In other words, D50 is the droplet size at which 50% of the distribution shows dimensions

lower than it and 50% higher than it. Similarly, D10 is the droplet size value in μm, below which 10 % of the distribution stands and D90 the droplet size value below which 90% of the droplets are sited. These three characteristics for a distribution curve metrics can demonstrate the span of the ellipsoid using the following equation:

$$Span = \frac{D_{90} - D_{10}}{D_{50}} \quad (21)$$

The span of a distribution curve is a dimensionless parameter, that gives vital information on the distribution range of the droplets in the formulation. Two emulsions can show the same median value D50 and yet have drastically different spans with one demonstrating a large range of droplet sizes and a very broad curve whereas the other exhibits a narrow curve and a high concentration of droplets sizes near its median value. In order to study the true effect of droplet size in retention it is optimal to have formulations that show low spans, preferably below 5, so that the study of the impact of that specific droplet dimension is ensured. The peak value is the droplet size in μm that showed the highest volume of droplets assuming it. The following, Table 4.3 and Figure 4.3, demonstrate an example of D10, D50, D90 and Peak, highlighted on a graph of one of the formulated model system emulsions, the SSD 40% sunflower oil emulsion.

Table 4.3: 40% sunflower oil emulsion droplet distribution metrics.

40% Sunflower oil	SSD
D10	1.41
D50	3.98
D90	7.94
Span	1.64
Peak	4.47

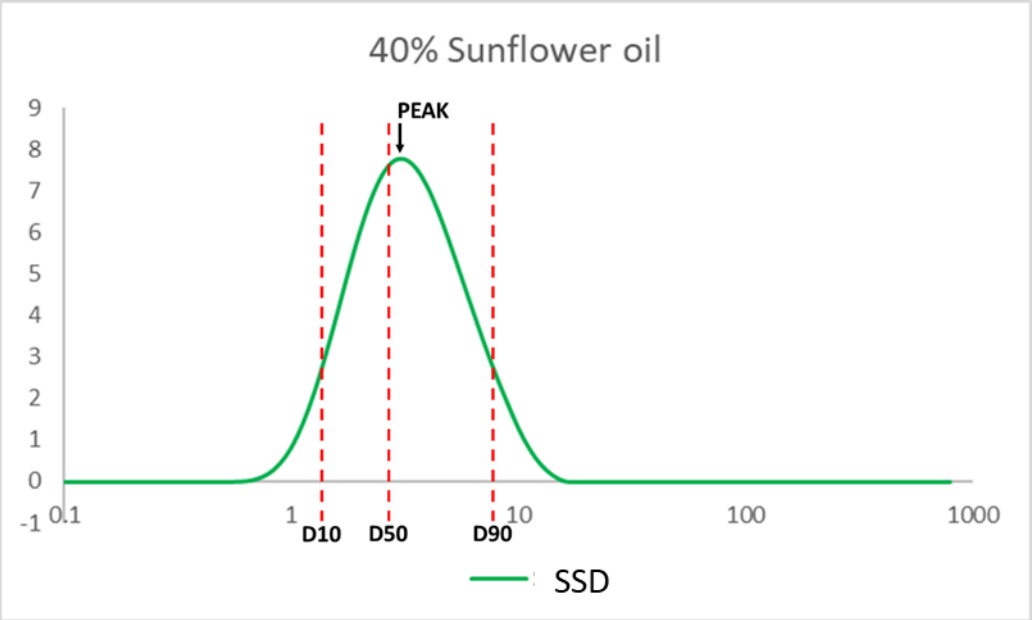

Figure 4.3: Mastersizer graph exhibiting the achieved droplet size distribution of the 40% sunflower oil emulsion.

As illustrated in Figure 4.3, the peak and median value do not necessarily overlap, however the more symmetric the distribution curve the closer these two values are. Additionally, the formulated emulsion exhibited a low span as shown in Table 4.3 and the corresponding Figure 4.3.

The following Tables demonstrate the D10, D50, D90 and peak values for all the fabricated emulsions.

Table 4.4: 20%, 40% and 60% petrolatum emulsions droplet distribution metrics. All concentrations demonstrated similar median values on the equivalent droplet sizes and low span values.

20% Petrolatum	LSD	MSD	SSD
D10	14.13	15.85	0.63
D50	141.25	31.62	1.26
D90	316.23	63.10	5.62
Span	2.14	1.49	3.97
Peak	177.83	31.62	1.26

40% Petrolatum	LSD	MSD	SSD
D10	22.39	19.95	1.26
D50	158.49	50.12	2.51
D90	316.23	100.00	5.01
Span	1.85	1.60	1.49
Peak	158.49	44.67	5.01

60% Petrolatum	LSD	MSD	SSD
D10	63.10	15.85	1.41
D50	141.25	44.67	3.16
D90	281.84	125.89	7.08
Span	1.55	2.46	1.79
Peak	199.53	35.48	6.31

In Table 4.4, the distribution metrics for the petrolatum emulsions are presented. We have chosen the median droplet size as the independent parameter of the study and the span as an indicator of formulation quality. As mentioned above we focused on the production of emulsions that demonstrated low levels of span so that the effect of droplet size can be evaluated more accurately.

The petrolatum emulsions demonstrated similar values of median droplet size in all tested concentrations but also in comparison to the formulations that incorporated sunflower and mineral oils, as shown in Tables 4.5 and 4.6.

Table 4.5: 20%, 40% and 60% sunflower oil emulsions droplet size distribution metrics. It is shown that all concentrations exhibit similar median values of the equivalent droplet sizes and low span values.

20% Sunflower oil	LSD	MSD	SSD
D10	15.85	7.08	1.26
D50	158.49	35.48	2.51
D90	398.11	141.25	5.01
Span	2.41	3.78	1.49
Peak	223.87	39.81	2.51

40% Sunflower oil	LSD	MSD	SSD
D10	25.12	12.59	1.41
D50	158.49	50.12	3.98
D90	316.23	199.53	7.94
Span	1.84	3.73	1.64
Peak	141.25	56.23	4.47

60% Sunflower oil	LSD	MSD	SSD
D10	35.48	4.47	1.41
D50	125.89	56.23	3.98
D90	562.34	223.87	8.91
Span	4.18	3.90	1.88
Peak	177.83	44.67	3.98

Table 4.5 demonstrates the metrics that characterize the sunflower oil formulation curves for all levels of concentration and droplet size. Once more, all equivalent size levels are similar with each other and to the formulations produced with the other two selected oil phases.

Table 4.6: 20%, 40% and 60% mineral oil emulsions droplet size distribution metrics that demonstrate similar median values on the equivalent droplet sizes and low span values in all concentration levels.

20% Mineral oil	LSD	MSD	SSD
D10	79.43	15.85	2.51
D50	158.49	39.81	5.62
D90	398.11	100.00	11.22
Span	2.01	2.11	1.55
Peak	158.49	44.67	6.31

40% Mineral oil	LSD	MSD	SSD
D10	89.13	11.22	2.51
D50	141.25	56.23	3.16
D90	398.11	158.49	7.08
Span	2.19	2.62	1.44
Peak	199.53	39.81	4.47

60% Mineral oil	LSD	MSD	SSD
D10	39.81	11.22	1.12
D50	141.25	56.23	3.98
D90	354.81	112.20	6.31
Span	2.23	1.80	1.30
Peak	177.83	50.12	6.31

Lastly, in Table 4.6, the characteristic distribution values of the mineral oil emulsions are illustrated. All curves showed comparable median values on the equivalent droplet size levels with each other and with their corresponding petrolatum and sunflower formulations. Additionally, low spans where shown in all formulations, allowing the effective study of the impact of droplet size on retention.

In conclusion, 27 model system emulsions where formulated successfully, demonstrating distinctive independent parameters of interest, so that their impact on

retention can be investigated. The first of the nominated independent parameters was the viscosity of the oil phase, where three levels were chosen by incorporating three different oils of characteristic rheological profiles, petrolatum, sunflower oil and mineral oil. The second independent parameter was oil concentration, three levels of which were chosen, 20%, 40% and 60% to evaluate the correlation of the oil portion in effective retention and potentially propose an optimal oil value that provides potent retention yet minimizes material loss. The third independent parameter was oil droplet size to produce formulations that demonstrated characteristic droplet size distributions in similar ranges for the corresponding formulations, trial and error experiments took place to correlate the shear energy during mixing to the produced droplet size distribution. The levels chosen were small size droplet emulsions with median droplet dimensions below 5um, medium size droplet emulsions with median values that ranged from 35-55um and lastly large droplet size emulsions that demonstrated median droplet sizes larger than 100um in diameter. All formulated emulsions demonstrated high control of the parameters of interest, long lasting stability, repetitive properties and enabled efficient characterization of their impact on oil retention.

4.6. Rheology of Produced Model System Emulsions

The rheological characteristics and especially the viscosity of the produced emulsions was evaluated using the rheometer. The higher viscosity oils were expected to generate emulsions with higher end product viscosities as well, which is shown in Table 4.7. The following graph demonstrates a typical rheology graph of a produced model

system emulsion, in this case the 20% petrolatum, small size droplet, showing its shear thinning behaviour.

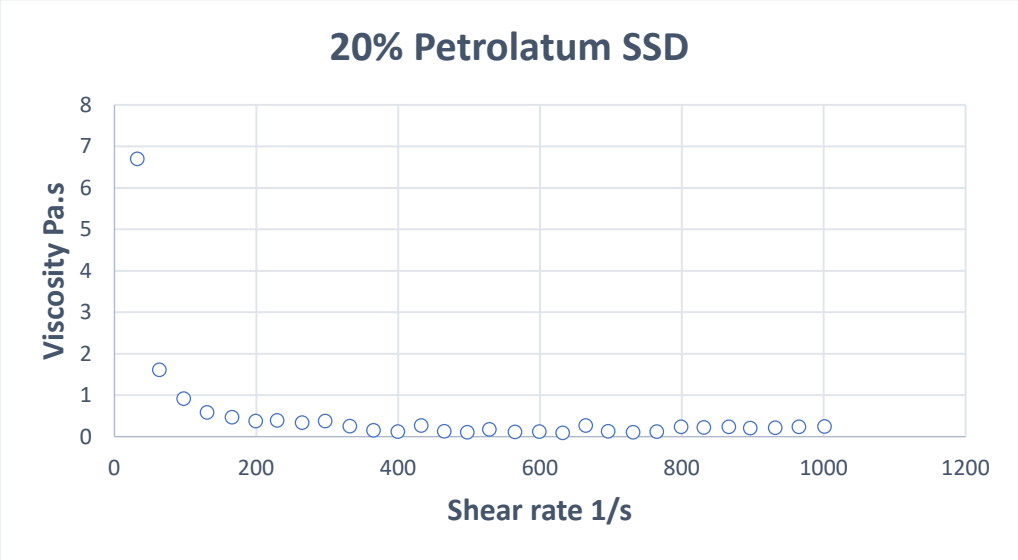

Figure 4.4: Rheology profile of 20% petrolatum emulsion, SSD. The shear thinning behavior of the emulsion is demonstrated.

The graph in Figure 4.4 demonstrates the shear thinning characteristics of the 20% petrolatum, SSD emulsion. The curve illustrates the correlation of the viscosity to shear rate and the reduction of the viscosity in duration of applied shear. This behavior is well known in the literature and is described as shear thinning of non-Newtonian fluids. In other words, increasing shear applied on a shear thinning material leads to lower values of resistance as it moves, hence lower viscosity values [5-7]. All formulated model system emulsions showed shear thinning behavior and rheological profiles similar to that of the Graph in Figure 4.4. Once the viscosity value reaches a lower plateau on the graph its value is no longer influenced by the shear force, this is then

considered a representative viscosity value for the characterization of that formulation. The viscosity values of all formulated emulsions are presented in Table 4.7.

Table 4.7: Measured viscosity figures (in Pa.s) for all the fabricated model system emulsions. Measurements took place in the rheometer at 25°C. Formulations containing Petrolatum, exhibited a clear advantage in viscosity due to the highly viscous behavior of petrolatum.

Viscosity (Pa.s)	20% Petrolatum	40% Petrolatum	60% petrolatum
SSD	0.75±0.11	0.97±0.10	1.71±0.19
MSD	0.68±0.08	0.88±0.9	1.34±0.32
LSD	0.73±0.02	0.94±0.11	1.39±0.47

Viscosity (Pa.s)	20% Sunflower oil	40% Sunflower oil	60% Sunflower oil
SSD	0.25±0.07	0.32±0.10	0.34±0.05
MSD	0.21±0.06	0.22±0.05	0.30±0.01
LSD	0.19±0.02	0.22±0.09	0.18±0.03

Viscosity (Pa.s)	20% Mineral oil	40% Mineral oil	60% Mineral oil
SSD	0.19±0.02	0.24±0.04	0.19±0.0
MSD	0.18±0.01	0.18±0.07	0.15±0.01
LSD	0.16±0.02	0.17±0.03	0.09±0.01

As shown in Table 4.7, petrolatum emulsions exhibited the highest viscosities in comparison to the other two oil phases, in all concentrations and droplet sizes. Additionally, in the case of petrolatum, higher oil concentrations lead to higher viscosity values of the product due to the viscous, semi-solid nature of petrolatum, something that was not detected in the other two oil phases that had similar viscosity values in all concentrations. Furthermore, SSD emulsions in all three oil phases, demonstrated higher viscosities than those of MSD and LSD. This is attributed to the formed lamellar

structure that thickens with increasing shear, which was higher in the case of SSD emulsions for the formation of the smaller droplets. The increased amounts of shear applied to the system lead to an improved lamellar structure orientation hence higher viscosity [8]. As shown in Table 4.6, there is a distinctive range of viscosities amongst the different oil phase emulsions, however the control parameter in this research was the initial oil viscosity and not that of the sheared product.

4.7 Optical Characterization of the Produced Microstructure of the Model System Emulsions

Our hypothesis was that the combination of anionic surfactant and fatty acid as a co-emulsifier would work synergistically towards the formation of a lamellar structure that would raise the viscosity of the chassis and allow the efficient distribution of the oily phase in a stable and homogenous way [9-14]. In low viscosity oils like mineral and sunflower oil, the formation of an oil in water emulsion is fairly straightforward and does not require a sophisticated structure for the oil to be dispersed in, just an adequate amount of surfactant for the emulsification of the two phases [15]. However, in high viscosity semisolids like petrolatum, an oil in water emulsion was challenging to produce since just the presence of surfactant and the applied mixing energy to the system were not sufficient to produce a homogenous and stable emulsion even at high levels of surfactant ratios and mixing energy [16]. The incorporation of the oily phase in a lamellar gel chassis enables the stable encapsulation of petrolatum between the lamellar vesicles and provides homogeneity and long-lasting stability of the product. To evaluate the achieved microstructure, the produced emulsions were visualized

using cryo-SEM, a common optical characterization technique in liquid formulation. Initially the samples were placed within the sample holder of the instrument where they were frozen with liquid nitrogen and then fractured within the chamber with a needle so that the microstructure of the emulsion could be revealed.

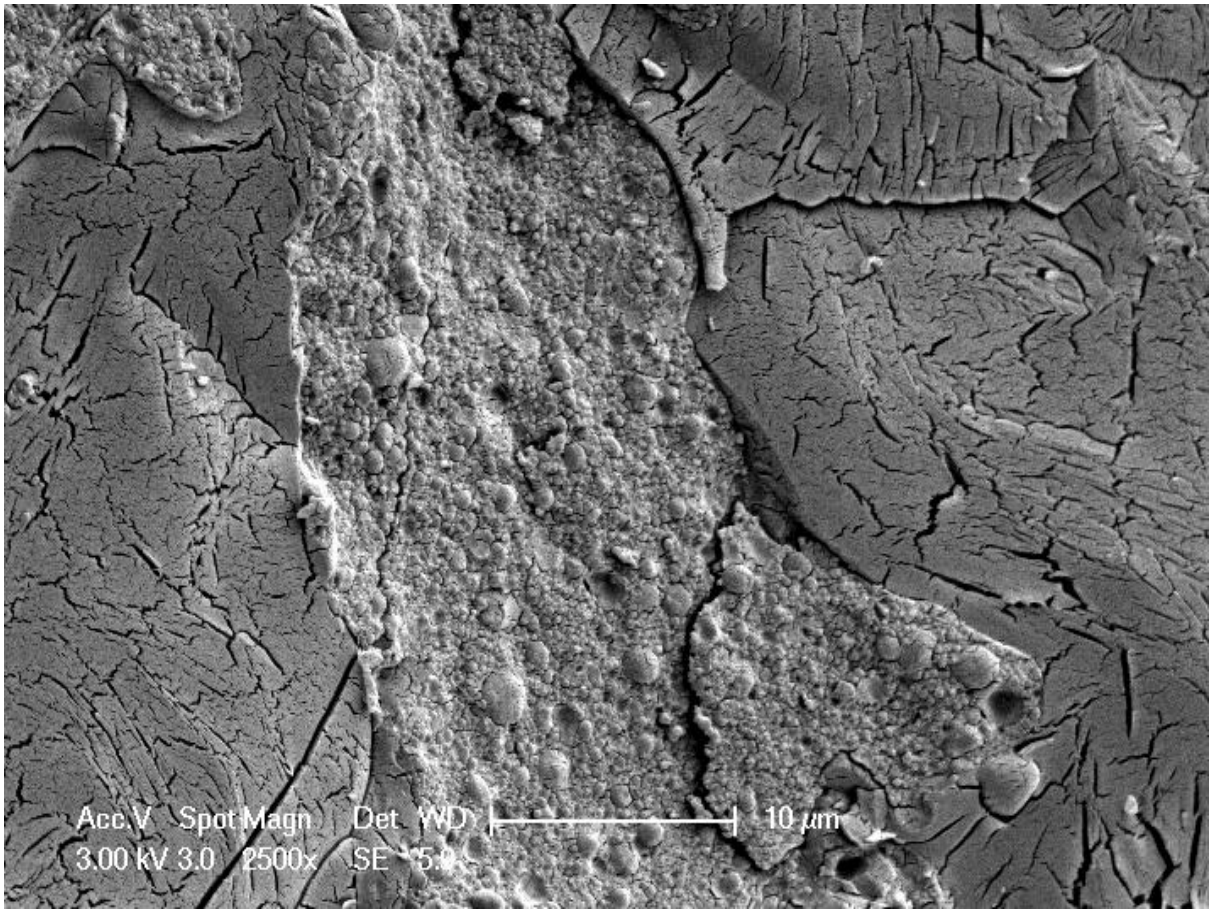

Figure 4.5: Cryo SEM image of the microstructure of the formulated model system emulsion, 20% petrolatum SSD emulsion. The lamellar sheets with deposited petrolatum droplet layers can be seen. The majority of the petrolatum droplets exhibit low dimensional size.

In Figure 4.5, an example of the achieved microstructure of the 20% petrolatum emulsion that exhibited small droplet size of oil is illustrated. The cracked area shown is the water phase of the emulsion, whereas the one with the integrated droplet structure is the oily phase. The lamellar sheets are clearly illustrated in Figure 4.5 and

the petrolatum droplets are deposited within the structure as highlighted. Using the image analysis software, ImageJ, the dimensions of the petrolatum droplets were evaluated, and the demonstrated values came to an agreement with the Mastersizer results which in this particular emulsion ranged between 1-10um. The produced lamellar structure enabled efficient oil phase dispersion in all oil types and concentrations, leading to stable and homogeneous products that demonstrated variable oil droplet sizes. Additionally, the lamellar gel structure provided a flexible and robust chassis that could be used as the base of various purpose cosmetic products.

4.8. Conclusions

Model system emulsions were fabricated towards the evaluation of different parameters on retention of hydrophobic actives on human skin after the use of a cosmetic formulation. The model system emulsions showed a very simplistic ingredients list to eradicate the effect of unwanted elements and focus on the variables of interest. In this project, three hydrophobic components were tested, petrolatum as a high viscosity oil choice, sunflower oil as a medium viscosity representative and mineral oil as a low viscosity option. The emulsions produced exhibited three levels of oil volume fraction, 20%, 40% and 60% and finally different amounts of shear were applied to generate a variance of oil droplet size samples and test the effect of the latter on oil retention. The produced emulsions were evaluated for their droplet size distribution using the Mastersizer, for their viscosity using the rheometer and for the achieved lamellar sheet microstructure using the Cryo-SEM.

4.9 References

1. Mineral Oil. Available at: https://www.arb.ca.gov/db/solvents/solvent_pages/Hydrocarbon-HTML/Mineral_Oil.htm. (Accessed: 8th November 2018)
2. MINERAL OIL (HIGH VISCOSITY). http://www.fao.org/fileadmin/user_upload/jecfa_additives/docs/Monograph1/Additive-282-rev.pdf?_sm_au_=iVVJ8pNb8skRcFH5
3. Viscosity | EXACT Dispensing Systems. Available at: https://exactdispensing.com/downloads/reference-data/exact-viscosity/. (Accessed: 8th November 2018)
4. Liquid Viscosities. Available at: http://plastics.fwwebb.com/Asset/Industrial-Meter-Catalog-Version-6-Page-68.pdf?_sm_au_=iVVJ8pNb8skRcFH5
5. Mezger, Thomas G. (2006). The rheology handbook: for users of rotational and oscillatory rheometers (2., rev. ed.). Hannover: Vincentz Network. p. 34.
6. An Introduction to Rheology - H A Barnes, J F Hutton, K Walters - Google Books. Available at: https://books.google.co.uk/books?hl=en&lr=&id=VKj8BAAAQBAJ&oi=fnd&pg=PP1&dq=rheology&ots=E-GybDfGTA&sig=Cw4HH1RSUqwkrPKVpR3PJJV0UxM#v=onepage&q=rheology&f=false. (Accessed: 8th November 2018)
7. Whorlow, R. W. Rheological Techniques. (Halsted Press/John Wiley & Sons, 1980).
8. Wunenburger A.S., Colin A., Leng J., Arnéodo A., Roux D., Oscillating Viscosity in a Lyotropic Lamellar Phase under Shear Flow. Physical Review Letters, American Physical Society, 86, pp.1374 (2001).
9. Battaglia, G. & Ryan, A. J. The evolution of vesicles from bulk lamellar gels. Nat. Mater. 4, 869–876 (2005).
10. Koynova, R. & Tenchov, B. Interactions of surfactants and fatty acids with lipids. Current Opinion in Colloid & Interface Science 6, 277-286, (2001)
11. Katsaras, J. & Raghunathan, V. A. Aligned Lipid—Water Systems. in Lipid Bilayers 25–45 (2001).
12. Grewe, F., Ortmeyer, J., Haase, R. & Schmidt, C. Colloidal Gels Formed by Dilute Aqueous Dispersions of Surfactant and Fatty Alcohol. in Colloid Process Engineering 21–43 (2015).
13. Anionic surfactants - an overview | ScienceDirect Topics. Available at: https://www.sciencedirect.com/topics/pharmacology-toxicology-and-pharmaceutical-science/anionic-surfactants. (Accessed: 8th November 2018)
14. Kaler, E. W., Herrington, K. L., Murthy, A. K. & Zasadzinski, J. A. N. Phase behavior and structures of mixtures of anionic and cationic surfactants. J. Phys. Chem. 96, 6698–6707 (1992).
15. Smith, A. L. & Society of Chemical Industry (Great Britain). Colloid and Surface Chemistry Group. Theory and practice of emulsion technology: proceedings of a symposium organized by the Society of Chemical Industry and held at Brunel University, September 16-18, 1974. (1976).

16. Shacketford, C. & Cordero, T. The Preparation of Liquid Petrolatum Emulsions Using Gelatin and Domestic Gum. J. Am. Pharm. Assoc. (Scientific ed.) 32, 163–165 (1943).

CHAPTER 5: DESIGN AND ENGINEERING OF THE DEPOSITION AND CLEANING SET-UPS

5.1 Background

Cosmetic product performance is strongly linked with the parameters that define its use. In a cleansing product, the parameters that impact deposition, including portion of product per skin area, lateral force of application, speed of application, number of cycles, etc, as well as the parameters of product removal, including flowrate of rinsing water, temperature of water, angle of flow, applied shear, etc, all affect the performance of the product both in cleaning the substrate and in depositing the moisturizing component. To enable the accurate comparison of hydrophobic active retention levels amongst the range of fabricated model system emulsions on the skin mimic substrates, it was crucial to ensure that the deposition method and the cleaning protocol would be highly controlled and repetitive to eliminate the impact of experimental error in these steps that would later influence retention levels. To achieve this, two highly controlled set-ups were designed, one for the deposition of the formulation on the mimics and one for the removal of the product of the substrate. In this chapter the deposition and cleaning set-ups will be discussed, and their parameters will be explained in detail.

5.2 Deposition Set-Up

To ensure a highly controlled deposition of the model system emulsions on the optimized skin mimic substrates, a tribometer was modified into a deposition set-up. The tribometer instrument compartments and capabilities are described in Chapter 2. The upper moving part of the instrument was modified by positioning a flat skin mimic face down on it, so that it could be in contact with the sample skin mimic on the sample base. Consequently, the product application took place by adding the material over the sample, and the skin mimic to skin mimic smearing lead to the formation of an even film of the product on the sample. Additionally, to represent more effectively real-life conditions, the bottom sample holder of the instrument was modified by adding a highly accurate heating plate so that the sample temperature could be added to the control parameters of this step. The importance of skin temperature in product deposition is crucial since some cosmetic ingredients like petrolatum exhibit melting points near human skin temperature, although they show semi-solid capabilities at room temperature, when applied on skin, the combination of skin temperature and shear liquify them and make them spread more effectively. Consequently, the need to control the skin mimic sample temperature at 35°C was paramount for the correlation of the project to real life conditions and to accurately study retention.

As far as this project is concerned, key parameters of the deposition step were the initial amount of emulsion, lateral force of application, number of cycles, speed of movement and the temperature of the sample skin mimic. The skin mimic area was 1x1 cm^2, the initial portion of emulsion selected was 2ml, the lateral force was 100g, the speed of movement 10mm per second, the number of cycles was 5 and the

temperature of the mimic was set at 35°C. Figure 5.1 is an illustration of the deposition set-up.

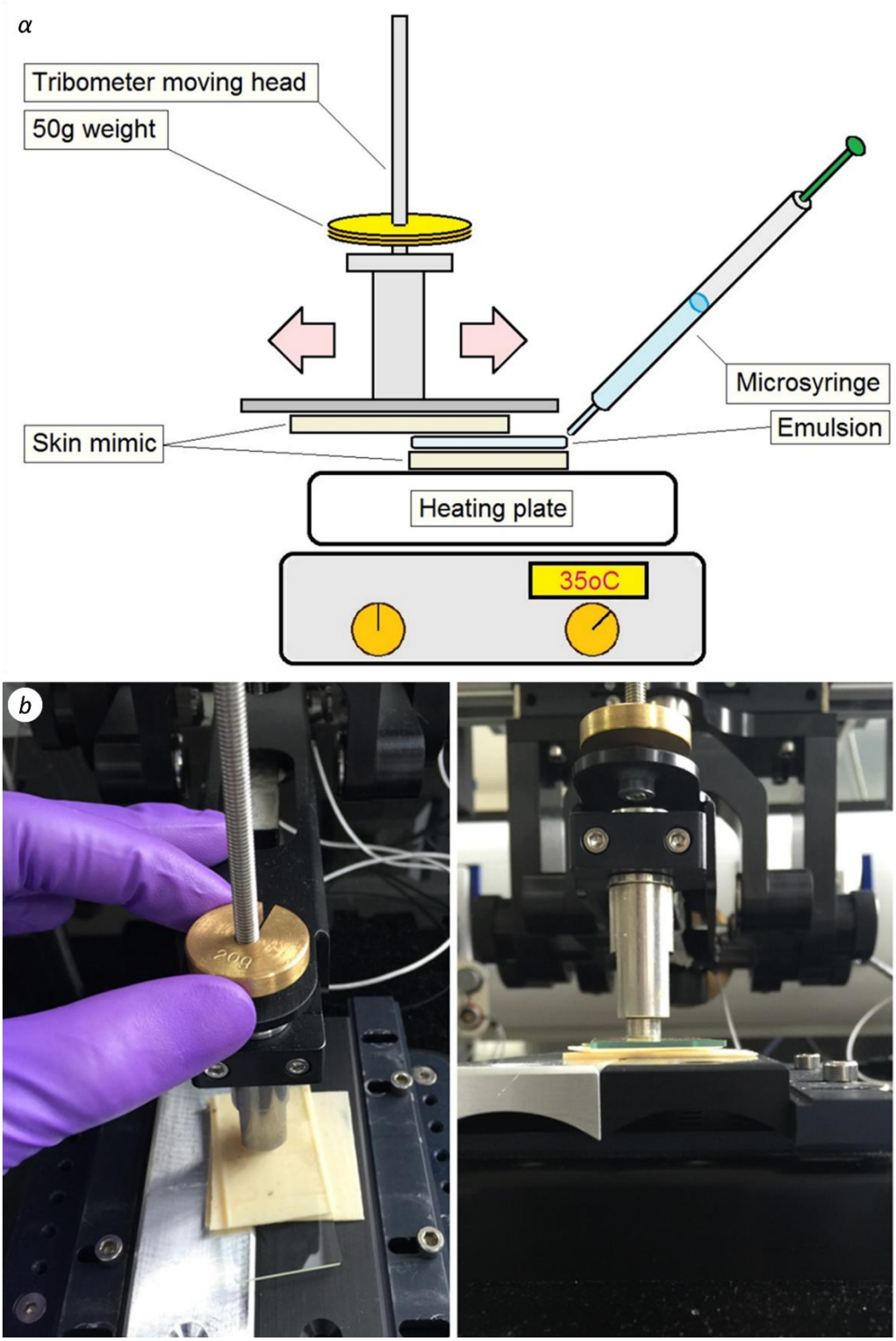

Figure 5.1: Deposition set-up (α) and corresponding image (b) where the skin mimic on skin mimic homologation is illustrated. The standard weight discs are used to control the lateral force whereas the

heating plate controls the temperature of the skin mimic sample. The speed and number of cycles are controlled by the panel of the tribometer instrument, leading to a controlled and repetitive deposition of the product.

In Figure 5.1, the schematics of the designed deposition set-up and the corresponding images are presented. The skin mimic on skin mimic contact was essential to represent effectively real-life conditions. The accurate moving arm ensured repetition of all deposition parameters in all test samples and an even distribution of shear forces, an important condition in comparative studies like this. Moreover, the addition of the heating plate, introduced temperature control to the system which was especially significant to better embody product use in vivo.

For the purposes of this project, four skin mimic samples were prepared for each model system emulsion and had product deposited on them. The samples were weighed before and after the application step. The controlled deposition set up provided a very repetitive product film of 2.02±0.03mg. The characteristically low standard deviation of the achieved film weight demonstrated the level of accuracy and repetition of the designed deposition system.

5.3 Cleaning Set-Up

The following step was the cleaning or rinsing step of the skin mimics with product deposited on them by introducing them to a cleaning apparatus. However, during showering, several product removal actions take place including direct rinsing of the area with water from the shower head, product removal by a film of water driven by gravity and slow dilution of the product as it moves, mechanical shear by hand followed by rinsing, etc. The cleaning habits of each consumer are subjective as well as the parameters that drive cleaning like water flow rate, temperature, etc. Hence, it was imperative to simplify this process and develop a repetitive and controlled rinsing method to accurately remove the produced emulsions from the mimics in a system that replicates shower conditions. Again, a novel set-up that demonstrated the required characteristics while providing high control for the user was created. In this project, cleaning by water rinsing only was assumed. The cleaning system was designed as a downscaled version of a shower head, limited to a single water jet but maintaining all the parameters that affect cleaning or product removal from the skin topography while rinsing.

The cleaning apparatus consisted of a water tank placed on a heating plate to ensure water temperature regulation, an accurate water pump that retrieved water from the tank and released it onto the sample at a certain flow rate, through a 3D printed exit nozzle of 1mm output diameter. Moreover, the skin mimic samples were placed on a variable angle sample holder within a collection container. A timer was used to keep rinsing times and a tripod and camera were employed to record videos of the cleaning process. Detailed information on the components used in the cleaning apparatus can be found in chapter 2. The parameters of focus at this step were water flow rate, water

temperature, duration of flow and angle of flow. The following Figure 5.2 illustrates the schematics and corresponding image of the designed cleaning apparatus.

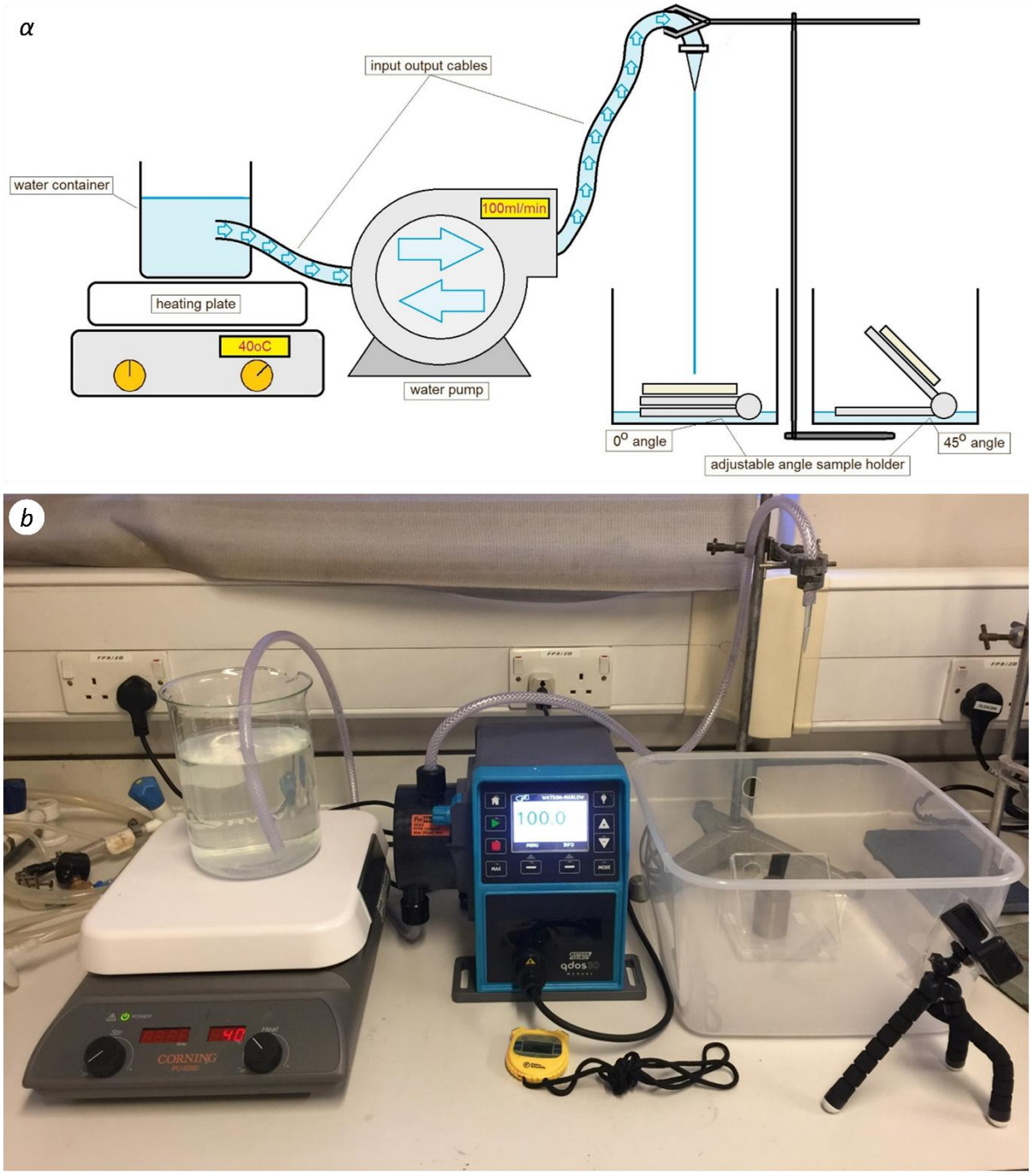

Figure 5.2: Cleaning apparatus schematic (α) and corresponding image (b) that shows the basic components of the system and represents a downsized version of a shower.

The water flow rate was calculated using the maximum flowrate value according to UK regulations as described by the UK government [1], which for traditional showerheads (non-aerating) was 8-10 l/min. Given that an average showerhead in the market consists of 80-100 single jets in its structure, the flow rate of each individual jet can be calculated by dividing the showerhead flowrate to the number of single jets. Consequently, the minimum calculated single water jet flowrate, assuming a total flow rate value of 800ml/min and 100 single jets per showerhead, was 80ml/min whereas the maximum single water jet flow rate, assuming a total showerhead flowrate of 1000ml/min and 80 single jets per shower, was 125ml/min. Hence a flowrate of 100ml.min was selected for the experiments carried out in this project.

As far as water temperature is concerned, the rinsing water was stored in a beaker and placed on a heating plate set at 40°C, which is an average shower temperature according to UK government reports [2,3]. The water temperature was ensured using a thermometer before the beginning of rinsing. The significance of this parameter is vital due to the dilution variance of materials in water at different temperatures. Higher water temperature leads to more effective removal of product from skin topography, hence it was crucial for all the samples to be treated at the same temperature.

The duration of rinsing is a subjective matter that only depends on consumer preference. It is expected that for longer rinsing times of the sample less product would remain within its microtopography. However, a lot of information can be retrieved by testing the retention levels at three different rinsing durations. The three levels selected were 30, 60 and 90 seconds and we assumed that the majority of the material would be removed in the first few seconds of rinsing and therefore the samples would reach a plateau of a minimum retention that would not change with further rinsing.

During showering, water from the showerhead hits human skin in various angles depending on the structure of the shower and preference of the consumer. In this project, the angle of flow was another independent parameter, due to the initial assumption that certain angles of flow might lead to improved water access into the topography of the skin and result in more efficient cleaning and reduced product retention. This assumption is based on the theory that retention is mainly driven by the physical entrapment of the product onto the skin microtopography and not by chemical bonding of the formulation molecules with the stratum corneum cells. To produce quantitative data of the impact of flow angle on retention, a variable angle sample holder was developed that enabled sample angles of 0, 45 and 60 degrees that translate in water flow angles of 90, 45 and 30 degrees respectively.

Consequently, the cleaning set-up was a clear representation of the shower process characterized by high levels of control on all the independent parameters involved. In this step, two of the independent parameters, the rinsing duration and rinsing angle, were evaluated for their impact on retention by choosing three levels of each of these and performing experiments. The flow rate and water temperature were kept as standard for all samples. The skin mimic samples were introduced to the cleaning set-up directly after the deposition step, and then moved to a fume cupboard to dry in ambient conditions. Once dried, the samples were weighed again to calculate the amount of retained product and then characterized visually using fluorescent microscopy.

5.4 References

1. Why think about showers? Available at: https:// www.opsi.gov.uk/si/si1999/19991148.htm. (Accessed: 26th September 2018)
2. Health Services – Scalding and burning. Available at: http://www.hse.gov.uk/healthservices/scalding-burning.htm. (Accessed: 26th September 2018)
3. Angel, C. & Director, C. Controlling Scalding Risks from Bathing and Showering 2 of 12 Guidance on Bathing and Showering-Version 3. (2010).

CHAPTER 6: UNDERSTANDING AND EVALUATION OF RETENTION OF HYDROPHOBIC ACTIVES FROM COSMETIC FORMULATIONS ON THE HUMAN SKIN

6.1 Retention Characterization

The aim of this project was the development of a method that would enable the understanding and evaluation of retention of hydrophobic actives from cosmetic formulations on human skin, while being simple to use, repetitive, accurate, representative of product use in real life, cost and time efficient and tuneable. In the previous sections, the developed method components and their characteristics were described, from the fabrication of the optimized skin mimic samples and the model system emulsions, to the development of highly controlled deposition and cleaning set-ups. In this section, the protocol followed, the retention characterization techniques and the results analysis will be presented and explained. As mentioned before, five independent parameters with three levels each were selected for this study and their impact on retention was characterized. Three of these parameters were related to the formulation and were oil viscosity, oil concentration and droplet size. The other two, were related to the rinsing method and were rinsing duration and angle. A

complementary, small scale, proof of concept experiment took place to study the effect of skin topography, where two different levels of substrate surface were evaluated.

Due to the high number of parameters, levels and limited time, a full factorial approach to this study was not feasible and as a result a full factorial approach only took place for the petrolatum model system emulsion of 20% concentration, all three droplet sizes, all three durations of rinsing and two levels of flow angle. A design of experiment approach was assembled to study the impact of all the selected parameters on all their levels, which will be explained in detail in the following Chapter 7. In this section the protocol followed is explained as well as the results and discussion of the full factorial approach.

6.1.1. Experimental Protocol

The protocol followed on the full factorial approach started with optical evaluation of the mimics and preparation of the investigated model system emulsion. Following, the mimics were weighed and labelled. The mimics were wetted and placed on the deposition set up sample holder and left for 5min until they reached a temperature of 35°C. Then 2ml of the emulsion were placed within the interface between the substrate and the mimic attached to the upper arm of the tribometer. The deposition process was then initiated, and an even film was created on the bottom mimic. Four skin mimic samples were prepared for each of the tested emulsions. The mimics were afterwards weighed again for the evaluation of the deposition process. Further, the samples were moved on the cleaning apparatus and placed on the sample holder, the angle of flow was selected and when the water temperature was set at 40°C, the rinsing process

could start. The time was kept using an electronic timer. After the rinsing was complete the samples were carefully removed and placed in a fume cupboard and left to dry in ambient conditions for 20 min. The samples were then tested visually using the fluorescent microscope. The produced images were analysed using imageJ software and the grey scale intensity data were used to produce graphs. Following that, the mimics were weighed, and those values fed into a gravimetric analysis of the retained product that complemented the image analysis data. Lastly the mimics were tested as for their coefficient of friction since the retained oil would act as a lubricant and lower the friction of the mimic in comparison to a clean one. The last method is a common conditioning product characterization method in the industry.

6.1.2 Retention Characterization Techniques

The three selected methods to evaluate retention, all targeted specific alterations of the sample due to the retained product portion. Fluorescent microscopy not only provided a visual illustration of the areas where the retained oily phase was deposited but also using image analysis, quantitative data could be retrieved. It is important to state here that only the oily phase was stained with the hydrophobic dye and as a result it was the only one emitting a fluorescent signal. Using image analysis, the fluorescent microscopy images were converted to an 8bit black and white image and then the shades of grey were divided into 256 levels of brightness and each pixel was graded as for its brightness level. Following that, the area of the sample was selected and assigned with a mean value of intensity that provided a representation of the retained oil amount on the tested sample. The mean intensity value is a dimensionless value

and it was used as a means of comparison amongst the samples. Advantages of this method included ease of use, visual and quantitative data generation and time efficient comparison of the mimics. However, in cases of overlapping layers of oil, this method is incapable of quantifying accurately the retained portion intensity and as a result further characterization was required to complement fluorescent microscopy data and lead to trustworthy conclusions. This technique was employed for both the 20% petrolatum full factorial and the design of experiment approach.

The gravimetric analysis represented a simpler and quicker characterization technique of retention levels. The initial weights of the skin mimic samples were recorded, as well as their weights after product deposition and after rinsing. This way the mass of product retained on the skin's topography could be calculated. To ensure that only the product portion was evaluated and not any amount of moisture, the samples were left to dry in ambient conditions within a fume cupboard. Advantages of this technique included its simplicity, ease of use, time efficiency and low requirements in sophisticated instrumentation, since the only piece of equipment needed was an accurate balance, measuring to 4 decimal places. Nevertheless, this method could not provide data of the consistency of the retained substance unlike the fluorescent microscopy that only targeted the hydrophobic active. Furthermore, due to the small portions of retained material, in low retention circumstances, this method could not provide useful data due to its low sensitivity that could not pick up minor mass differentiations. Mostly due to the latter, this technique was only employed for the 20% petrolatum full factorial approach.

The last technique, tribology, targeted the ability of the retained oily substances to perform as lubricants. As well as moisturization, oily substances provide a slippery,

smooth feel to the skin and thus benefit the consumer perception of product performance. The higher the oil amount retained, the lower the friction of the surface. Based on that fact, the samples were tested for their coefficient of friction and the results were analysed and compared to complement the previous results. Benefits of this method include that a better indication of the distribution and performance of the hydrophobic active was provided. However, it required a significant amount of time and could not provide quantitative retention data unless a correlation curve was developed, and thus this technique was only used for the full factorial approach on the 20% petrolatum emulsion.

6.2. Full Factorial Approach

LSD, MSD and SSD, 20% petrolatum emulsions were prepared and characterized as described in the previous chapters. The emulsions were applied on skin mimics using the deposition set-up and then the samples were rinsed using the cleaning set-up. Three levels of rinsing duration were chosen and 2 levels of flow angle, 45 and 90 degrees. The results of fluorescent microscopy, gravimetric analysis and coefficient of friction are presented and analysed.

6.2.1. Fluorescent Microscopy Characterisation

The following fluorescent microscopy images illustrate the areas of the skin mimics where petrolatum has been retained. Of all the formulation ingredients, only petrolatum has been stained with a pyrromethene and as a result only this component emits

fluorescent signal, as a result the non-black, grey to white areas indicate the presence of petrolatum. As shown in Figure 6.1 the samples were treated with large, medium and small droplet size 20% petrolatum emulsions (from left to right) and then rinsed for 30 seconds at 90 degrees angle of flow.

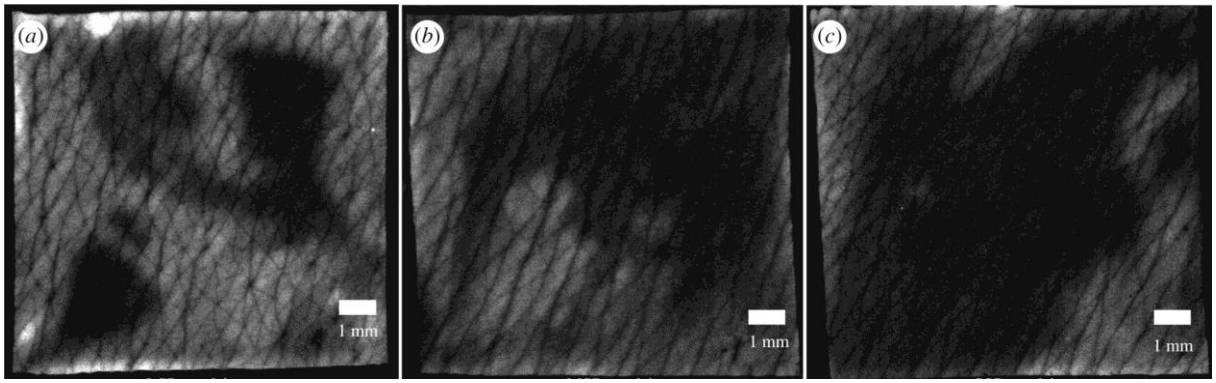

Figure 6.1: Fluorescent microscopy images of stained petrolatum retained on human skin mimics. The lighter grey to white areas, indicate emission of fluorescent signal and consequently the presence of retained petrolatum. (a) illustrates the mimic treated with an LSD emulsion, (b) MSD emulsion and (c) SSD emulsion. All samples in this case were rinsed for 30 seconds at 90 degrees of vertical flow. The superiority of LSD emulsion in driving higher levels of retention is obvious.

In Figure 6.1, the LSD treated samples exhibited considerably higher levels of petrolatum retention, with clear film formation that covered the majority of the skin mimic area after rinsing. The MSD emulsion showed less film forming abilities and less retained petrolatum amount on the skin mimic after rinsing in comparison to LSD emulsion treated samples, however it was more effective than the SSD emulsion which showed the lowest amount of retained petrolatum. It is known in literature that petrolatum is a potent occlusive material, with strong film forming capabilities. Due to the contact of the formulation with skin, the increased body temperature and the shear during the deposition of the product, petrolatum liquifies and spreads freely creating occlusive films on the stratum corneum. However, the surfactant molecules of the cleanser, the removing force applied by the rinsing water and the high temperature of

the water contribute to the removal of petrolatum and rupture of the formed films. The balance between the two forces determine the levels of retention. In Figure 6.1, the superiority of larger droplet sizes of petrolatum in the formulation is apparent. Figure 6.2 demonstrates the control sample images, showing the blank, untreated skin mimic and the mimic right after the emulsion deposition step with no rinsing whatsoever.

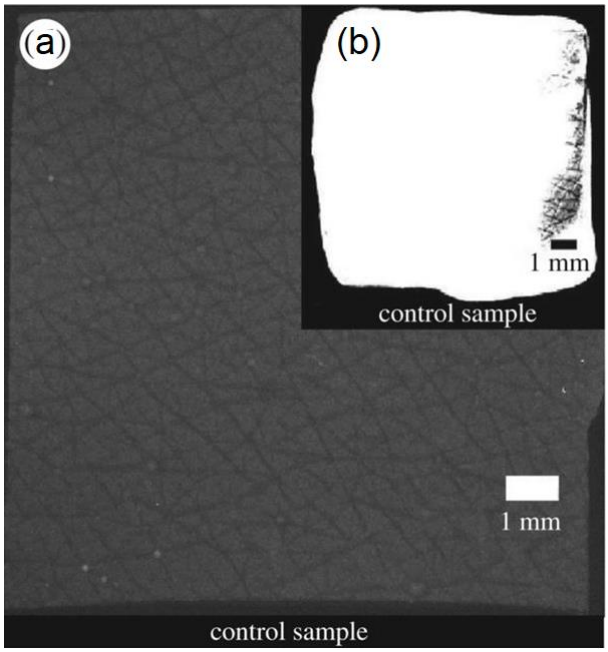

Figure 6.2: Fluorescent images of control samples. (a) The untreated sample is dark grey due to the lack of any substance that emits fluorescent signal, while the control sample that shows a layer of petrolatum emulsion right after the deposition step, (b) appears completely white due to the high intensity of fluorescent petrolatum within the film.

The blank, clean skin mimic has a dark grey colour due to the absence of any fluorescent material on it. However, the image is not totally black and as a result it demonstrates a value of brightness. This intensity value was measured using image analysis tools and found to be 72.57 ±2.66 out of 256 grey intensity levels. The grey scale intensity is a dimensionless value. The intensity of the blanc control mimic, which is attributed to white light interference to the instrument, was used as a baseline ‘noise’,

and the intensity values measured for the petrolatum treated samples were normalized using this background noise and the following equation:

$$Normalized\ sample\ intensity = \frac{Sample\ intensity}{Background\ intensity} \quad (22)$$

The control sample that illustrates the deposited product film on the skin mimic right after the deposition step exhibits an intense white colour throughout the test area showing the complete coverage of the mimic by the emulsion.

The tested sample fluorescent images were examined using the image analysis software ImageJ for their mean grey intensity value. The following intensity graphs in Figure 6.3 and Table 6.1 demonstrate the results of the image analysis of all the retrieved fluorescent images.

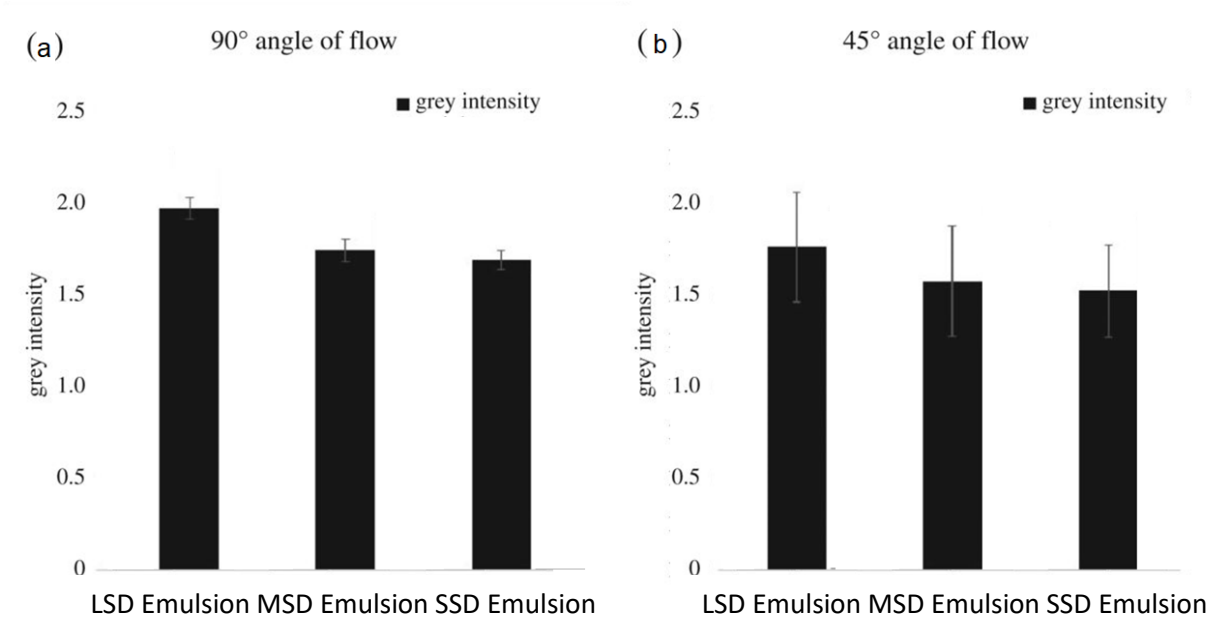

Figure 6.3: Grey intensity levels of LSD, MSD and SSD emulsions of 20% petrolatum, rinsed for 30 seconds at (α) 90 degrees and (b) 45 degrees of flow. Image analysis has shown that LSD emulsion deposition demonstrated enhanced retention in both angles of flow. 45 degrees of flow resulted in improved cleaning of the mimic and lower retention of hydrophobic actives in all droplet size levels.

Table 6.1: Mean grey intensity values of LSD, MSD and SSD emulsions of 20% petrolatum, rinsed for 30 seconds at 90 degrees and 45 degrees of flow.

Intensity (30sec rinse)	**LSD**		**MSD**		**SSD**	
90 degrees	1.94	±0.04	1.65	±0.03	1.58	±0.02
45 degrees	1.79	±0.30	1.55	±0.34	1.51	±0.22

In Figure 6.3, the intensity analysis of the LSD, MSD and SSD petrolatum emulsion is illustrated for the samples rinsed for 30 seconds at 90 and 45 degrees of flow. It is shown that in both levels of flow angle the LSD emulsions show improved performance as far as retention is concerned. However, 45 degrees of flow has led to lower values of retention in comparison to vertical flow in all tested droplet sizes proving that a slight angle enables better introduction of water into the skin topography, hence more efficient cleaning. In more detail, in Table 6.1, the superiority of LSD emulsion in petrolatum retention is observed, with approximately a 18% increased intensity than MSD and 22% increased than the SSD when rinsed at 90 degrees. For the samples rinsed at 45 degrees, LSD emulsions showed a 15% higher intensity than the MSD and a 18% higher intensity than the SSD. Conclusively, LSD demonstrated optimal performance as far as hydrophobic active retention is concerned, showing a strong correlation of large oil droplets and retention. Moreover, at 45 degrees of flow, optimal cleaning was observed, with LSD emulsions showing best retention, but a smaller performance deviation with the MSD and SSD emulsions. However, in the case of 45 degrees angle of flow, the errors are significantly higher than those in 90 degrees of flow. This effect is attributed to the complexity of human skin topography that makes it impossible to generate samples of the same topographic features. Hence the water flow at 45 degrees interacts with a significantly different topography from sample to

sample, leading in variable cleaning phenomena depending on the micropatterns on the hit point of the water flow. This way the error of our measurements is increased in comparison to the 90 degrees of flow cleaning where the topography doesn't affect significantly the water flow. Given that the errors are greater than the identified trends, for this specific system, the results cannot be considered conclusive and further evaluation with other means of evaluation of retention need to take place to cross check the results and ensure that the trend is repetitive. In the following section, the results from the gravimetric analysis align with those of the fluorescent microscopy, validating the conclusions made in this section.

The following graphs in Figure 6.4 demonstrate the intensity results of the image analysis of skin mimics treated with LSD, MSD and SSD emulsions and rinsed for 60 seconds and both 45 and 90 degrees of flow.

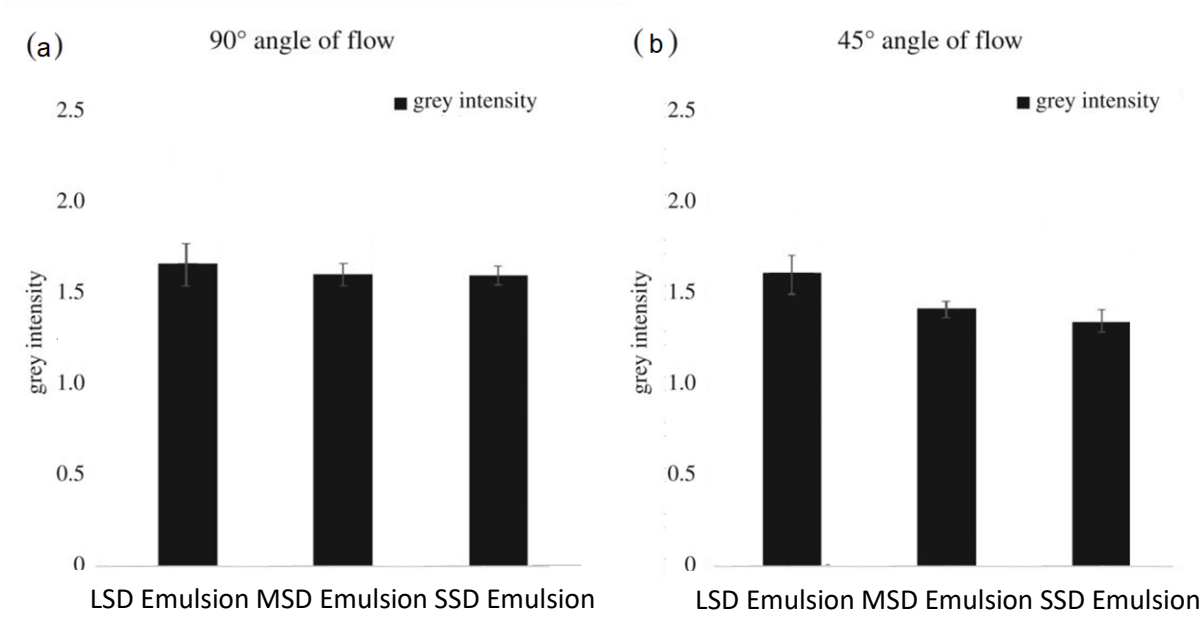

Figure 6.4: Grey intensity levels of LSD, MSD and SSD emulsions of 20% petrolatum, rinsed for 60 seconds at (α) 90 degrees and (b) 45 degrees of flow. Image analysis has shown that LSD emulsion deposition demonstrated enhanced retention in both angles of flow. 45 degrees of flow resulted in improved cleaning of the mimic and lower retention of hydrophobic actives in all droplet size levels.

Table 6.2: Mean grey intensity values of LSD, MSD and SSD emulsions of 20% petrolatum, rinsed for 60 seconds at 90 degrees and 45 degrees of flow.

Intensity (60sec rinse)	**LSD**		**MSD**		**SSD**	
90 degrees	1.69	±0.15	1.57	±0.09	1.53	±0.07
45 degrees	1.55	±0.11	1.43	±0.02	1.34	±0.07

Again, LSD emulsions showed the highest levels of intensity in both angles of flow and SSD emulsions showed the lowest. In 90 degrees of flow, LSD emulsions showed mean intensity values that were approximately 7% higher than those of MSD emulsions and 10% higher than SSD emulsions. The 45 degree rinsing flow, resulted in more efficient cleaning of the samples in comparison to the equivalent emulsions rinsed at 90 degrees flow. Once more LSD emulsions showed higher intensity levels and therefore improved petrolatum retention. The increase of rinsing duration, caused a reduction of the retained petrolatum on the skin mimics, leading to lower mean intensity values in samples treated with all levels of droplet size emulsions and rinsed at all levels of flow. The fluorescent deviations amongst the samples become narrower with longer rinsing and improved angle. This fact leads to the conclusion that droplet size has a strong impact in retention levels of the hydrophobic active, however, prolonged cleaning and improved angle rinsing shortens the impact of oil droplet size and leads to a minimum petrolatum portion that stays physically entrapped within the topography of the stratum corneum. As seen in Figure 6.5 and Table 6.2 this portion is more and more difficult to be removed leading to the conclusion that product removal is most effective in the first seconds of rinsing and that the impact of rinsing angle also becomes less in longer rinsing times. The following graphs demonstrate the intensity results of the samples rinsed for 90 seconds at both levels of flow angle.

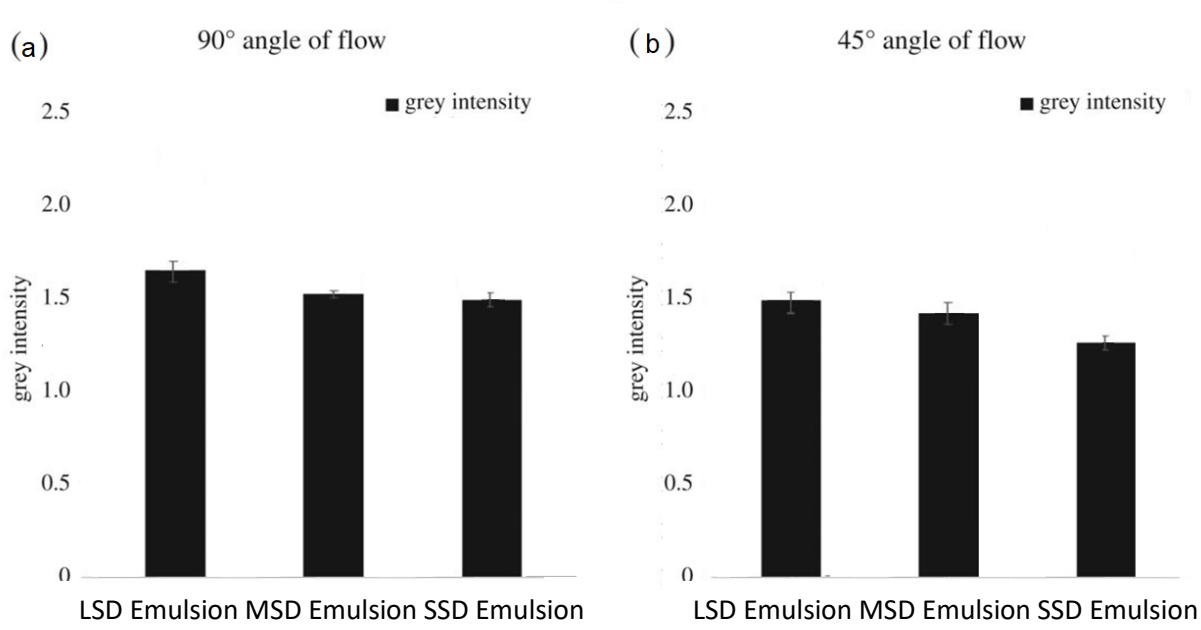

Figure 6.5: Grey intensity levels of LSD, MSD and SSD emulsions of 20% petrolatum, rinsed for 90 seconds at (α) 90 degrees and (b) 45 degrees of flow. Image analysis has shown that LSD emulsion deposition demonstrated enhanced retention in both angles of flow. 45 degrees of flow resulted in improved cleaning of the mimic and lower retention of hydrophobic actives in all droplet size levels.

Table 6.3: Mean grey intensity values of LSD, MSD and SSD emulsions of 20% petrolatum, rinsed for 90 seconds at 90 degrees and 45 degrees of flow.

Intensity (90sec rinse)	**LSD**		**MSD**		**SSD**	
90 degrees	1.60	±0.09	1.53	±0.01	1.51	±0.05
45 degrees	1.49	±0.07	1.43	±0.12	1.36	±0.04

In Figure 6.5, LSD emulsions showed the highest levels of grey intensity which translates in higher levels of petrolatum retention, followed by MSD emulsions and SSD emulsions. However, in this set of experiments, the LSD showed an improvement in intensity of only 4% against MSD and 6% against the 90 degrees rinsing. This indicates that prolonged rinsing was detrimental in the film forming abilities of petrolatum leading to restricted retention even by the high performing LSD emulsion. The superficial layers of petrolatum were susceptible to longer rinsing, leaving only the

physically entrapped petrolatum retained within the pores and wrinkles of the mimic. Again, 45 degrees of flow showed improved cleaning, however the impact of the flow angle was significantly lower in the highest duration of flow, with MSD emulsion treated samples, showing an intensity deviation of as little as 10% between the two levels of rinsing angle.

The retention variances between the first two levels of rinsing duration were notably higher than the differences between the final two. Taking the LSD emulsion treated samples, rinsed at 90 degrees, as an example, from 30 seconds of rinsing to 60 seconds of rinsing the intensity value dropped by approximately 13%, whereas from 60 seconds rinsing to the longest 90 seconds of rinsing, the intensity dropped by only 5%, proving that the majority of product removal takes place in the very first seconds of rinsing. Additionally, this fact proved that an entrapped portion of petrolatum within the topography of the mimic, was not been affected by prolonged rinsing or variances in rinsing angles and that portion was affected by droplet size, with the LSD emulsion outperforming the other two levels of droplet size emulsions.

In conclusion, image analysis and visual evaluation of the fluorescent images showed that LSD emulsions exhibited optimal performance in retention of petrolatum, followed by MSD emulsions and SSD emulsions. Moreover, the angle of flow was an impactful parameter that determined the performance of petrolatum removal, with 45 degrees of flow exhibiting lower amounts of retained petrolatum in all levels of flow duration. Lastly, prolonged rinsing resulted in lower active retention as was expected, however retained petrolatum levels tended to reach a minimum plateau after which further rinsing did not significantly alter the retention levels, at any angle of flow. Also, the

impact of droplet size and rinsing angle in petrolatum retention, although noticeable, was not as significant in the highest level of rinsing duration.

6.2.2 Gravimetric Analysis

Following the fluorescent microscopy evaluation of the samples and the image analysis, the samples were weighed, and the retained mass was calculated by subtracting the initial mimic weight from the final weight. The following Figure 6.6 and Table 6.4 show the results of the gravimetric analysis for the retention of petrolatum emulsions, rinsed for 30 seconds at both rinsing angles, 45 and 90 degrees.

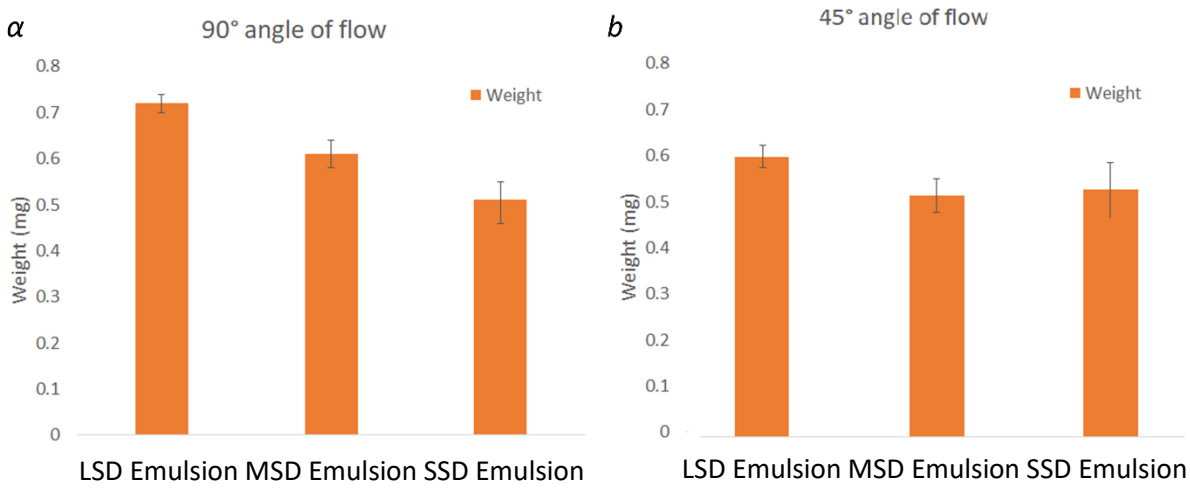

Figure 6.6: Grey intensity levels of LSD, MSD and SSD emulsions of 20% petrolatum, rinsed for 30 seconds at (α) 90 degrees and (b) 45 degrees of flow. Image analysis has shown that LSD emulsion deposition demonstrated enhanced retention in both angles of flow. 45 degrees of flow resulted in improved cleaning of the mimic and lower retention of hydrophobic actives in all droplet size levels.

Table 6.4: Gravimetric analysis, retained mass values of LSD, MSD and SSD emulsions of 20% petrolatum, rinsed for 30 seconds at 90 degrees and 45 degrees of flow.

Weight mg (30sec rinse)	**LSD**		**MSD**		**SSD**	
90 degrees	0.72	±0.02	0.61	±0.03	0.51	±0.04
45 degrees	0.59	±0.02	0.52	±0.03	0.53	±0.05

In Figure 6.6, the superiority of LPS emulsions in retained product portion is clear in both angles of flow. SSD showed the lowest retention values with approximately 30% less product retention at 90 degrees and approximately 15% less product retention at 45 degrees in comparison to LSD emulsion treated samples. It is shown that the span from the highest recorded retention to the lowest is smaller in the case of 45 degrees rinsing, proving that rinsing at this angle results in more effective removal. These results come to an agreement with the image analysis results demonstrated in the previous section and prove that the LSD is the most effective emulsion as far as retention is concerned whereas 45 degrees is the most efficient in removing the product. The following graphs in Figure 6.7 and Table 6.5, demonstrate the gravimetric results of the samples rinsed for a higher duration, in this case 60 seconds.

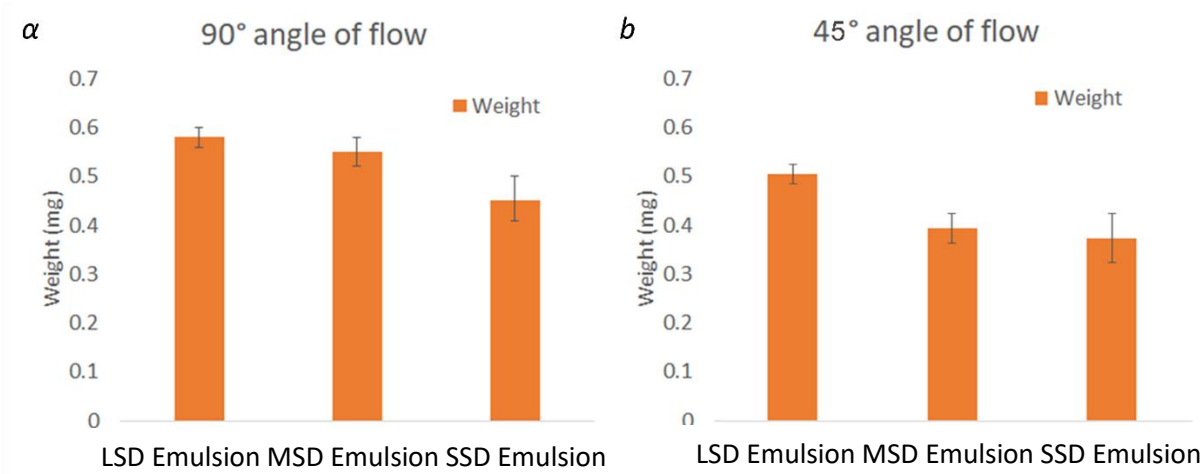

Figure 6.7: Grey intensity levels of LSD, MSD and SSD emulsions of 20% petrolatum, rinsed for 60 seconds at (α) 90 degrees and (b) 45 degrees of flow. Image analysis has shown that LSD emulsion deposition demonstrated enhanced retention in both angles of flow. 45 degrees of flow resulted in improved cleaning of the mimic and lower retention of hydrophobic actives in all droplet size levels.

Table 6.5: Gravimetric analysis, retained mass values of LSD, MSD and SSD emulsions of 20% petrolatum, rinsed for 60 seconds at 90 degrees and 45 degrees of flow.

Weight mg (60sec rinse)	**LSD**		**MSD**		**SSD**	
90 degrees	0.60	±0.01	0.55	±0.02	0.46	±0.04
45 degrees	0.54	±0.02	0.46	±0.03	0.42	±0.07

Again, from Figure 6.7 and Table 6.5, the LSD emulsions exhibited the highest levels of retention in both 90 and 45 degrees of flow. At 90 degrees, LSD emulsion retained more than MSD emulsion by almost 9% and more than SSD by 30%. At 45 Degrees, LSD emulsion retained more than the MSD emulsion and SSD emulsion by 12% and 29% respectively. Moreover, 45 degrees of flow showed lower retention values on the equivalent emulsion treated samples rinsed at 90 degrees proving again the high efficiency of cleaning skin mimics at this angle. The higher duration of rinsing resulted in lower levels of retention, something that was also noted in the fluorescent image analysis. The following graphs in Figure 6.8 and Table 6.6 illustrate the gravimetric analysis results for the samples rinsed for the longest level of rinsing duration, 90 seconds.

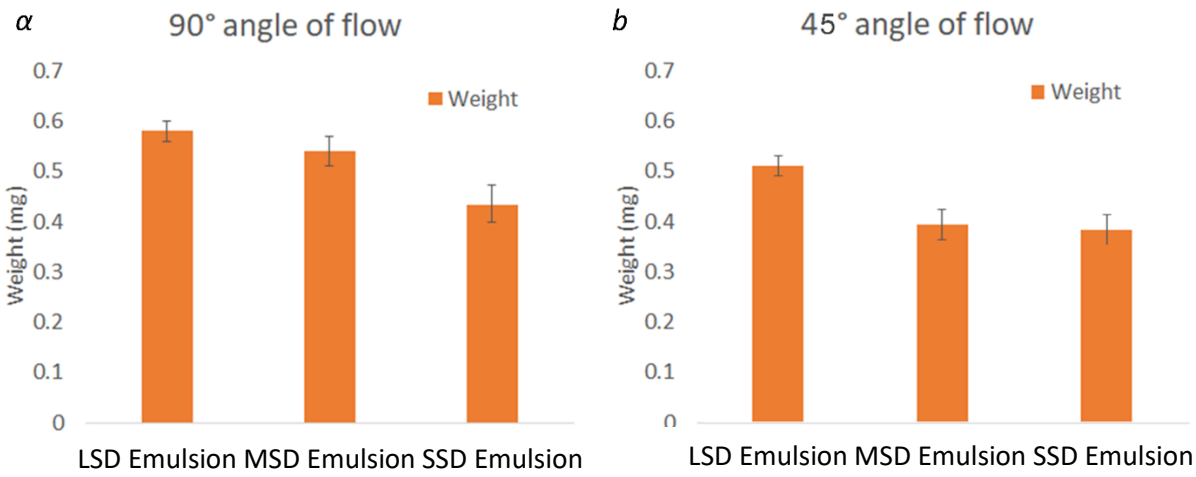

Figure 6.8: Grey intensity levels of LSD, MSD and SSD emulsions of 20% petrolatum, rinsed for 90 seconds at (α) 90 degrees and (b) 45 degrees of flow. Image analysis has shown that LSD emulsion

deposition demonstrated enhanced retention in both angles of flow. 45 degrees of flow resulted in improved cleaning of the mimic and lower retention of hydrophobic actives in all droplet size levels

Table 6.6: Gravimetric analysis, retained mass values of LSD, MSD and SSD emulsions of 20% petrolatum, rinsed for 90 seconds at 90 degrees and 45 degrees of flow.

Weight mg (90sec rinse)	**LSD**		**MSD**		**SSD**	
90 degrees	0.58	±0.01	0.55	±0.01	0.45	±0.04
45 degrees	0.50	±0.01	0.39	±0.03	0.37	±0.05

In Figure 6.8, the gravimetric analysis results for the samples rinsed for 90 seconds are presented. Similar to the previous samples pattern was observed with the LSD emulsions showing optimal levels of retention and SSD showing the lowest retention. Furthermore, similarly to the fluorescent evaluation results, a higher duration of rinse resulted in reduced product retention portion, but not in a linear way, since the retained portion variance from 30 to 60 seconds of rinse is much higher than that from 60 to 90 seconds, leading us to the assumption that there is an amount of petrolatum, a plateau, that is entrapped in the stratum corneum topography that further rinsing is incapable of removing significantly at any angle of flow. Taking the LSD emulsion rinsed at 90 degrees. For example, the variance of retained mass between the first two levels of rinsing duration was a 20% drop in mass, whereas in the last two levels it was a significantly lower 3% drop. The massive difference between the two indicates that the superficial layers of product were removed in the very first moments of cleaning and that the retained portion that was entrapped within the topography was tough to remove further.

6.2.3 Friction Evaluation

The treated samples were evaluated for their friction coefficient. A tribometer was employed for the purposes of this set of measurements, using a sphere on surface structure was selected. The sphere was made out of polypropylene and its diameter was 15mm. The lateral force selected was 100g and was controlled by using standard weights provided by the instrument manufacturer. The skin mimic samples were placed on the sample holder of the instrument and the sphere was placed at the edge of the sample. Since the dimensions of the skin mimic samples were 1x1 cm^2, the travel distance of the sphere was set at 1cm so that it covers the whole length of the mimic. The speed of movement was set at 10mm per second and the number of cycles selected was 5. The instrument has accurate force sensors, one for the lateral and one for the linear force, these feed the data to the instrument's computer. The lateral force is known and set at 100g of force, however, reading the sensors value of lateral force is a good indication of the instrument's accuracy. The coefficient of friction, μ, was then measured for all samples by dividing the linear or friction force, f, by the lateral or normal load, N. The following equation 23 illustrates this calculation:

$$\mu = \frac{Linear\ force}{Lateral\ force} \tag{23}$$

The coefficient of friction, as seen in the above equation, is a dimensionless number, and the following Table 6.7 demonstrates the calculated coefficient of friction for all tested skin mimics. The initial assumption was that retention of petrolatum on the skin mimics would have a strong correlation to the coefficient of friction since petrolatum works as a lubricant reducing the friction of skin and providing a silky and smooth feel.

Table 6.7: Calculated coefficient of friction for all treated samples. Retention of petrolatum is strongly connected to the friction values of the mimics, with higher levels of retention leading to better lubrication of the sample, hence a reduced coefficient of friction.

Coefficient of friction		**LSD**		**MSD**		**SSD**	
30 sec rinse	90 degrees	0.17	±0.01	0.22	±0.03	0.23	±0.02
	45 degrees	0.23	±0.04	0.27	±0.05	0.26	±0.04
60 sec rinse	90 degrees	0.31	±0.06	0.37	±0.07	0.38	±0.08
	45 degrees	0.36	±0.07	0.39	±0.03	0.38	±0.05
90 sec rinse	90 degrees	0.35	±0.04	0.38	±0.01	0.41	±0.03
	45 degrees	0.37	±0.08	0.39	±0.09	0.39	±0.07

The coefficient of friction for all treated samples was evaluated and compared with each other and with our control, untreated, sample. The control skin mimic sample exhibited a coefficient of friction of 0.59 ±0.09, which was higher than all the treated samples showing that even small amounts of retained petrolatum lead to notable lubrication and smoother skin. In literature, Zhang et al. [1], performed human skin in vivo friction measurements on several skin body areas and their results showed a mean coefficient of friction of 0.46±0.15 and a highest recorded coefficient of friction in the human hand, which was 0.61±0.21. The fabricated mimic coefficient of friction showed a value that is representative of that of real human skin [2]. The slightly higher friction value of the coefficient of friction of the mimic than the human skin in vivo mean value is attributed to the complete absence of natural lipids from the mimic that make the mimic less smooth in comparison to live skin. However, the introduction of

petrolatum reduced the mimic friction to levels significantly lower than those of skin in literature, especially for the samples that exhibited high retention of the hydrophobic active. As expected, higher levels of retained petrolatum portion lead to lower levels of coefficient of friction. LSD emulsions showed the best results as far as smoothness is concerned, with lower coefficients of friction than the MSD emulsions and SSD emulsions. For the samples rinsed for 30 seconds at 90 degrees, LSD emulsion showed the lowest coefficient of friction with a value of 0.17±0.01. The highest value of friction coefficient was reported for the sample rinsed for 90 seconds at 90 degrees and that was treated with SSD emulsion and showed a coefficient of friction of 0.41±0.03. The graphs in Figure 6.9 demonstrates the results of friction coefficient evaluation that were presented in Table 6.7.

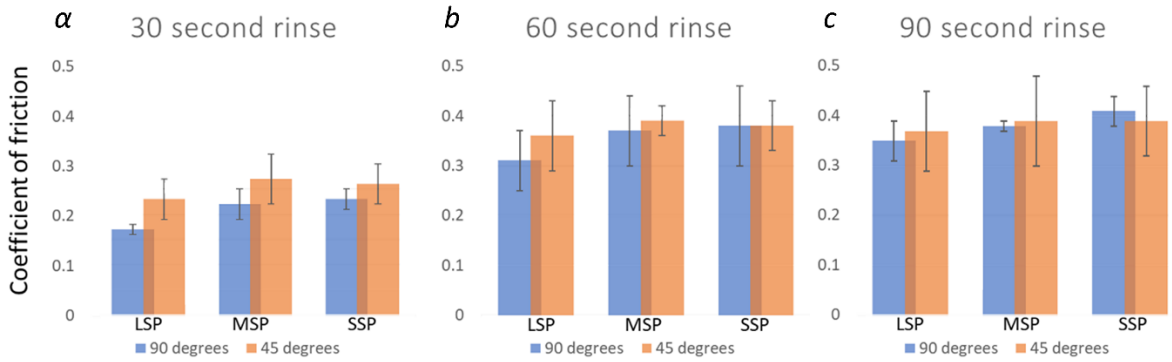

Figure 6.9: Coefficient of friction characterization of petrolatum treated samples. LSD emulsions exhibited lower coefficients of friction in all rinsing durations and angles in comparison to their equivalent MSD and SSD emulsions, showing improved lubrication due to higher amounts of petrolatum retained on the samples' topographic features.

The data supports the fluorescent and gravimetric analysis results mentioned in the previous sections that showed the significant impact of oil droplet size in petrolatum retention and more specifically the superiority of large droplet size emulsions in retention of hydrophobic active. Longer durations of rinsing resulted in higher levels of

coefficient of friction which is attributed to lower levels of petrolatum retained on the topography of the mimic. A similar impact is shown for the samples rinsed at 45 degrees of flow. The cleaning at that angle was more effective, leading to restricted petrolatum retention and as a result lower friction in comparison to the equivalent samples rinsed at 90 degrees. However, at 90 seconds of rinsing, there were a few results that did not follow the prementioned pattern. With samples rinsed at 45 degrees, MSD emulsions showed lower friction than LSD. This phenomenon was attributed to the fact that at this level of rinsing duration and angle, the retention deviation between the three emulsions is low, and although the LSD emulsion might have shown best retention in all other evaluation methods in tribology it is not only the portion of petrolatum retained that affects friction but also the distribution of it. As a result, it is assumed that in this particular sample, the distribution of retained petrolatum might not been even and as a result showed a higher friction value. Nevertheless, all the treated samples demonstrated coefficient of friction values lower than the untreated control sample, showing that even at low retention amounts the friction of the sample is notable affected making tribology a valid method of product performance evaluation method.

6.2.4 Retention Comparison Between a Skin Mimic and a Flat Polyurethane Substrate

The initial assumption for the mechanism of retention was that the petrolatum droplets would enter the topography of the stratum corneum during the deposition step, forced by the applied shear, and following, during the rinsing step, the superficial petrolatum layers would be removed due to the force of the water jet hitting the sample surface,

whereas the inner petrolatum layers that would be physically entrapped within the roughness of human skin would be harder to remove due to being protected by the topographic features and the adhesive properties of petrolatum.

To evaluate the effect of skin topography in product retention, a flat sample surface was produced using the same materials as the skin mimics and was treated with the LSD emulsion using the deposition set up and following the same rinsing protocol for 30 seconds duration, at 45 and 90 degrees of flow. Fluorescent microscopy evaluation as well as gravimetric analysis showed that the flat surface samples exhibited lower retention levels, compared to the skin mimics. Figure 6.10 illustrate the fluorescent images of the control flat surface samples and one with the retained petrolatum film as well as the graphs showing the results of the image analysis data and the gravimetric analysis.

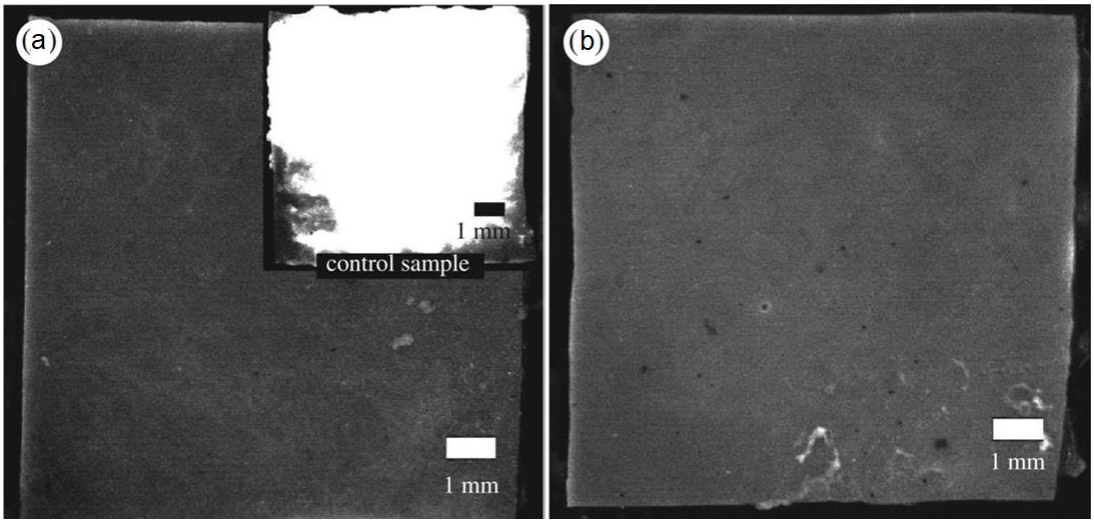

Figure 6.10: (a) Fluorescent images of the flat surface control samples with inset the flat surface with a layer of fluorescent petrolatum. (b) shows the flat surface sample treated with LSD emulsion showing the retained petrolatum film.

From Figure 6.10, a significant difference in brightness cannot be reported between the treated sample and the control. However a slightly lighter grey colour is observed in the treated sample, indicating the presence of a very thin petrolatum layer. Image analysis tools enabled the quantification of the differences that could not be evaluated by eye and are presented in the graph in Figure 6.11.

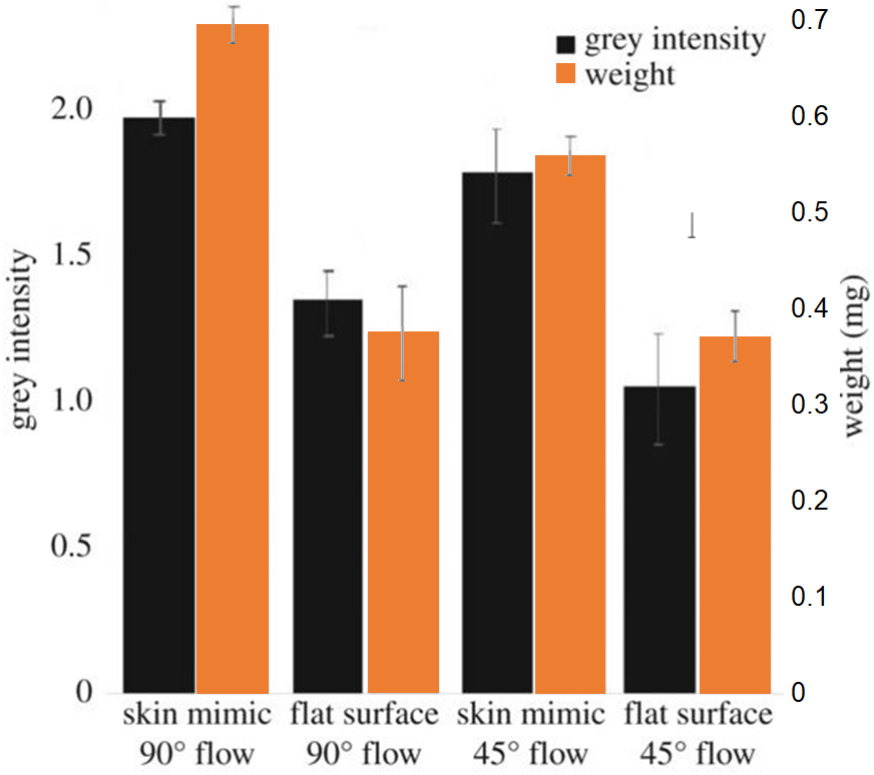

Figure 6.11: Fluorescent image analysis and gravimetric analysis data, illustrating the comparison between retention levels on skin mimics and flat surface samples, treated with LSD petrolatum emulsions, and rinsed for 30 seconds at both 45 and 90 degrees. The impact of skin topography is clear, leading to higher retention levels attributed to the physical entrapment of petrolatum within the roughness of the mimic.

Table 6.8: Fluorescent intensity and weight analysis data comparison for retention on flat substrates and skin mimics. Skin mimics showed higher levels of intensity and residue weight in equivalent angle of flow than the flat surfaces, showing that the topography of the skin has a positive impact on retention by enabling physical entrapment.

Flat sample	**Intensity**		**Weight**	
90 degrees	1.37	±0.12	0.39	±0.05
45 degrees	1.04	±0.23	0.38	±0.02
Skin Mimic	**Intensity**		**Weight**	
90 degrees	1.94	±0.04	0.72	±0.02
45 degrees	1.79	±0.30	0.59	±0.02

The graphs in Figure 6.11 and the results presented in Table 6.8 demonstrate the impact of skin roughness in retention. Gravimetric analysis data demonstrated that the skin mimics retained petrolatum in significantly higher levels than the flat surface samples, more specifically by 84% for those rinsed at 90 degrees and 55% for those rinsed at 45 degrees. The outstanding differences in retained portion showed what a powerful impact the topography has on retention and supports our assumption that the major driving mechanism of retention of hydrophobic actives on human skin is physical entrapment within the roughness of the stratum corneum. Moreover, insignificant differences in retention levels in flat samples rinsed at 45 degrees and those rinsed at 90 degrees was detected, showing that this parameter was only significant in samples that demonstrated some degree of surface roughness.

Consequently, this experiment proved that physical entrapment demonstrated a major impact in retention of petrolatum on the tested surfaces and provided better understanding of the mechanism of retention. Furthermore, the impact of angle of flow was evaluated, and although it showed no significant difference on retention for flat

surfaces, it demonstrated important differences in retention on skin mimics and it should be evaluated further.

6.3 Discussion and Conclusions

The full factorial approach on the 20% petrolatum emulsions generated useful data towards the understanding of retention and identifying its major driving factors. The selected independent parameters included the oil droplet size of the emulsions with three levels produced, the LSD the MSD and the SSD emulsion, the rinsing duration of the samples during the cleaning step with again three levels, 30 second rinsing, 60 second rinsing and 90 second rinsing, and finally the rinsing angle with two levels the 90 degrees of flow and the 45 degrees. Retention was evaluated by fluorescent microscopy towards the generation of intensity data that indicates petrolatum retention, film formation and mapping of the areas where petrolatum was deposited, by gravimetric analysis of the samples that evaluated the retained mass of product on the topography of the mimics and tribology to characterize the lubricating effect of the retained portion. All methods employed showed that the impact of the selected independent parameters on retention was significant. LSD emulsions exhibited the highest retention levels in all rinsing durations and angles, a result supported by all evaluation methods used. LSD exhibited the highest intensity levels, showing improved retention and optimal film forming abilities of petrolatum on the sample surface. This shows a strong connection of the oily phase droplet size within the emulsion with its ability to retain on the surface after cleaning. Increased durations of flow exhibited lower retention levels which was an expected outcome. However, the results showed

that the majority of the deposited product was removed within the first seconds of rinsing, and after the superficial layers of petrolatum were removed, further rinsing was not as effective in removing the product that was physically entrapped inside the features of stratum corneum. Consequently, we concluded that the product removal is not linear to rinsing duration, on the contrary at high rinsing durations, the levels of retention showed a tendency to reach a minimum plateau of retained petrolatum. Further petrolatum removal should require some form of mechanical shear or increase of the flow rate to an unrealistic for shower use value. Furthermore, 45 degrees of angle showed improved cleaning by resulting in lower petrolatum amounts retained on the mimics' topographic features. We attributed this behaviour to the morphology of the stratum corneum and the ease of water to penetrate within the wrinkles and pores of the skin at a tilted angle, leading to improved product displacement by the water. Tribometry characterization showed that the samples that exhibited higher petrolatum retention and a wider spread petrolatum film, also showed lower coefficient of friction values. LSD emulsions again exhibited improved performance, with the sample rinsed at 90 degrees for 30 second showing a friction coefficient of 71% lower than the control, untreated, sample. A flat sample to skin mimic comparison took place, by following the described protocol for both types of samples from depositing the material to cleaning and evaluating retention. This enabled us to draw conclusions on the impact of skin morphology and physical entrapment to the post-wash retention of the hydrophobic active, since the flat surface does not demonstrate any roughness, hence no entrapment. The results outlined the strong impact of topography on retention with skin mimics showing higher retention levels, in one case by an excessive 84%. The information presented, and the generated data, indicate that the mechanism with which

petrolatum retains on human skin is by being introduced through the inner, fine topographic features of the stratum corneum during the deposition step, pushed by mechanical shear and physically remaining entrapped inside the roughness of the skin, making it difficult to be removed by water displacement.

The strong impact of oil droplet size in retention was the most valuable information derived from this full factorial approach with LSD emulsions showing enhanced retention in all cleaning conditions. We studied the behaviour of the model system emulsions and came up with a few hypotheses that underline these phenomena and elucidate the superiority of larger size droplets of oil on retention.

Initially, the large droplet size emulsions differ to the medium and small size droplet emulsions in interfacial surface area. Due to the smaller size of oil droplets in SSD and MSD emulsions, the interfacial area between oil and water is significantly higher than in LSD emulsions. To calculate the interfacial oil in water area of the emulsions for comparison purposes, we made the assumptions that the droplets of oil within the emulsions are spherical and that all droplets exhibit diameters equal to the median diameter of the droplet size distribution of the tested emulsion according to the Mastersizer data. Consequently, for the LSD, 20% petrolatum emulsion that has a median droplet size of 141.25μm, the calculated surface area equals to 0.0085m^2 per 1ml of emulsion. For the MSD emulsion with a median droplet size of 31.62μm, the surface area was calculated to a value of 0.0380m^2, a significantly higher value than that of the LSD emulsion. Finally, the SSD emulsion that showed a median droplet size value of just 1.26μm showed a surface area of 0.9524m^2, an impressive level of area in comparison to the MSD and LSD emulsions. The highest amount of oil area exposed to water indicates the coverage of this area with surfactant monomers towards the

reduction of the interfacial tension between the oil and the water phase and the production of a stable formulation. However, the presence of surfactants, especially anionic, creates a counter effect in deposition of oils, a well-studied effect in cosmetic projects. Surfactants are established for their cleaning properties and their ability to target and remove oily substances during rinsing. As a result, a large amount of the oils within the emulsions that are designed to deposit and retain on human skin during use of the product, are encapsulated and removed by the surfactants instead. Due to the critically higher interfacial area in SSD emulsions than in MSD and LSD emulsions, the surfactant to oil ratio per oil droplet is significantly higher in SSD and hence this counter effect has a larger impact on its retention. LSD emulsions, on the other hand, demonstrate low surfactant to oil ratios in their droplets and as a result the surfactant counter effect on deposition is low favouring the retention of actives on skin [6-9]. In Figure 6.12 (a), a schematic representation of the higher surface area is demonstrated in SSD emulsions in comparison to LSD emulsions.

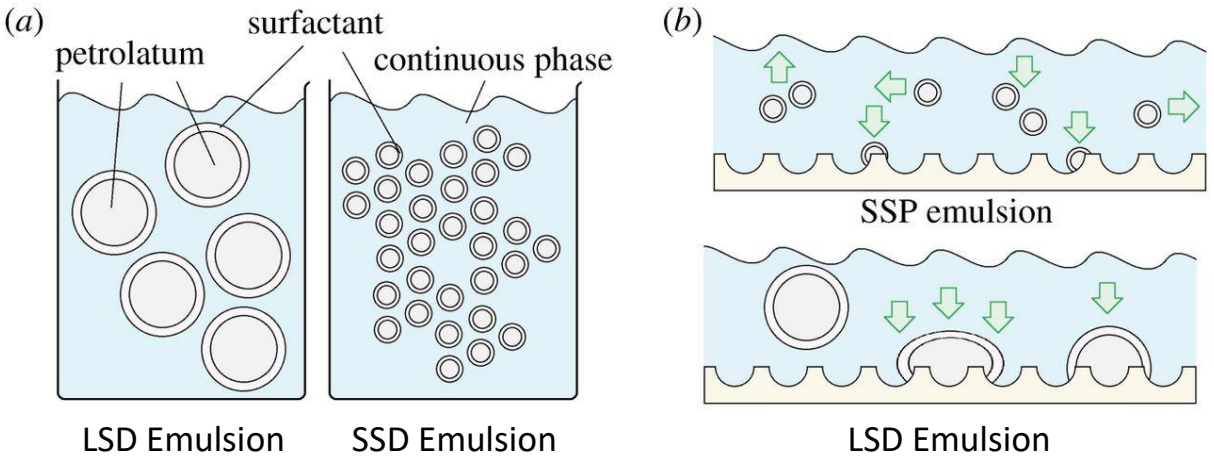

Figure 6.12: Schematic illustration of, (a) the surface area variance between LSD and SSD emulsions and (b) skin mimics with an applied layer of SSD and LSD emulsions: for the LSD emulsion, the considerable effects of gravity and shear forces lead to the droplets' deformation and break-up and, thus, higher retention values. By contrast, in the SSD emulsions, the droplets are more stable and resistant to thermal and mechanical stresses, and exhibit high mobility and enhanced Brownian diffusion forces, all enabling an ease of removal during the cleansing process, without adhering or releasing oils onto the skin mimic's topography.

Moreover, it is well established that the oily phase within the emulsion is encapsulated in a layer of surfactant. This surfactant interface needs to be broken for the hydrophobic active to be released onto the skin, so effective deposition and retention can take place. However, smaller dimension oil droplets exhibit great stability and endurance to mechanical shear and thermal stress when compared to droplets of larger dimensions [9-10]. The higher amounts of energy required to compromise the stability of the smaller oil droplets makes them less favourable to disintegration and releasing the hydrophobic active on the skin substrates. Consequently, the SSD emulsion resulted in lower levels of retention due to the highest mechanical and thermal energy required to release the oil from the droplets on the mimics in comparison to larger droplets that require less energy to break and when they do they release a considerably larger amount of oil than the smaller droplets. Lyer et. al. [11], presented the superior stability of small droplets and compared their difference to larger dimension droplets. Their

results showed that the smaller droplets have optimal endurance in shear and high energy requirements to demulsify in comparison to larger droplets. Tjarwat et. al. [10], studied the stability of droplets in correlation to their dimensions, especially the energy required to compromise their structure. They concluded that larger size droplets, are more affected by gravitational forces in comparison to smaller submicron droplets that are affected by Brownian diffusion forces with kT values that overcome the gravitational forces making them more stable and not prone to phase separation within an emulsion structure. The gravitational effect to droplets and its correlation to droplet dimensions is described by the following equation 24:

$$kT > \frac{4}{3}\pi R^3 \Delta\rho g L, \tag{24}$$

In equation 25, k is the constant of Boltzman, T represents the temperature, R the radius of the droplets, Δρ the variance of density of the oil and the medium, g is the gravitational force and L the height of the vessel. By assuming that the droplet dimensions of all droplets are equal to their median values, gravitational forces were calculated for the droplets of LSD emulsions and SSD emulsions by employing the following equations 25 and 26.

$$\mathrm{LSP_{GRAV}} = \frac{4}{3}\pi R^3 \Delta\rho g L \tag{25}$$

and

$$\mathrm{SSP_{GRAV}} = \frac{4}{3}\pi \mathrm{R_{SSP}^3} \Delta\rho g L. \tag{26}$$

Moreover, we assumed that both emulsions were kept in a similar height vessel that demonstrated the same value of L and that all the other components of the equation

were identical for both emulsions. The calculated forces were only affected by the droplet diameter value of each emulsion, with:

$$LSD_{GRAV} > SSD_{GRAV} \Leftrightarrow 141.253 > 1.263 \quad (27)$$

Consequently, the gravitational force impact was calculated to be approximately 1.4×10^6 times higher in the larger droplets of LSD emulsions than in the oil droplets of the SSD emulsions. Larger droplet dimensions exhibited a crucial impact in the gravitational forces that make phase separation and demulsification of the emulsion more likely to take place, when they overcome the Brownian diffusion forces.

Additionally, larger droplets, being more affected by gravity and showing significantly less mobility as well as mechanical shear and thermal resistance than smaller droplets, they are more prone to deformation and breakage, leading to efficient release of the larger amounts of hydrophobic active on human skin hence improved retention. The higher mobility smaller droplets are more stable and easily float away with rinsing, leading to poor retention performance by the SSD emulsions. The synergistic effect of the low energy requirements to deform and release oil from the large LSD emulsion and the low counter effect of surfactant on them enables efficient deposition of large amounts of the active on human skin with low shear required leading to higher amounts of film forming and retention.

6.4 References

1. Zhang, M. & Mak, A. F. In vivo friction properties of human skin. Prosthet. Orthot. Int. 23, 135–41 (1999).
2. Asserin, J., Zahouani, H., Humbert, P., Couturaud, V. & Mougin, D. Measurement of the friction coefficient of the human skin in vivo: Quantification of the cutaneous smoothness. Colloids Surfaces B Biointerfaces 19, 1–12 (2000).
3. Wilke K, Bie SS. A short history of sweat gland biology. Int J Cosmet Sci 29, 169–179. (2007)
4. Krawczyk J. Surface free energy of the human skin and its critical surface tension of wetting in the skin/surfactant aqueous solution/liquid system. Skin Res. Technol. 21, 214–223 (2015)
5. Wilke K, Bie SS. A short history of sweat gland biology. Int J Cosmet Sci 29, 169–179. (2007)
6. Goodwin J. Colloids and interfaces with surfactants and polymers. New York, NY: John Wiley & Sons (2009).
7. Corazza M, Virgili A. Surfactants, skin cleansing protagonists. J. Eur. Acad. Dermatol. Venereol. 24, 1–6. (2010)
8. Blank IH. Action of soaps and detergents on the skin. The Practitioner202, 147–151, (1969)
9. Cameron DR, Weber ME. Determination of interfacial areas in emulsions using turbidimetric and droplet size data: correction of the formula for emulsifying activity index. J. Agric. Food Chem. 39, 655–659, (1991)
10. Tjarwat FT. Emulsion formation, stability and rheology. New York, NY: Wiley-VCH (2013)
11. Lyer V, Cayatte C. Impact of formulation and particle size on stability and immunogenicity of oil-in-water emulsion adjuvants. Hum. Vaccin. Immunother. 11, 1853–1864, (2015).

CHAPTER 7: DESIGN OF EXPERIMENTS AND MODELLING

7.1 Introduction

Further to the full factorial experiment of the 20% petrolatum emulsions it was decided that it would not be feasible to perform the excessive amount of experiments required to test all the formulations using the full factorial approach, given the limited time of this project. However, this allowed the opportunity to employ a well-known approach in statistical experiments, the design of experiment. This process included the fitting of a statistical model, to generate results and information for all independent factors, excluding the need to perform an excessive number of experiments. The statistical analysis software JMP, pronounced ‘jump’, which was developed in 1980 by the SAS institute, was employed for this purpose. This software, is mainly used to analyse the data output from experimental projects where the exploration of all parameters in all levels is not possible. The data from a selected number of experiments, that consist of a specific combination of levels for each tested parameter, are used to generate graphs and models that further enable understanding of the impact of the selected independent parameters on the response value and evaluate the initial hypothesis. The fitting of the model to the experimental data is also evaluated and more suitable parameters and /or correlations of them can be chosen to generate more efficient models that contribute further to the understanding of the system. Clear identification

of the independent parameters leads to more accurate models and better understanding of the system. It is crucial to ensure that the working parameters have no effect to each other to avoid misconceptions in the generated data [1-2].

In this project, our aim was to use JMP to generate a model that would describe the impact of the selected parameters, which were oil viscosity, oil concentration, droplet size, rinsing time and rinsing angle, on the response parameter which was the retention of oil identified as fluorescent intensity. The generated graphs are expected to provide useful feedback on which of the above parameters has the strongest statistical significance on the response, to understand what drives retention and to allow better selection of working parameters in future researches.

The limitations of the software mainly correlate with the poor identification of the independent parameters. Factors may have an overlapping impact on the response parameter hence misconceptions might occur from the generated model. To tackle this, clear definition of the initial independent parameters is essential as well as the interactions amongst them. The careful choice of those as well as ensuring that the documentation of the method is sufficiently detailed can output trustworthy data that enable the understanding of their influence in the response parameter and reduce the risk of measurement error. Other concerns in experimental design include the establishment of validity, reliability, and replicability of the results. Additional concerns include accomplishing appropriate levels of statistical power and sensitivity of the model [2].

JMP can be used for the development of various types of design of experiments in numerous disciplines, saving millions of dollars in manufacturing, processing and research companies.

7.2 Initial Design

First and foremost, the independent factors were identified as well as their levels, and they are presented in Table 7.1:

Table 7.1: Independent parameters and their levels.

Independent parameter	Low Level	Medium Level	High Level
Oil Viscosity (40°C)	4.7±0.1cP (mineral oil)	9.2±0.3cP (sunflower oil)	20.5±0.1cP (petrolatum)
Oil Concentration	20%	40%	60%
Oil median droplet size	<5um	35-55um	>100um
Rinsing duration	30 seconds	60 seconds	90 seconds
Rinsing angle	45 degrees	67.5 degrees	90 degrees

Following, these parameters and their levels were entered into a design of experiment software, JMP. The ‘JMP’ software used these parameters to generate a schedule of experiments that needed to be performed, to provide data and information on the system, equivalent to a full factorial approach but with only a fraction of the experiments required. For this purpose, the software combined the levels of the independent factors towards the creation of a list of experiments, in a way that the impact of all parameters

would be sufficiently studied, in a more feasible timeframe. A fraction of the experiments scheduled to be performed would feed the model and another set of experiments would evaluate the fit of the produced model. To achieve improved accuracy, in parameters like oil droplet size which we know by now that demonstrates a significant impact on oil retention, the values entered in JMP were the specific values for each fabricated emulsion, as defined by the Mastersizer characterization. The response or dependent parameter of this study was fluorescent intensity, as derived from image analysis of the produced fluorescent microscopy images of the tested samples without being normalized with the control value of the blanc mimic. Table 7.2 demonstrates the generated design of experiment by the software.

Table 7.2: Design of experiments as generated by the software 'JMP'. Combination of the selected independent parameters resulted in a plan of experiments in random order that would generate data equivalent to full factorial approach.

Original Dox No	Description	Viscosity oil, Pa.s	Volume fraction oil	droplet size, micron	Rinsing Angle	Rinsing Time
2	training	Mineral oil	60	SSD	90	30
19	training	Mineral oil	40	MSD	45	120
11	training	Mineral oil	20	LSD	67.5	75
26	training	Sunflower oil	60	LSD	90	30
14	training	Sunflower oil	60	SSD	45	30
1	training	Mineral oil	60	LSD	90	120
36	validation	Petrolatum	20	LSD	45	30
33	training	Mineral oil	20	LSD	45	30
30	training	Sunflower oil	20	MSD	45	75
37	validation	Petrolatum	20	SSD	45	120
15	training	Mineral oil	20	SSD	45	120
10	training	Petrolatum	60	SSD	90	30
25	training	Petrolatum	40	SSD	90	75

35	training	Sunflower oil	40	MSD	67.5	75
28	training	Petrolatum	40	LSD	45	30
29	training	Mineral oil	60	SSD	45	75
9	training	Sunflower oil	60	SSD	90	120
6	training	Petrolatum	60	LSD	90	120
5	training	Petrolatum	60	LSD	45	75
4	training	Sunflower oil	20	SSD	90	30
31	training	Mineral oil	40	LSD	90	30
40	validation	Petrolatum	20	LSD	90	120
17	training	Mineral oil	20	SSD	90	120
16	training	Mineral oil	20	LSD	90	120
3	training	Mineral oil	60	LSD	45	30
41	validation	Mineral oil	40	SSD	67.5	30
24	training	Petrolatum	60	SSD	45	120
12	training	Petrolatum	20	MSD	90	120
21	training	Mineral oil	60	SSD	67.5	120
8	training	Petrolatum	20	SSD	45	30
38	validation	Petrolatum	60	LSD	45	120
39	validation	Mineral oil	60	MSD	90	75
23	training	Petrolatum	60	MSD	67.5	30
20	training	Sunflower oil	40	LSD	67.5	120
32	training	Petrolatum	20	LSD	90	30
18	training	Petrolatum	20	SSD	67.5	120
22	training	Mineral oil	60	LSD	45	120
27	training	Petrolatum	20	LSD	45	120
34	training	Sunflower oil	40	MSD	67.5	75
7	training	Mineral oil	20	SSD	45	30
13	training	Mineral oil	20	MSD	90	30

Table 7.2 illustrates the plan of experiments and shows the essential experiments that were required to generate enough data to produce a model that was trustworthy and provided equivalent data that a full factorial approach would. The first column of the Table 7.2 named ‘Original DOX No’ shows the original number assigned to the

experiment that would be performed with the parameters of that row. It is a common statistical step to randomize the order of the experiments, in order to minimize the error, hence the numbers of the original DOX are not in order from 1 to 41. The second column named ‘Description’ indicates which of these experiments would feed the model and which would be used for the validation of fitting of the produced model. The third column Illustrates the first independent parameter which is the oil viscosity. Mineral oil showed a viscosity of 0.01 Pa.s, sunflower oil showed the medium level of viscosity with a value of 0.02 Pa.s, and finally petrolatum that demonstrated the highest viscosity level with a value of 2.33 Pa.s. These values were obtained from rheological measurements using the rheometer at 40°C. The next column represented the oil volume fraction of the emulsion used for that experiment and it showed three levels 20%, 40% and 60% of oil. Next, the droplet size of the oil droplets within the emulsion was demonstrated in the following column. Although in this design of experiment column, the droplet size levels were written as SSD, MSD and LSD, the actual values of each emulsion as measured using the Mastersizer were fed to the statistical software, to evaluate accurately the impact of oil droplet size on retention. The following two columns demonstrated the two independent parameters regarding the cleaning step which were the rinsing angle with three levels of 45 degrees, 67.5 degrees and 90 degrees, and rinsing duration with three levels again of 30, 75 and 120 seconds of rinsing. Different levels were selected for these values from our previous full factorial approach to the petrolatum emulsions so that we could enable further understanding on the retention mechanism and its driving parameters.

7.3 Design of Experiments Protocol

The experiments took place in the order defined by the first column of the design of experiments Table 7.2. A full factorial approach of 5 independent parameters of 3 levels each would translate into 243 experiments of 4 sample repetitions which is equal to 972 experiments. With the design of experiment approach only 41 combinations of experimental conditions were tested and 4 samples for each combination which equals to 164 experimental repetitions.

Each row represented one experiment, or one combination of experimental parameters. For each row, an emulsion was fabricated given the specification of oil viscosity, oil volume fraction and droplet size as described by the row. The emulsion was then characterized as for its droplet size distribution and the median value was recorded. Following, the deposition step and the cleaning step took place with rinsing duration and angle of flow as described by the specification for this experiment. Four samples were tested in each experiment and further characterized as for their grey scale intensity, the target property, by employing image analysis of the fluorescent microscopy images. Following, the mean value of fluorescent intensity of the samples and the standard deviation were calculated, recorded and later introduced to the statistical analysis software together with the median droplet size value of the emulsion used, towards the generation of the statistical model. It is important to state here that the values of retention fed to the model were the raw intensity values as retrieved from the fluorescent microscope and the image analysis software, to minimize the experimental error and improve time efficiency of the method.

For example, the first day of experiments, a 60% emulsion of mineral oil in water was fabricated. Sufficient shear was applied to produce small size oil droplets. The homogenizer RPM used during the mixing step, that ensured the production of small size droplets, were defined on a previous step which is described in chapter 3.2. The model system emulsion was then tested to ensure it demonstrated the desired oil droplet size, and then it was applied on four mimics using the deposition set up, followed by rinsing at 45 degrees of flow for 30 seconds. The mimics were then placed under the fluorescent microscope, images were captured for all of them and following image analysis and grey intensity evaluation took place. The values of intensity were recorded and then added to the statistical analysis software.

This process was followed for every row of the Table 7.2 in the order stated by it, and every emulsion was fabricated and characterized on the day of the experiment to avoid stability issues and to ensure repeatability of the results. Four samples per experiment ensured repetition of the results and enabled the evaluation of the standard deviation.

7.4 Results and Model Generation

The following Table 7.3 demonstrates the intensity results for each row.

Table 7.3: Fluorescent intensity results of the designed experiment plan.

Original Dox No	Viscosity oil, Pa.s	Volume fraction oil	droplet size, μm	Rinsing Angle	Rinsing Time	Retention-Intesity	stdev
2	0.01	60	3.98	90	30	157.92	3.64
19	0.01	40	56.23	45	120	116.59	3.77
11	0.01	20	158.49	67.5	75	145.62	6.74
26	0.02	60	125.89	90	30	207.59	4.72
14	0.02	60	4.47	45	30	147.5	3.27

1	0.01	60	141.25	90	120	185.84	13.99
36	2.33	20	141.25	45	30	192.82	4.86
33	0.01	20	158.49	45	30	145.7	2.97
30	0.02	20	35.48	45	75	101.54	6.24
37	2.33	20	1.26	45	120	166.9	1.99
15	0.01	20	7.94	45	120	92.15	2.26
10	2.33	60	3.16	90	30	196.35	11.32
25	2.33	40	2.51	90	75	190.1	7.71
35	0.02	40	50.12	67.5	75	123.18	3.27
28	2.33	40	158.49	45	30	212.56	8.39
29	0.01	60	3.98	45	75	110.31	5.72
9	0.02	60	4.47	90	120	130.23	12.44
6	2.33	60	141.25	90	120	225.8	8.37
5	2.33	60	141.25	45	75	215.26	6.82
4	0.02	20	2.51	90	30	105.66	3.57
31	0.01	40	141.25	90	30	183.11	5.19
40	2.33	20	141.25	90	120	193.09	11.07
17	0.01	20	5.62	90	120	94.967	3.97
16	0.01	20	158.49	90	120	142	6.37
3	0.01	60	141.25	45	30	194.97	11.02
41	0.01	40	3.16	67.5	30	110.2	3.11
24	2.33	60	3.16	45	120	177.27	3.95
12	2.33	20	31.62	90	120	176.17	7.98
21	0.01	60	3.98	67.5	120	120.48	1.37
8	2.33	20	1.26	45	30	160.14	0.55
38	2.33	60	141.25	45	120	199.84	9.02
39	0.01	60	141.25	90	75	140.48	7.92
23	2.33	60	44.67	67.5	30	211.18	7.23
20	0.02	40	158.49	67.5	120	147.47	14.92
32	2.33	20	141.25	90	30	202.81	7.48
18	2.33	20	1.26	67.5	120	152.54	9.55
22	0.01	60	141.25	45	120	189.63	3.53
27	2.33	20	141.25	45	120	165.74	11.74
34	0.02	40	50.12	67.5	75	125.19	10.11
7	0.01	20	5.63	45	30	100.67	2.28
13	0.01	20	39.81	90	30	104.86	3.07

From Table 7.3, it is hard to draw any conclusions as parameters that affect retention are combined in a random manner and their individual impact cannot be identified at

first glance. However, by feeding the data into the statistical analysis software, JMP, and by applying a statistical approach, in this case the least square model, we were able to produce data towards the understanding of the impact of each independent parameter on retention. The following Images demonstrate the results of the statistical analysis as derived from the model generator and will be explained.

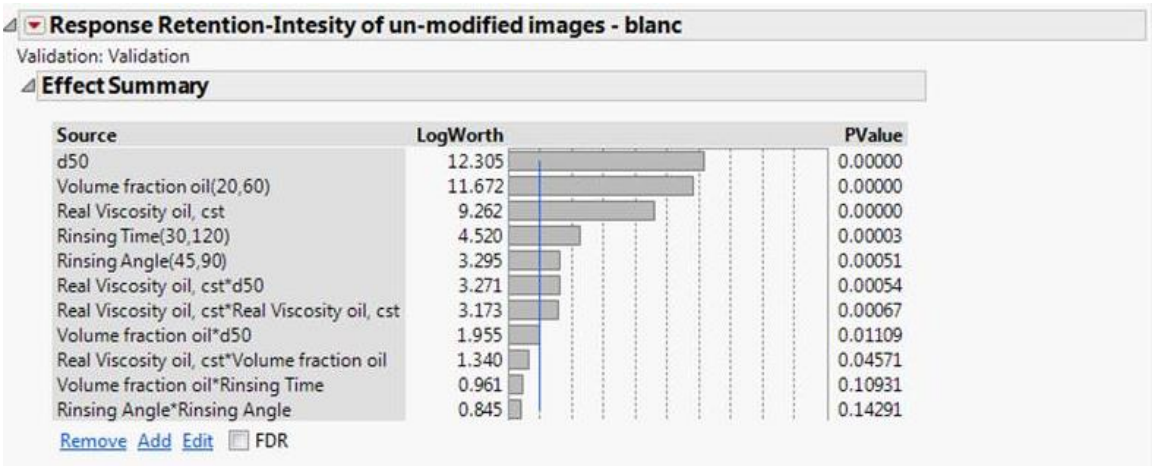

Figure 7.1: A table of the effect of independent parameters, combinations of them as well as quadratic parameters on the response variable is presented. By quadratic parameters we mean those whose effect is tested in relation to themselves, for example Viscosity*Viscosity.

The response parameter in our study is the fluorescent intensity of the fluorescent images that indicated hydrophobic active retention. The table illustrated in Figure 7.1, conclude that the parameter that had the most statistically significant impact on retention was d50 which is the median droplet size of the oil droplets within the fabricated emulsions. From the full factorial approach that was carried out for petrolatum emulsions and was presented in the previous chapter, we concluded that oil droplet size demonstrated a crucial impact on retention and the results of the DOE support these findings, by showing this impact to be present in all oil viscosities and again being the most significant parameter that drove retention of hydrophobic actives

on human skin. The second most impactful parameter was volume fraction of the oil phase within the emulsion, an expected outcome since increased amounts of oil within the formulation, naturally lead to improved retention of those on human skin. Oil viscosity was a significant independent parameter as well, with higher viscosity oils leading to optimal retentions for the same conditions of cleaning. As a result, petrolatum emulsions have shown increased retention in comparison to their equivalent mineral and sunflower oil emulsions. Rinsing duration showed the next highest impact on retention, with higher durations of rinse leading to lower amounts of retained oil portion on the mimics. Lastly the rinsing angle was the last independent parameter in terms of retention impact. Combinations of some of those parameters as well as quadratic parameters were evaluated for their impact on retention. In more detail, the relation of oil viscosity to oil viscosity as well as volume fraction to droplet size showed an important statistical significance on retention [1].

In the Figure 7.1, the PValue of each tested parameter is presented. In this case, PValue represents the probability of this parameter to not be impactful to the response. As a result, the lower this value is the more statistically significant the corresponding parameter was on retention. Again, the significance of oil droplet size followed by oil volume fraction and oil viscosity were shown. The results of this approach complemented our results on the full factorial approach to petrolatum emulsions, with oil droplet size being the most impactful parameter on retention, followed by the rinsing duration and angle of flow. The following Figure 7.2 illustrates the fit of the model, an indication of how accurate the generated prediction model is compared to the experimental results.

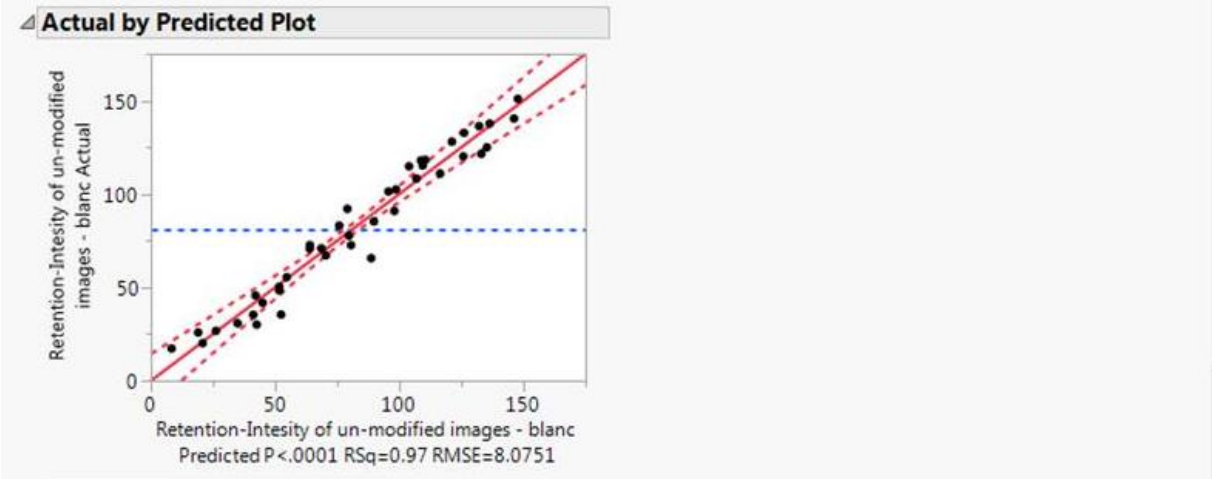

Figure 7.2: Illustration of the predicted curve, red line, against actual experimental data. This chart enables us to evaluate the fit of the generated model curve and calculate the Rsquare value, which is an indication of the achieved accuracy of the model.

In this graph, the generated prediction model against the experimental results is presented. The black dots represent the actual experimental results of retention and the red line shows the predicted results curve as generated by the statistical model. It is shown that the experimental results concentrate near the solid red line, exhibiting an effective fit of the real results to the model. Rsquare, is a value that indicates the fit of the curve to the experimental results and the closer this value is to 1 the better the fit is. The calculated Rsquare value for our system was 0.97, showing a high accuracy of the generated model and the effectiveness of the prediction curve. The following curve demonstrates a number summary of data fit for the least square technique that was employed.

Summary of Fit

RSquare	0.972562
RSquare Adj	0.959439
Root Mean Square Error	8.075061
Mean of Response	81.14429
Observations (or Sum Wgts)	35

Analysis of Variance

Source	DF	Sum of Squares	Mean Square	F Ratio
Model	11	53159.378	4832.67	74.1132
Error	23	1499.752	65.21	Prob > F
C. Total	34	54659.130		<.0001*

Lack Of Fit

Source	DF	Sum of Squares	Mean Square	F Ratio
Lack Of Fit	22	1497.7318	68.0787	33.7015
Pure Error	1	2.0200	2.0200	Prob > F
Total Error	23	1499.7519		0.1352
				Max RSq
				1.0000

Figure 7.3: Summary of the achieved fit, analysis of variance and fit evaluation of the method. The data demonstrates a fit analysis of the statistical model on the, experimental, data. The statistical approach was the least square method.

In the summary of fit the Rsquare value of 0.97 can be seen, indicating a highly efficient fit of the model to the actual experimental values. Moreover, the probability of the curve not fitting the actual values is very low, as shown in the analysis of the variance table, indicating the accuracy of the created model. A probability of the independent parameters not to be impactful to the accuracy of the curve is demonstrated in the following Figure 7.4.

Parameter Estimates

Term	Estimate	Std Error	t Ratio	Prob>|t|
Intercept	1.5773202	4.462246	0.35	0.7269
Real Viscosity oil, cst	1538.0187	151.1043	10.18	<.0001*
Volume fraction oil(20,60)	20.824657	1.545996	13.47	<.0001*
d50	0.3064357	0.021199	14.46	<.0001*
Rinsing Angle(45,90)	6.2438054	1.544693	4.04	0.0005*
Rinsing Time(30,120)	-8.135325	1.571917	-5.18	<.0001*
(Real Viscosity oil, cst-0.02661)*(Real Viscosity oil, cst-0.02661)	93486.998	23793.88	3.93	0.0007*
(Real Viscosity oil, cst-0.02661)*Volume fraction oil	-254.8509	120.643	-2.11	0.0457*
(Real Viscosity oil, cst-0.02661)*(d50-70.5173)	-6.770118	1.684221	-4.02	0.0005*
Volume fraction oil*(d50-70.5173)	0.0649945	0.023529	2.76	0.0111*
Rinsing Angle*Rinsing Angle	5.6129443	3.700158	1.52	0.1429
Volume fraction oil*Rinsing Time	-2.78129	1.669604	-1.67	0.1093

Figure 7.4: Parameter estimates table and the probability of impact of each independent parameter or combination of parameters.

Again, the most impactful parameters on the response were oil droplet size median values d50, oil viscosity, oil volume fraction and duration of rinsing. The independent parameter that exhibited the lowest impact on the model fit was the angle of rinsing flow with a probability of 0.0007. The following Figure 7.5 demonstrates the achieved Rsquare values for the training experiments and the one for the validation experiments.

Crossvalidation

Source	RSquare	RASE	Freq
Training Set	0.9726	6.546	35
Validation Set	0.8449	12.816	6

Figure 7.5: Cross validation of the model showing the achieved Rsquare for the training experiments and the one for the Validation experiments.

Out of the 41 experimental conditions that took place 35 of those fed data towards the creation of a model curve, the training experiments, and 6 were used to validate the model. In Figure 7.5, it is shown that the training data demonstrate Rsquare fit of 0.97 to the model prediction. However, the validation data demonstrate a fit of 0.85. The fit of the validation points is lower than that of the training points, this is a normal consequence since the training points were the ones used to fabricate the model.

However, the demonstrated validation fit is still more than efficient, hence the prediction curve is considered accurate and precise in indicating the impact of the independent parameters on retention.

Sorted Parameter Estimates

Term	Estimate	Std Error	t Ratio	Prob>|t|
d50	0.3064357	0.021199	14.46	<.0001*
Volume fraction oil(20,60)	20.824657	1.545996	13.47	<.0001*
Real Viscosity oil, cst	1538.0187	151.1043	10.18	<.0001*
Rinsing Time(30,120)	-8.135325	1.571917	-5.18	<.0001*
Rinsing Angle(45,90)	6.2438054	1.544693	4.04	0.0005*
(Real Viscosity oil, cst-0.02661)*(d50-70.5173)	-6.770118	1.684221	-4.02	0.0005*
(Real Viscosity oil, cst-0.02661)*(Real Viscosity oil, cst-0.02661)	93486.998	23793.88	3.93	0.0007*
Volume fraction oil*(d50-70.5173)	0.0649945	0.023529	2.76	0.0111*
(Real Viscosity oil, cst-0.02661)*Volume fraction oil	-254.8509	120.643	-2.11	0.0457*
Volume fraction oil*Rinsing Time	-2.78129	1.669604	-1.67	0.1093
Rinsing Angle*Rinsing Angle	5.6129443	3.700158	1.52	0.1429

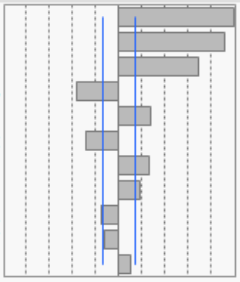

Figure 7.6: Impact evaluation of the sorted parameters as well as probability of impact for them.

In Figure 7.6, the impact of the independent parameters used to produce the prediction model is illustrated as well as their impact on the response, positive or negative, and its level. The dashed blue line in the horizontal bar chart indicate the impact above which an independent parameter is considered significantly important to the response. Oil droplet size showed the highest positive impact on retention, with higher oil droplet dimensions resulting in higher fluorescent intensity values, hence improved retention levels of oil on the human skin mimics. The second most impactful parameter was oil volume fraction, again with a positive impact on retention, which indicated that higher oil fractions within the model system emulsions resulted in higher intensity levels. Oil Viscosity was third on the impact of retention, with a positive effect on intensity as well. The rinsing time was the only independent parameter with a negative impact on retention, which was a logical consequence, given that longer rinsing results in more

effective cleaning hence less oil portion retained on the human skin mimics and a lower fluorescent intensity signal recorded. Rinsing angle showed a positive signal up to the 90 degrees of flow, a result that was also demonstrated on the petrolatum emulsion full factorial approach presented in the previous chapter. However, it is expected that if higher than 90 degrees rinsing angles were tried the retention levels would start falling again due to improved cleaning due to rinsing at an angle. This result would be of no scientific benefit and hence the range of angles selected was from 45 to 90 degrees. Figure 7.7 demonstrates the prediction profiler of the independent parameters chosen and their relation to retention fluorescent intensity.

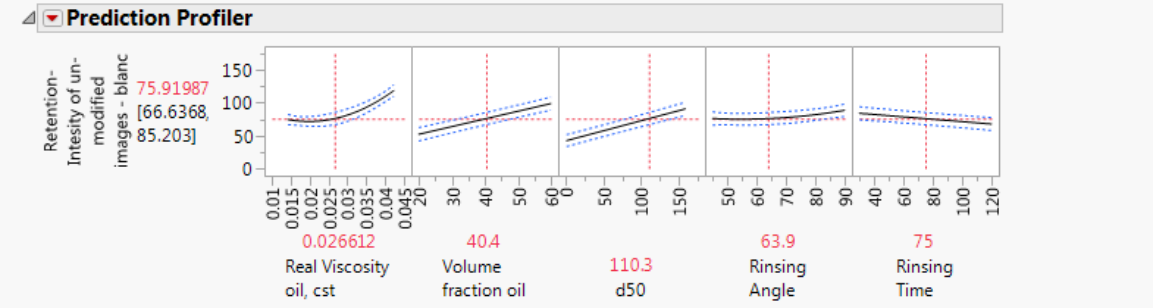

Figure 7.7: Prediction profiler for the selected independent parameters. A useful tool in performance prediction of a cosmetic formulation as far as retention of the hydrophobic active is concerned.

This set of graphs comprises of 5 graphs, one for each independent parameter and their impact on fluorescent intensity. Each graph has a moving cross, labelled in red, that can move along the curve, changing the value of each parameter as well as the corresponding retention-intensity value of the Y axis. The values indicated in red are the values currently marked by the red cross. Each curve indicates the impact of each independent variable to the response intensity. The higher the slope of the curve the

greater the impact of this parameter on the response value. Even by observing the graphs it can be concluded that oil viscosity, oil volume fraction and oil droplet size are the most influential parameters on the response value.

This tool enables the user to predict the retention performance of a formulation, given its specifications and the cleaning parameters. For example, in this snapshot, the information provided is the model system emulsion made using an oil of a viscosity of 0.027 Pa.s, at 40.4% volume fraction and droplet size of 110.3um, rinsed at 63.9 degrees for 75 seconds would result in an intensity value of 75.92. Hence, this tool enables the researcher to predict results of experiments that have not been performed. If a calibration curve that connected the fluorescent intensity to actual oil portion retained on mimics was present then this tool could feed data towards the accurate portion evaluation of retention. However, it can be used as it is for comparison purposes, efficiently and repetitively.

The other way that this tool can prove beneficial from a research and development point of view is by choosing the desired performance levels and then predicting the recipe of the formulation. For example, if a company wanted to produce a cosmetic formulation, which after use results in oil retention of specific levels, using this tool can provide the parameter combinations that deliver the desired levels of performance. It is optimal for industries to achieve the same results with smaller amounts of actives, due to huge cost savings, hence this tool can help towards this direction by showing the droplet size and oil viscosity values that would be optimal for lower volume fractions of oil within the formulation.

For the purposes of this project, fluorescent intensity was selected as the response parameter, as it absolutely correlates to the amount of retained oil portion on the mimics. However, other response parameters could be used that better suit different projects as suggested by the previous chapter. For example, the response parameter could be the coefficient of friction of the samples treated with these model system emulsions. Then the effect of each parameter to the smoothness of the skin would be studied, and personal care companies could employ this method to assist product development given the targeted skin smoothness they want to achieve. This method was easy to perform, cost and time efficient, and the substantial information and understanding provided is of great value and with profitable potential.

The following graph in Figure 7.8 demonstrates the interaction profile of the independent parameters and their correlation to the response.

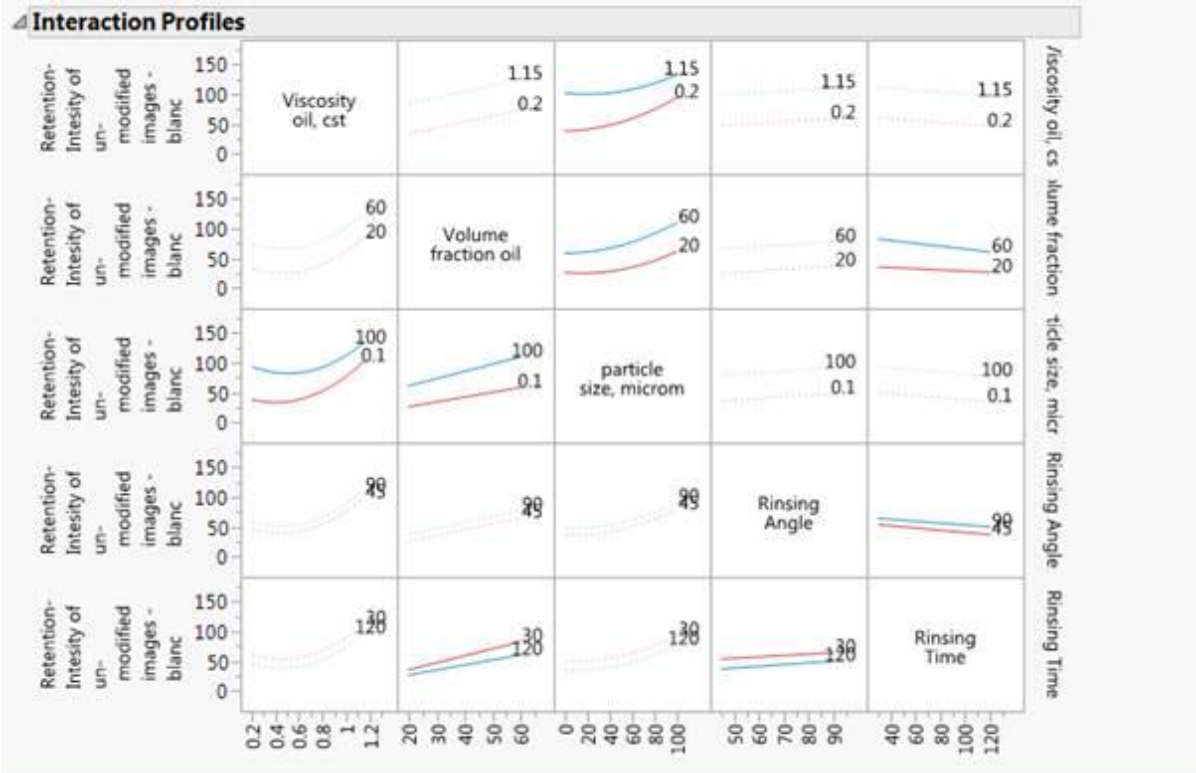

Figure 7.8: Interaction profiles of the selected parameters, showing the effect of each independent parameter to another independent parameter combination to the response parameter, in this case fluorescent intensity.

In Figure 7.8, the interaction profiles of the independent parameters in correlation to the response parameter is illustrated. These 20 graphs show the value range of predicted fluorescent intensity that the mimics exhibited for the interaction of two parameters per graph. For example, in the 3rd graph of the first, upper, row, the correlation of viscosity to droplet size is demonstrated. The blue line represents the curve that correlates droplet size to intensity of the model system emulsion fabricated with the high viscosity oil, the red line demonstrates the graph of droplet size to intensity for the model system emulsion produced with the low viscosity oil. The values between the two curves are the points of intensity and droplet size interactions for model system emulsions of viscosities between the two limits tested.

7.5 Discussion and Conclusions

The design of experiment approach enabled us to study a wider range of independent parameters and levels in a fraction of the time required to perform the significantly large number of experiments and focus on their impact on retention. The independent parameters selected were the oil viscosity, oil volume fraction, oil droplet size, rinsing duration and rinsing angle. Three levels for each parameter were selected. The response parameter of this study was the fluorescent intensity of the retained active portion on the test substrate that indicated the levels of retention. The produced model showed an impressive accuracy, with a great fit of the experimental data. The parameters selected were evaluated for their statistical significance in retention. The parameter that showed the highest impact on retention was the oil droplet size, with LSD emulsions exhibiting the highest retention levels in comparison to the MSD and SSD emulsions, a result that complemented our previous full factorial approach where LSD emulsions also resulted in effective retention of petrolatum. The second highest impact parameter was oil volume fraction followed by oil viscosity. The volume fraction was expected to have a significant statistical impact on retention since larger deposited amounts of active on the substrates would logically result in higher retained levels as well. Oil viscosity on the other hand showed a positive impact on retention, with higher oil viscosities leading to optimal retention. This was attributed to the physical difficulty that viscous materials show to flow making them harder to remove than less viscous materials. Lastly the rinsing duration and angle showed a vital impact on retention with higher durations of flow leading to effective cleaning of the substrate and rinsing at an angle reducing the amount of retained hydrophobic active, supporting our assumptions

of physical entrapment of the active being the major mechanism of retention. The design of experiment approach proved to be a valid proposition to test a larger number of parameters and levels with the accuracy of a full factorial approach in a cost and time effective manner. All results came to an agreement with our previously presented results and complemented them with further understanding on the impact of the selected independent variables. This approach could be used in further research by tuning the levels of the parameters or changing the response parameter towards the evaluation of other properties that the use of a cosmetic product provides, like reduction of friction, etc.

7.6 References

1. SAS Institute Inc. JMP® 10 Modeling and Multivariate Methods. Cary, NC: SAS Institute Inc, (2015).
2. First Look – JMP Pro,. Taylor James, JTonEDM (2012).

CHAPTER 8: SUMMARY AND FUTURE OUTLOOK

8.1 Summary

The aim of this project was the development of a method that would enable the study of retention of hydrophobic actives from cosmetic formulations on human skin, in an accurate, repetitive, cost and time effective manner. Towards the development of this method, the fundamental steps of cosmetic product use were identified and replicated in a highly-controlled environment.

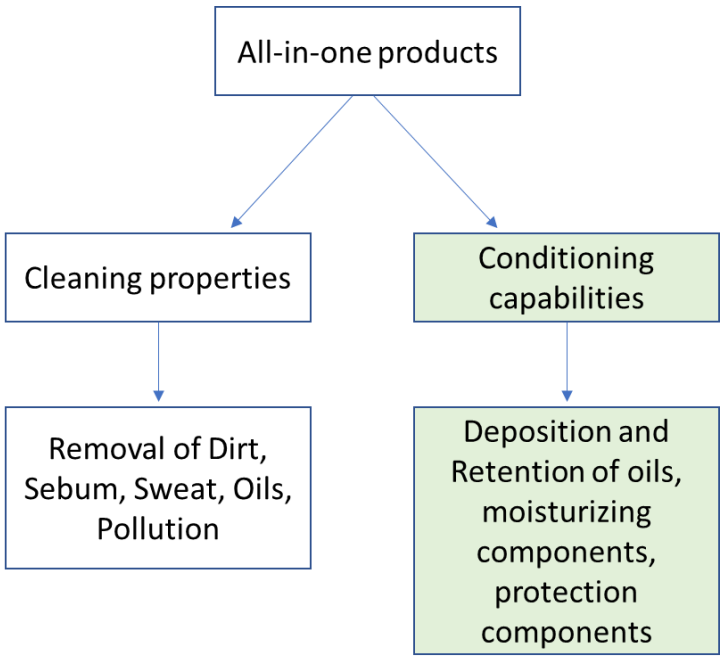

Figure 8.1: An overview flow-chart illustrating the multifunctional capabilities of all-in-one cleansing products. The overall work focused on the conditioning properties of these formulations and developing a method that enables the evaluation of retention levels of hydrophobic conditioning components such as petrolatum, sunflower and mineral oil.

The method included the fabrication of an optimal skin mimic of the area of interest that exhibited representative topographic features, surface energy, roughness and mechanical properties to human skin *in-vivo.* The skin replication technique proved to be a challenge, but we were able to produce robust, accurate and durable skin mimics that required low maintenance and a long shelf-life. The mimics were characterized for their accuracy in replicating human skin properties and demonstrated optimal precision, outperforming commercially available replicas.

Furthermore, the developed method involved the fabrication of model system emulsions that showed simplicity in their chassis while maintaining the major components of cosmetic products. This study focused on three formulation parameters including oil viscosity, oil volume fraction and oil droplet size within the product.

Following the development of the emulsions, a deposition set up that would apply the formulations on the skin mimics repetitively and in a controlled manner for the normal load, speed and number of cycles was essential and the tribometer set-up that provided this level of control along with modifications that allowed control of temperature and skin mimic to skin mimic interaction enabled the deposition of the product in an effective and controlled way.

Furthermore the single ,cleaning, water jet set up provided a controlled and representative of shower conditions environment to rinse the mimics in various angles and enabled the study of the impact of rinsing angle and duration on retention.

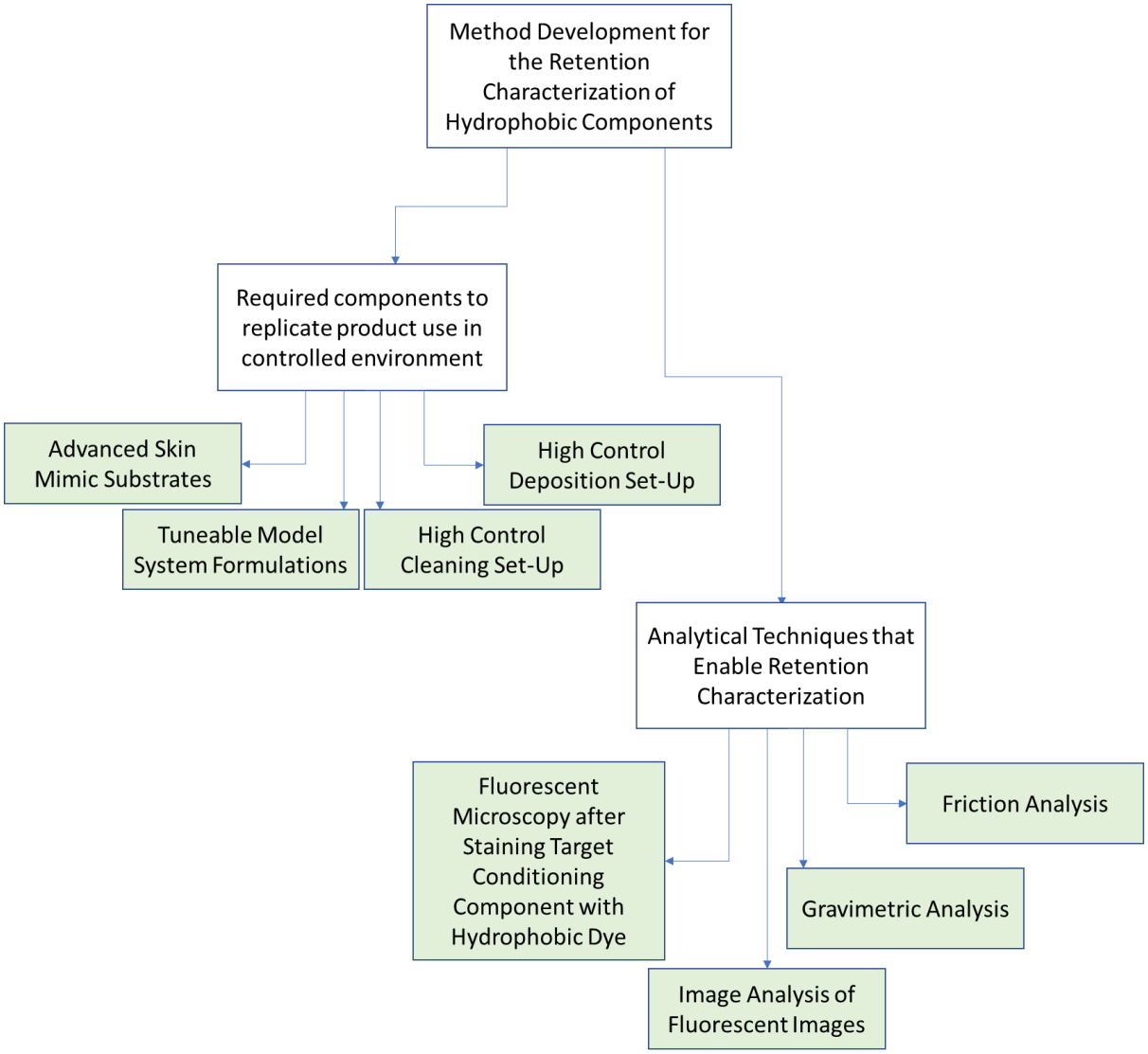

Figure 8.2: Illustration of the essential steps towards the development of a method to characterize retention. The project was divided in two major pillars. The first describes the vital replication of all parts of product use, from skin substrates and cosmetic formulations, to deposition and removal of the material. The second pillar describes the techniques and methods that were employed for the characterization of the retained portion of the hydrophobic component on the skin substrate's topography. These methods needed to be cost effective, accurate, repetitive and time efficient.

The full factorial approach, that tested the impact of droplet size, rinsing duration and rinsing angle in petrolatum retention, showed that LSD emulsions exhibited the highest performance in retention leading to elevated amounts of petrolatum retaining on the skin topography after rinsing. This was attributed to the lower stability of larger droplets, making them prone to breakage and therefore more efficient oil deposition on human

skin, their low mobility that resisted the water flow and low surface area that reduced the surfactant counter effect. Retention was evaluated on three aspects, fluorescent intensity of the stained active, gravimetric analysis of the substrates and coefficient of friction measurements. All characterization techniques came to an agreement, supporting the results and outlining the defining superiority of larger droplets in retention. Rinsing duration resulted in lower retention levels as well as rinsing at an angle, with 45° of flow leading to the most effective active removal.

Following, the design of experiment took place that enabled the study of a larger number of parameters including three levels of oil viscosity, three levels of oil volume fraction and three levels of rinsing angle. This approach provided valuable data towards the understanding of retention by allowing the evaluation of the statistical significance of a larger number of parameters in a feasible time schedule. The produced prediction model showed an effective fit to the experimental parameters and once more the effect of droplet size on retention was crucial, with larger droplets dominating the smaller ones. Additionally, the oil volume fraction showed an important impact on active retention, followed by oil viscosity, with higher viscosity oils enabling higher levels of retention. This fact was attributed to the resistance in flow of more viscous materials rendering them harder to rinse off. Rinsing duration showed a negative impact on retention with higher values leading to lower retained portion, however the effect was nonlinear. Moreover, rinsing at an angle of 45° showed the most effective sample cleaning, complementing the results of the full factorial approach.

The developed method, in combination with the design of experiment approach is a valid proposition in studying retention, being a quick, tuneable and cost-effective

method that evaluates the effect of various parameters. What is more, other effects of retention could be studied as the response parameter of the produced model, like the coefficient of friction, to study the impact of the independent parameters on skin smoothness. The proposed methodology enabled the data generation of hydrophobic active retention and contributed to the understanding of its drivers. Future researches could feed to retention understanding by studying the impact of more parameters.

8.2 Future Research Outlook

Further research might include the development of calibration curves of fluorescent intensity to hydrophobic active mass to enable retained portion calculations, only by employing fluorescent microscopy and image analysis, saving time and reducing experiment numbers. Additionally, the correlation of retained oil portion and coefficient of friction could be studied, focusing on the impact of both retained mass and distribution of oil on friction. As far as skin mimics are concerned, different levels of skin roughness mimics could be developed to study its effect on retention and evaluate the impact it might have to hydrophobic active physical entrapment. Furthermore, different surfactant systems could be studied as for their impact on retention. It is well established that cationic surfactants promote retention on skin by attaching to its surface, hence it would be interesting to study diverse surfactant systems and their effect on retention of the active component. Also, different amounts of shear during the deposition step could be examined to assess the effect of mechanical shear during the use of the product. Finally, the development of a more realistic product formulation and the retention evaluation of its actives in comparison to the model system emulsions

could take place to show the expected values of retention from a real cosmetic product and the effect of the complementary components to its conditioning performance.

APPENDIX A: DESIGN OF EQUIPMENT AND 3D PRINT

During the method development, few parts/equipment needed to be designed and built tailored, specifically for the purposes of this project. The cad designing software AUTODESK TINKERCAD, were used for the design of required equipment and a 3D printer, with the model name Ultimaker 2+, was employed for the production of the designs. The materials chosen for these parts were the polymers ABS and PLA. Both perform similarly in the temperatures used in the developed method. The following figure demonstrates the 3D printer Ultimaker 2+ that was used.

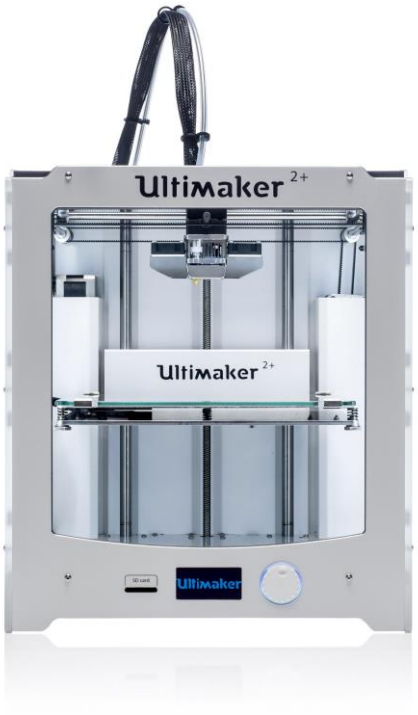

Figure A.1: 3D Printer Ultimaker 2+. Image found in '*https://ultimaker.com*'

Main features of this printer include the following:

- Build area of 223x223x205mm
- Heated base
- LCD screen
- Nozzle thickness of 0.02-0.60mm
- Swappable nozzle

The prementioned software, Tinkercad, as well as the 3D printer, were used for the development of two variations of water flow chambers and for the 1mm nozzle used in the cleaning set-up described in chapter 5.3. The two water flow chambers were designed and used for a proof of concept experiment, for the evaluation of different cleaning set-ups for the purposes of this project and the developed method. The results of this experiment are further presented in the following Appendix B. The following images demonstrate the Tinkercad designs of the flow chambers and the single water jet nozzle.

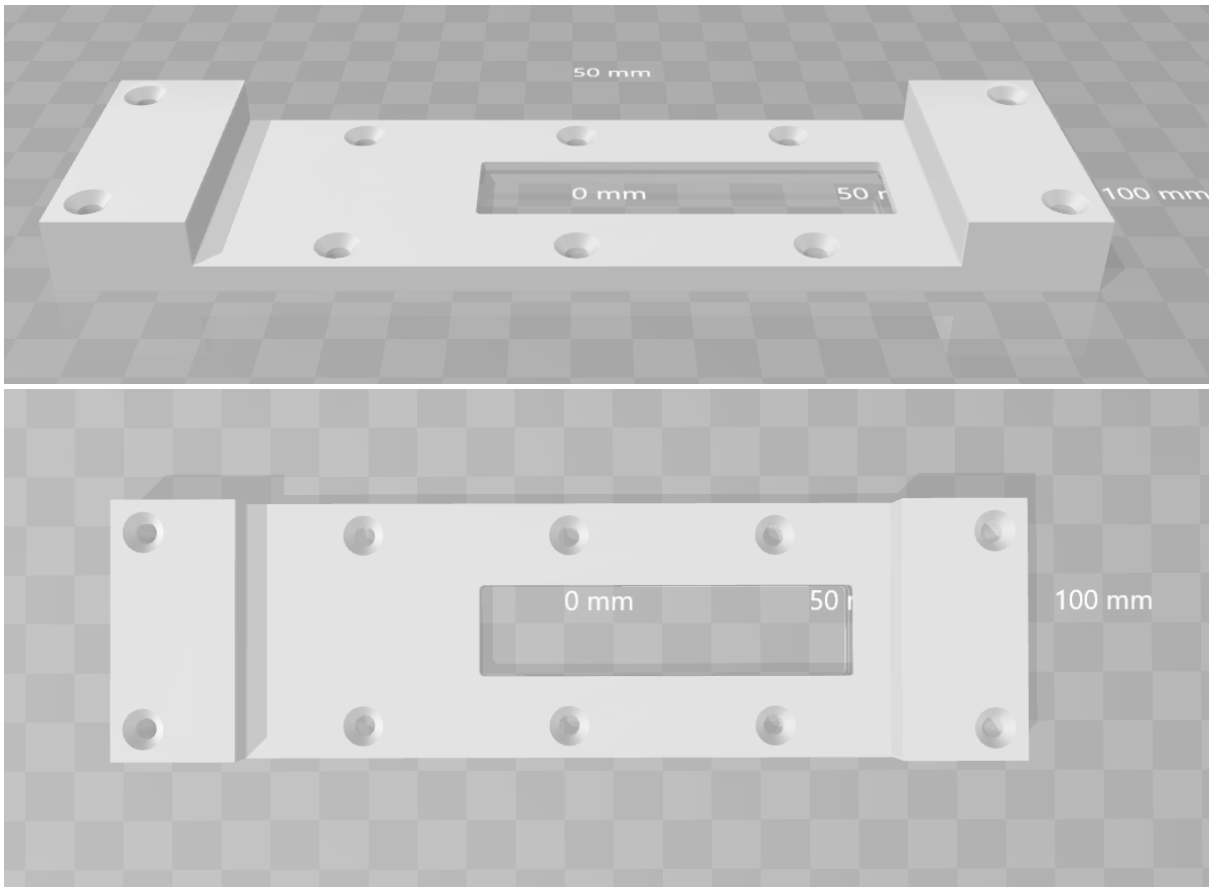

Figure A.2: Water flow chamber upper part. In this design, there is a hole were a glass is supposed to be glued so that the rinsing of the substrate can be monitored. The two boxes at both ends of the chamber are hollow and work as water tanks to eliminate turbidity coming from the water input cable and allow laminar flow in the chamber.

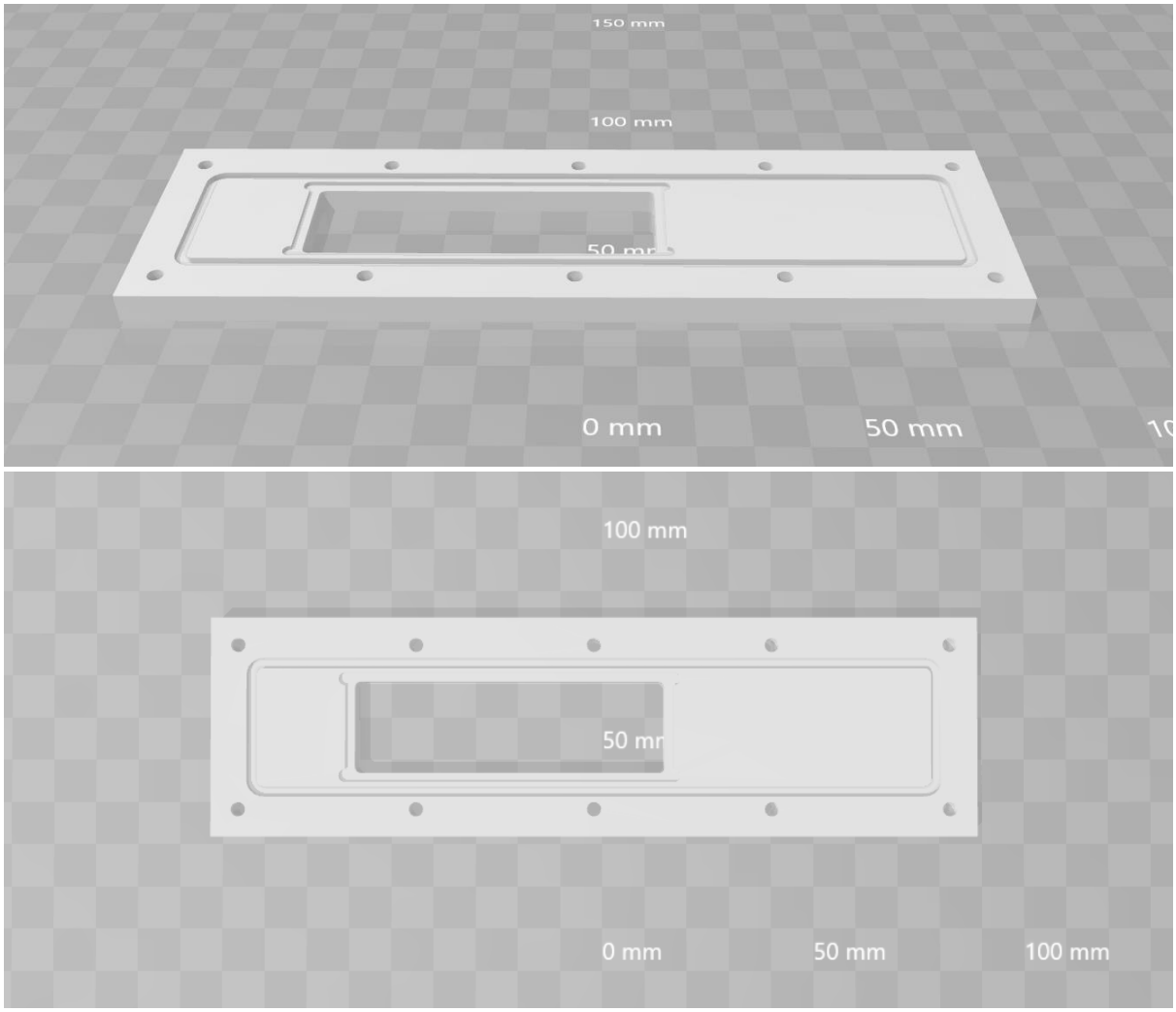

Figure A.3: Water flow chamber bottom part. In this design, there is again a place holder were a is supposed to be fitted. Also, in this design, hollow markings around the sample holder can be seen were a sealing rubber gasket is placed and then the top and bottom arts are connected using screws.

The water flow chamber shown in Figure A.2 and Figure A.3 was a design provided by University of Birmingham's mechanical workshop. This design was normally used for the generation of metallic flow chambers using laser etching. Subtle changes to the design took place to ensure that the 3D printed product would be functional. However, this chamber was produced t perform better in higher flow rates than the ones used in this project hence a compact, bespoke design was generated for this project. The following Figure A.4 demonstrates this design.

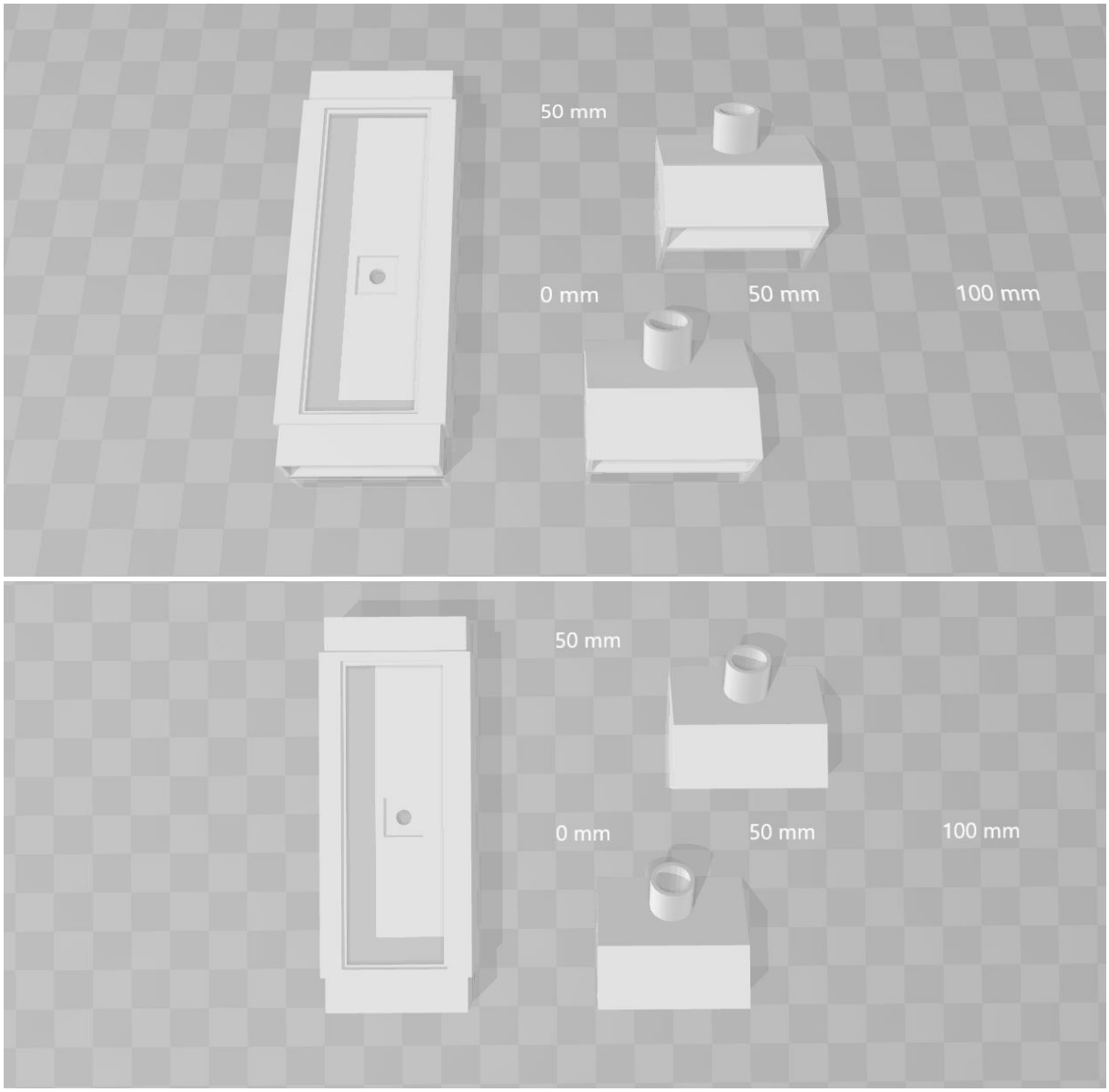

Figure A.4: Flow chamber design. In this bespoke design a sample holder can be seen on the bottom of the chamber were the skin bio-mimic sample is placed. Additionally, there is a hole or the placement of a demonstration glass that allows monitoring of the rinsing. Input and out put compartments were separately designed and printed.

The design in Figure A.4 illustrates the chamber that was printed and employed for the proof of concept experiment of the evaluation of the impact of different cleaning methods on retention. This chamber managed to provide an even flow over the test substrate. Also, the incorporated sample holder that demonstrated depth equal to the

samples' thickness enabled steady hold of the bio-mimics that didn't influence the laminar flow of the water feed.

The following Figure A.5 demonstrates the developed conical output nozzle used in the single water jet deposition set-up.

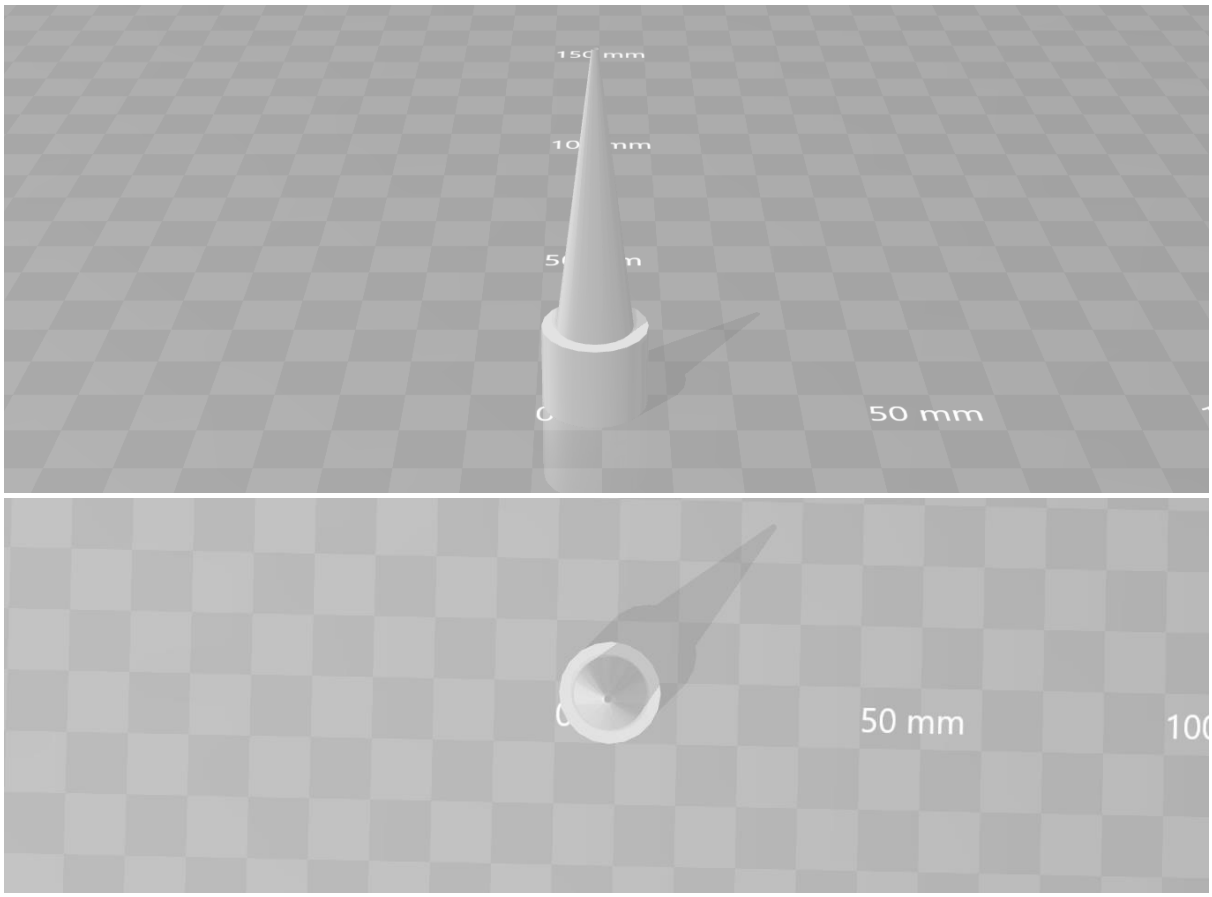

Figure A.5: 1mm output conical nozzle used in the single water jet cleaning set-up.

APPENDIX B: SINGLE WATER JET CLEANING SET-UP AND WATER FLOW CHAMBER COMPARISON

During shower, a few mechanisms of post-wash rinsing can be identified. In the case of skin cleaning we could observe three main cleaning/rinsing procedures. The irst one is rinsing the area directly with water coming from the showerhead water jets, without any additional mechanical scrubbing. Following, the second rinsing method is driven by a film of water flowing over human skin driven by gravity. This is usually found in the lower parts of the body, during rinsing, where the water from the showerhead that hits the upper body parts flows driven by gravity and eventually goes down the drain. The third rinsing mechanism that was identified was the combination of rinsing the skin surface with water and applying mechanical shear using hands for more efficient cleaning and product removal from the area. However, due to this being a very subjective process and because there are no values of mechanical shear applied on skin in literature, this process could not be replicated accurately in the lab. The first two cleaning mechanisms, were studied in depth and two cleaning set-ups were suggested for the purposes of this project. The first one is the one we decided that provided the highest accuracy and repetition and hence we used for the evaluation of retention and method development. However, in this Appendix, we will demonstrate the designed flow chamber that enabled controlled replication of rinsing the skin substrates by a gravity driven flow of water.

Firstly we designed a flow chamber that would enable the laminar flow of water, driven only by gravity. The chamber would be 3D printed out of PLA using an Ultimaker 2+ 3D printer. The chamber demonstrated a sample holder that enabled positioning of the sample and showed a depth equal to the substrate's thickness so that its edges would not obscure the laminar flow of water. Water input and output cables were connected to the edges of the chamber and the chamber was held in a vertical position using clamps and a lab stand. The input cable was connected with a beaker that was positioned 1m above the chamber middle point and a standar amount of water was used for the rinsing. The water would flow from the water beaker/container through the cable into the chamber and the to the output cable and waste container. The following Figures demonstrate the initial schematics and the 3D printed chamber.

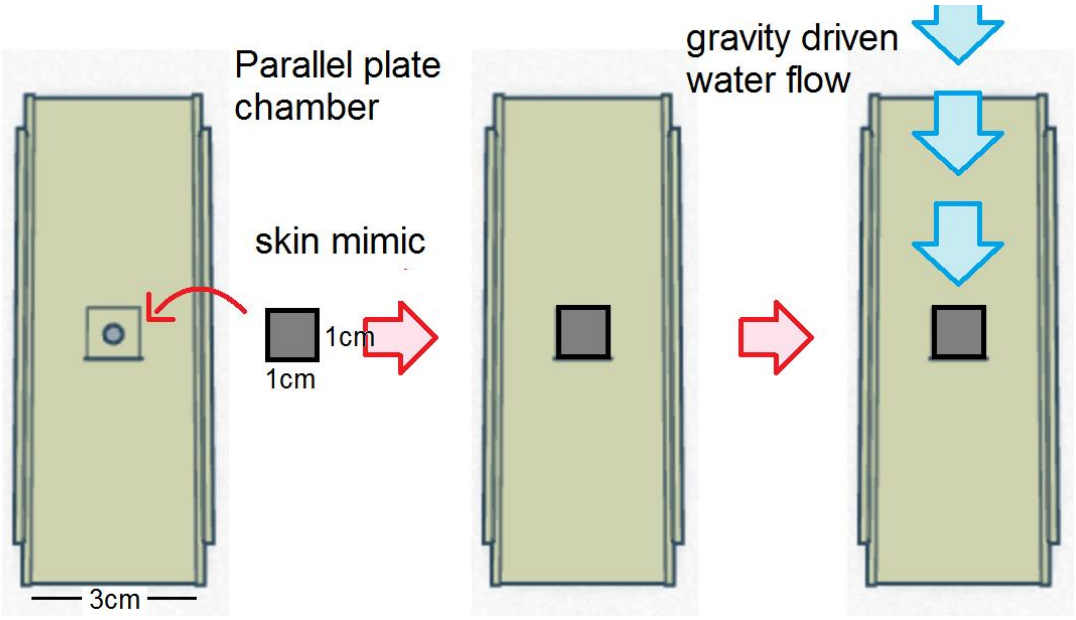

Figure B.1: Schematics of the gravity flow chamber showing the sample holder and the gravity driven flow of water.

Figure B.2: images of the printed water flow chamber.

The chamber was then used in comparison to the single water jet cleaning set-up on skin-mimic substrates following the experimental protocol described in detail in Chapter 6. The samples were then evaluated using fluorescent microscopy.

In the gravity flow chamber, we cannot control the flow rate since the flow is driven only by gravity. However, we can control the amount of water that will go through the mimics. For comparison purposes the water portion that was used to rinse a single substrate in the flow chamber was calculated so that it would be equivalent to the water used to rinse one substrate with the single water-jet cleaning set-up. The single water-jet set-up emitted water for 30 sec at a flow rate of 100ml/min, resulting in a total of 50ml of water. The chamber was designed to have a width of 3 cm in order to allow laminar flow over the middle point were the sample holder is positioned and not being affected by the walls of the chamber. The rinsing area is 3 times the width of the sample so 3 times more water is required for rinsing, using the chamber, so a total of 150ml of water was used. The model system formulation used for this experiment was 20% petrolatum, MSD and was deposited according to the protocol developed and explained in Chapter 5. The following Figure B.3 demonstrates the fluorescent microscopy, post rinse images of retained emulsion in samples cleaned with the flow chamber and the singe water jet set-up.

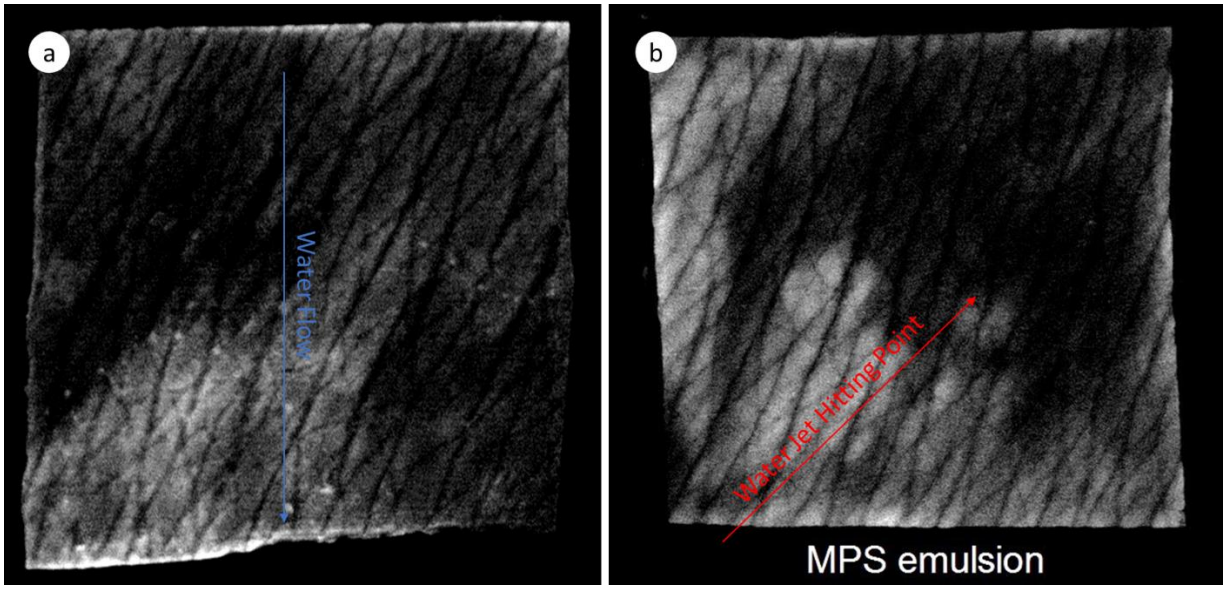

Figure B.3: Fluorescent Microscopy images of samples rinsed with (a) the gravity flow chamber and 9B0 the single water jet set-up. The big difference shown in those is the cleaning mechanism of the set-up with the first showing better cleaning in the top area of the substrate and less in the bottom whereas in the water-jet set-up, more effective cleaning is shown in the area were the water-jet hits rather than the edges of the sample.

In Figure B.3 the differences in cleaning of the two systems are illustrated. The flow chamber rinses the substrate from up to down showing improved cleaning in the top areas of the substrate rather than the bottom, whereas the water jet shows effective cleaning in the area where the water jet hits the sample and less effective in the edges. Additionally, the grey areas in the flow chamber sample show less intensity that the ones in the water-jet cleaned samples. We attribute this to the mechanistic differences of cleaning in the two set-ups, with the chamber removing more by means of dilution of the product in water and then rinsed by a gentle flow whereas in the water jet we have a stronger mechanical removal of the material from the area where the water hits the surface. To explore more the mechanism that the flow chamber rinses the substrate, experiments using 6 different water portions of flow were carried out to show

the effect of that on retention. This is the equivalent of rinsing time in the water jet set-up.

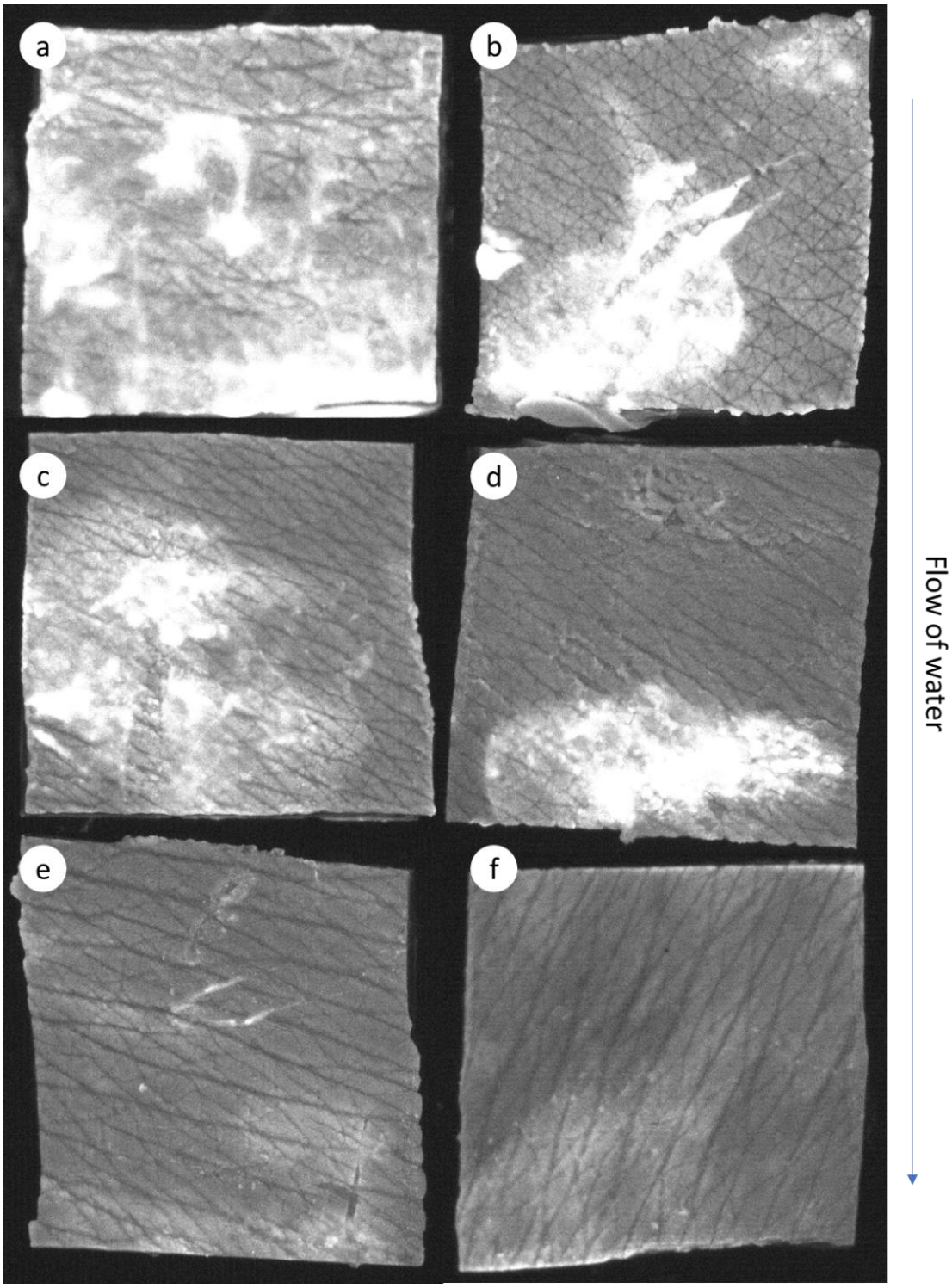

Figure B.4 demonstrates the rinsing effectives of product from human skin mimic substrates in function of rinsing water portion. Once more, it is observed that cleaning is affected by the direction of flow with top parts of the substrates retaining less material than the bottom parts.

This small-scale experiment provided a basic understanding of how different cleaning mechanisms might affect retention of hydrophobic actives on human skin. The substrates rinsed with the flow chamber show similar levels of retention with those cleaned with equivalent amount of water using the water jet set-up. However different characteristics of retention were observed that could potentially provide significant input on the mechanistic understanding of retention.

The flow chamber was not as accurate or repetitive as the high control water jet set-up, hence the second was used for the method development in this project.

APPENDIX C: VISCOSITY GRAPHS OF OIL PHASES

The following figures demonstrate the viscosity graphs of the three oil phases used in the model system emulsions, mineral oil, sunflower oil and petrolatum. The measurements took place at 40°C and the viscosity results are demonstrated in Chapter 4, Table 4.1.

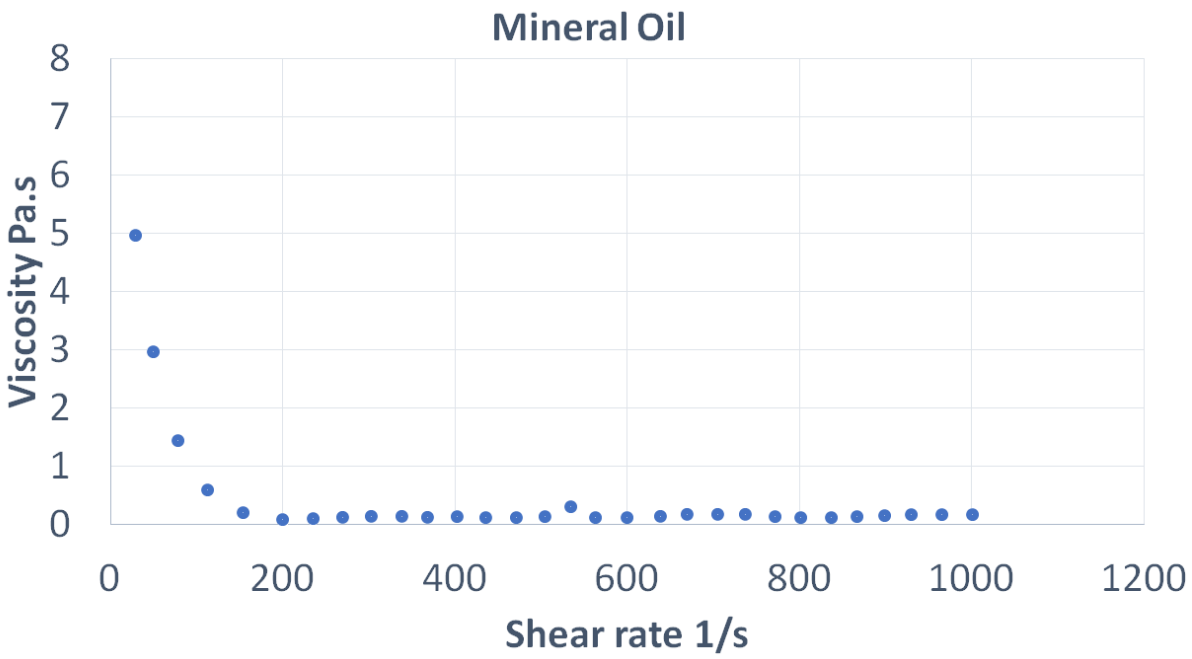

Figure C.1: Viscosity profile of mineral oil at 40°C

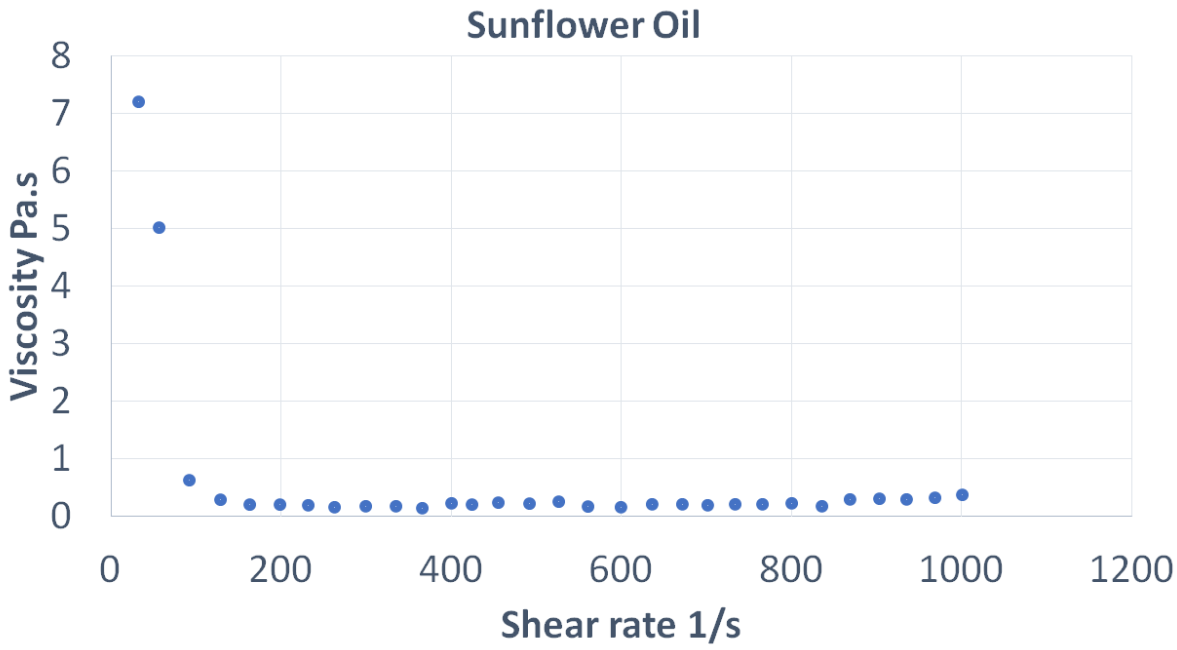

Figure C.2: Viscosity profile of sunflower oil at 40°C

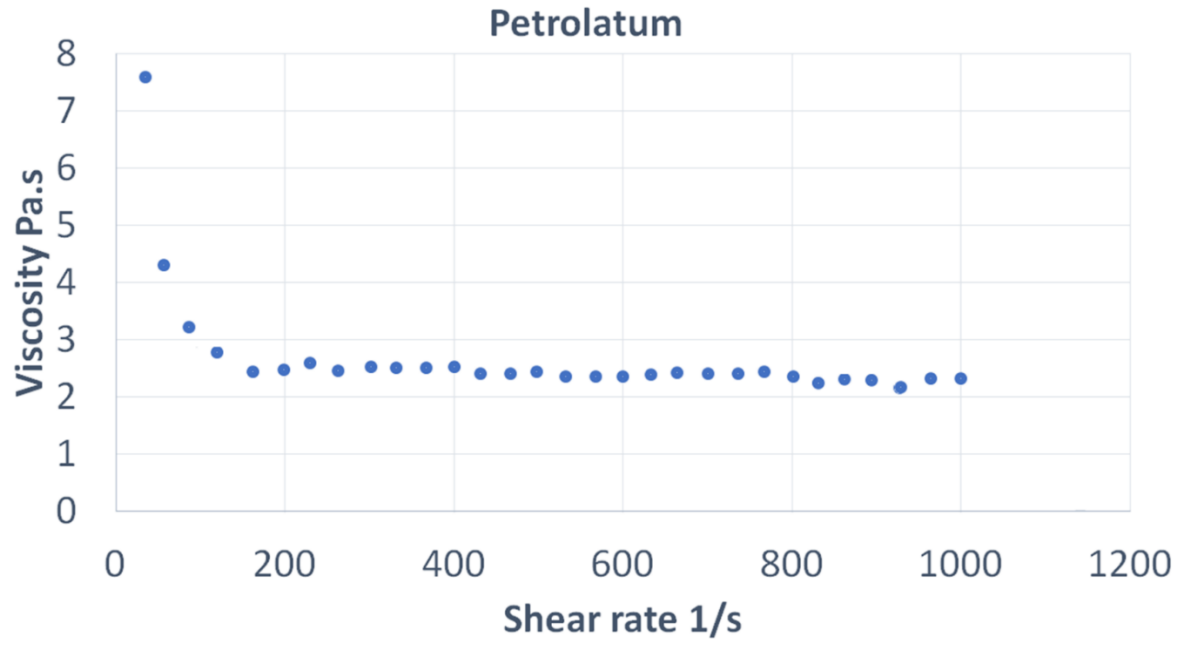

Figure C.3: Viscosity profile of petrolatum at 40°C